



Eidgenössische Technische Hochschule Zürich
Swiss Federal Institute of Technology Zurich

IMPACT OF SYNTROPHIC INTERACTIONS ON THE STABILITY OF MICROBIAL COMMUNITIES UNDER CHEMOSTAT CONDITIONS

AUTHOR Léo Buchenel

Zürich, May 12, 2020

SUPERVISORS IN THE IBZ GROUP

Dr. Alberto Pascual-García
Prof. Dr. Sebastian Bonhoeffer

SUPERVISOR IN THE D-PHYS DEPARTMENT

Prof. Dr. Manfred Sigrist

Master's Thesis submitted as part of the MSc Physics Program from ETH Zürich

It's not what you get out of life that counts. Break your mirrors! In our society that is so self-absorbed, begin to look less at yourself and more at each other. You'll get more satisfaction from having improved your neighborhood, your town, your state, your country, and your fellow human beings than you'll ever get from your muscles, your figure, your automobile, your house, or your credit rating. You'll get more from being a peacemaker than a warrior.

R. Sargent Shriver, quoted by Arnold Schwarzenegger

Contents

1	Introduction	5
1.1	CRMs in microbial ecology	5
1.2	General framework	7
1.2.1	Description of the model	7
1.2.2	General strategy	8
1.3	Feasibility	9
1.3.1	Respecting physical laws	9
1.3.2	Feasibility region	11
1.4	Dynamical stability	12
1.4.1	Local dynamical stability	12
1.4.2	How to determine local dynamical stability	13
1.4.3	The locally dynamically stable region $\mathcal{D}_{L,x}^{G,A}$	14
1.4.4	Evaluating the size of the basin of attraction	14
1.4.5	Global dynamical stability	15
1.5	Structural stability	16
1.6	Tactics used to simplify the problem	18
1.6.1	Metaparameters	18
1.6.2	Matrix properties	19
1.7	Goals of the Thesis	21
2	Methods	23
2.1	Domain of study	23
2.1.1	Choice of metaparameters and numerical constants	23
2.1.2	Set of matrices	24
2.1.3	Syntrophy scenarios	24
2.2	Feasibility	26
2.2.1	Building feasible systems	26
2.3	Dynamical stability	28
2.3.1	Master equation for local dynamical stability	28
2.3.2	Bounds on the eigenvalues: Gershgorin circle theorem	28
2.3.3	Reductio ad absurdum	28
2.3.4	Monte Carlo algorithm for the optimal matrix	29
2.4	Structural stability	30
2.4.1	Numerical estimate of the critical structural perturbation	30
3	Results	33
3.1	Feasibility	33
3.1.1	Estimating the fully feasible region $\mathcal{F}_1^{G,A}$	33
3.1.2	The feasibility region in the absence of syntropy	33
3.1.3	Impact of syntropy on the feasible region	37
3.2	Dynamical stability	47
3.2.1	The quest for dynamical stability	47
3.2.2	LRI regime	49
3.2.3	General numerical observations	58

3.2.4	Fully dynamically stable region	58
3.2.5	Largest eigenvalue of the Jacobian	66
3.2.6	The influence of the matrix dimensions	69
3.3	Structural stability	74
3.3.1	Domain of analysis	74
3.3.2	Critical dynamical syntrophies	75
3.3.3	Critical structural perturbation	78
4	Discussion	83
5	Appendices	87
5.1	Supplementary methods	87
5.1.1	Dynamical stability	87
5.2	Supplementary results	90
5.2.1	Feasibility	90
5.2.2	Dynamical stability	92
5.3	Declaration of originality	104
Bibliography		105

1 Introduction

1.1 Consumer-Resource Models in microbial ecology

Biology and Physics are tightly intertwined. Especially the years following the end of World War II saw many famous physicists getting interested in the blooming field of Biology [1], Leo Szilard or Erwin Schrödinger and his *What is Life? The Physical Aspect of the Living Cell* [2] among others. That exodus is no surprise, many biological phenomena at different scales are well modelled with Physics weaponry: from the use of Statistical Physics to solve protein folding problems [3] and find phase transitions in ecological communities [4] to the application of Hamiltonian dynamics to describe the movement of starling flocks [5].

However, many problems are not solved yet: the study of microbial communities remains one of the biggest and most interesting challenges of contemporary microbiology. Indeed microbes and their complex interactions have a substantial, non trivial and very large impact on humans and their environment in various ways: we only start to understand the role of microbiological interactions in vertebrates' guts [6], or how they shape our soils [7] and oceans [8].

Until recently [9], microbial ecologists focused their attention on competition and predation and overlooked the role of syntrophy as a factor in the shaping of microbial communities. Syntrophy, which is largely observed in microbial communities [9], by definition occurs when microbes release, through a metabolic process, byproducts that are consumed by some members of the microbial community. That mechanism is mutualistic at the community level: on one hand microbes release metabolites for others, which is costly, but on the other they receive additional resources from others. Similarly to microbial ecologists, only recently have theoretical ecologists focused on mutualistic systems like plants-pollinators networks [10, 11], and the role of mutualistic interactions on the stability of communities is still very debated. For instance Bastolla et al. argue that mutualism increases the persistence – *i.e.* the capacity to resist to perturbations – of plants-pollinators networks. Although other studies agree with that result [11, 12], the impact of mutualistic interactions on the stability of communities is still disputed by recent literature [13].

Grasping how syntrophy affects the stability of microbial communities is a step further towards the comprehension of the biological principles that govern these ubiquitous communities. Understanding such principles would allow us to control these communities which could lead to technological breakthroughs such as personalized medicine [14]. To develop a general understanding of microbial communities, we need a model that works well for a large range of number of microbial species. This rules out Flux Balance Analysis (FBA) [15], which is known to scale badly with the system size [16]. Because microbial communities are very diverse, we also need a model over which we can have a large analytical¹ control such that we can understand the effect of each parameter separately. This naturally leads us to population dynamics models.

Population dynamics in ecological communities are often approximated by variations of the Lotka-Volterra model [17]. This approach works well when the mediators of the competitive interaction between species, *i.e.* the resources, reach a steady state fast enough such that their own dynamics can be eliminated [18]. However, such an assumption is not

¹Of course, another advantage of having a good analytical grasp is that it allows us to extract the governing principles in a much easier way.

always true and one must in general always ask themselves whether it may be applied [19]. For microbial communities, previous literature shows that the population dynamics are not always well captured by a Lotka-Volterra model [18], which explains the need of a more mechanistic approach, where the dynamics of both the microbes and their resources are explicitly modelled. Robert MacArthur is one of the first ecologists to establish and study such a *Consumer-Resource Model* (CRM) [20], launching a field still active today [21].

We propose in this Thesis a CRM of microbial communities that explicitly models syntrophic interactions. We will focus on such microbial communities under chemostat conditions because, *inter alia*, these are very easy to set up experimentally. The general aim of our study is to determine and quantify how syntropy impacts the feasibility and the stability of microbial communities.

1.2 General framework

Before explaining the general strategy that will be followed in this Thesis, we briefly describe the model we will study.

1.2.1 Description of the model

We write down a CRM which describes the coupled evolution of the biomass of N_S different species and their N_R resources in a chemostat². Resources are labelled $\mu = 1, \dots, N_R$ and consumers $i = 1, \dots, N_S$. The coupled time evolution of their respective abundances $\{R_\mu, S_i\}$ is given by:

$$\frac{dR_\mu}{dt} = l_\mu - m_\mu R_\mu - \sum_j \gamma_{j\mu} R_\mu S_j + \sum_j \alpha_{\mu j} S_j \quad (1.1a)$$

$$\frac{dS_i}{dt} = \sum_\nu \sigma_{i\nu} \gamma_{i\nu} R_\nu S_i - d_i S_i - \sum_\nu \alpha_{\nu i} S_i \quad (1.1b)$$

The set of quantities $\{l_\mu, m_\mu, \gamma_{i\mu}, \alpha_{\mu i}, \sigma_{i\mu}, d_i\}$ has no explicit dynamics and is taken as constant. On the other hand, $\{R_\mu, S_i\}$ may dynamically evolve. Note that there are in this model a lot of different symbols that link different quantities and may be easy to confuse. We will at least try to keep the following conventions:

- Quantities related to resources have subscripts in Greek alphabet (e.g. the resource μ has abundance R_μ).
- Quantities related to species have subscripts in Latin alphabet (e.g. the species i has abundance S_i).
- Finally, quantities related to both have both indices.

Our model takes numerous phenomena into account and it may be helpful to take the time to explain the different terms of each differential equation. The temporal evolution of the biomass R_μ of a resource μ is essentially driven by the following processes:

- Constant external inflow coming from the experimental setup: this corresponds to the constant $+l_\mu$ term.
- Natural diffusion/deterioration at rate m_μ : this corresponds to the $-m_\mu R_\mu$ term.
- Consumption by the species j at a rate $\gamma_{j\mu}$: $-\gamma_{j\mu} R_\mu S_j$. Summing up the contributions of every species, we get the Lotka-Volterra style [17] term $-\sum_j \gamma_{j\mu} R_\nu S_j$,
- Intrasystemic inflow coming from the syntropy of species j at a rate $\alpha_{\mu j}$: $+\sum_j \alpha_{\mu j} S_j$.

On the other hand, biomass of species S_i changes because of the following processes:

²In a chemostat, new nutrients are continuously added, while at the same time microorganisms and resources are removed in order to keep the culture volume constant [22].

- Consumption of resource R_ν at a rate $\gamma_{i\nu}$. Only a fraction $\sigma_{i\nu}$ of this is allocated to biomass growth: $+ \sum_\nu \sigma_{i\nu} \gamma_{i\nu} R_\nu S_i$.
- Cell death/diffusion at rate d_i : this is the $-d_i S_i$ term.
- Syntrophic interaction : release of resource ν at rate $\alpha_{\nu i}$. In total $- \sum_\nu \alpha_{\nu i} S_i$.

1.2.2 General strategy

In general, we are interested in the existence and stability of fixed points (or *equilibria*) of Eq.(1.1). More precisely, an *equilibrium* is defined as abundances³ $\{R_\mu^*, S_j^*\}$ that are fixed points of the model, *i.e.* for which the LHS of Eq.(1.1) is zero:

$$\left\{ \begin{array}{l} 0 = l_\mu - m_\mu R_\mu^* - \sum_j \gamma_{j\mu} R_\mu^* S_j^* + \sum_j \alpha_{\mu j} S_j^*, \\ 0 = \sum_\nu \sigma_{i\nu} \gamma_{i\nu} R_\nu^* S_i^* - d_i S_i^* - \sum_\nu \alpha_{\nu i} S_i^*. \end{array} \right. \quad (1.2a)$$

$$\left\{ \begin{array}{l} 0 = l_\mu - m_\mu R_\mu^* - \sum_j \gamma_{j\mu} R_\mu^* S_j^* + \sum_j \alpha_{\mu j} S_j^*, \\ 0 = \sum_\nu \sigma_{i\nu} \gamma_{i\nu} R_\nu^* S_i^* - d_i S_i^* - \sum_\nu \alpha_{\nu i} S_i^*. \end{array} \right. \quad (1.2b)$$

The procedure we will follow (Fig.1.2.1) is split in three stages, each of them is detailed in its dedicated own section below. We will first address the question of the *feasibility* of our model, which tells us in what conditions equilibria of Eq.(1.1) exist. We will then focus on its *dynamical stability*, which answers the question of how the system responds when the equilibrium points $\{R^*, S^*\}$ are perturbed. Finally, we will study how microbial communities described by Eq.(1.1) respond when they are confronted to environmental perturbations, *i.e.* the issue of their *structural stability*.

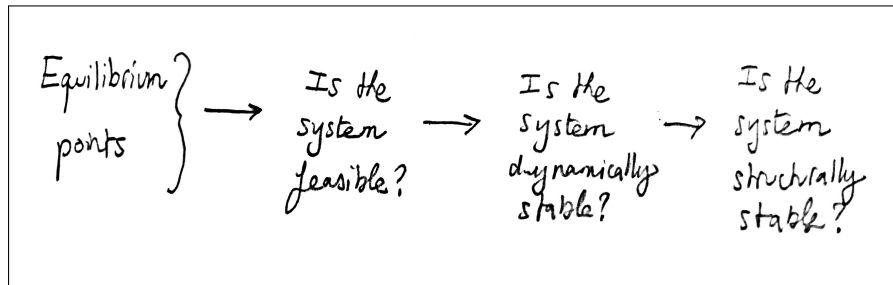


Figure 1.2.1: General procedure we will follow to study systems describing microbial communities.

³For the sake of brevity, we will sometimes drop the μ and j subscripts and simply write $\{R^*, S^*\}$.

1.3 Feasibility

The study of ecological interactions has been since its very inception [23], and still is today, tightly close to the one of random matrices [24, 25, 26]. Usually, the procedure is to study an equilibrium point which we assume is feasible. Some matrix of the model (*e.g.* the species-interaction matrix or the Jacobian) is approximated as random, and the dynamical or structural stability of said equilibrium point is investigated.

That framework is not satisfying for the study we would like to conduct, because it does not take time to study whether random parameters make sense in the first place. Indeed, before studying whether a microbial community can sustain perturbations, we need to know if said community actually *exists*. Biological systems, like any other natural systems, are constrained by laws, whether they arise from physical or biological considerations. For instance, it would not make sense to consider microbial communities that *e.g.* violate the laws of thermodynamics. In the following Section, we explain how such considerations can help determining the answer to the **feasibility** question:

Can microbial communities arising from a random set of parameters make sense on a physical and biological level? If not, what are the conditions that should be imposed and how are these translated mathematically?

1.3.1 Respecting physical laws

As explained above, we want to impose conditions such that we only study systems that are compatible with biological and physical laws. Choosing such restrictions is a crucial task: we want to be as close to nature as possible but we also need to stay simple enough such that the model remains mathematically tractable. Our choice is the following: any system deemed as feasible must have “biological” model parameters and conserve biomass.

Asking for the model parameters to be “biological” means we want them to carry their intended biological interpretation. This means *e.g.* that any syntrophic interaction has to be non-negative $\alpha_{\mu i} \geq 0$ otherwise it cannot be interpreted as a syntrophic interaction, because the mutual effect must be positive. More generally, the values of the parameters will be restricted. Firstly, we are looking for positive-valued equilibria. Also, we require that every consumer can allocate some of each resource it consumes to growth⁴: zero efficiencies are forbidden. Finally, every resource external feeding rate should be non-zero in order to avoid resource depletion and every resource and consumer must eventually die out in the absence of interaction. Taking into account the sign conventions in the model, these considerations result in:

$$R_\mu^*, S_i^*, l_\mu, d_i, m_\mu, \sigma_{i\mu}, \alpha_{\mu i} > 0 \text{ and } \gamma_{i\mu}, \alpha_{\mu i} \geq 0. \quad (1.3)$$

That condition already greatly restricts the choice of parameters $p \in \mathcal{P}$. However, additional complexity arises from the relationships parameters have to follow by definition. Indeed, the $3N_R + 2N_S + 3N_R N_S$ parameters are constrained by the $N_R + N_S$ equations (1.2). So if

⁴It would not make sense to say that species i eats resource μ with efficiency 0, since this is equivalent to species i not eating resource μ , and this is already encoded in the network structure.

we choose $2N_R + N_S + 3N_R N_S$ parameters, the remaining $N_R + N_S$ are instantly determined. Traditionally, we would solve for R^* and S^* and choose the rest of the parameters, but for mathematical reasons specific to the form of the fixed points equations (1.2), it is easier to solve for the consumers death rates d_i and the resources diffusion rate m_μ . This means that if we choose non-negative $\gamma, \alpha, \sigma, \tau, l, R^*$ and S^* , Eqs.(1.3) can be combined with Eqs.(1.2) into:

$$\begin{cases} d_i = \sum_{\nu} (\sigma_{i\nu} \gamma_{i\nu} R_{\nu}^* - \alpha_{\nu i}) > 0 & \forall i = 1, \dots, N_S. \\ m_\mu = \frac{l_\mu - \sum_j (\gamma_{j\mu} R_{\mu}^* - \alpha_{\mu j}) S_j^*}{R_{\mu}^*} > 0 & \forall \mu = 1, \dots, N_R. \end{cases} \quad (1.4)$$

In addition to these constraints, any feasible system should conserve biomass at equilibrium⁵: no species should be able to produce more biomass than it physically uptakes. More specifically, a consumer i attains, from resources consumption, a total biomass of $\sum_{\nu} \gamma_{i\nu} R_{\nu}^* S_i^*$. From this available biomass, only $\sum_{\nu} \sigma_{i\nu} \gamma_{i\nu} R_{\nu}^* S_i^*$ is devoted to growth. Out of the remaining $\sum_{\nu} (1 - \sigma_{i\nu}) \gamma_{i\nu} R_{\nu}^* S_i^*$, a part $\sum_{\nu} \alpha_{\nu i} S_i^*$ is given back to the resources as a syntrophic interaction. We simply impose that the syntrophic interaction is smaller than or equal to the available remaining biomass:

$$\sum_{\nu} (1 - \sigma_{i\nu}) \gamma_{i\nu} R_{\nu}^* \geq \sum_{\nu} \alpha_{\nu i} \quad \forall i = 1, \dots, N_S. \quad (1.5)$$

From now on, we will say that a parameter set p is *feasible* if it satisfies Eqs.(1.4) and (1.5). This is completely deterministic, in the sense that for a given parameters set $p \in \mathcal{P}$ one can without a doubt say whether it is feasible or not. Hence we define the *parameters set feasibility function* $\mathfrak{F} : \mathcal{P} \rightarrow \{0, 1\}$, which takes a parameters set as an input and tells whether this parameter set is feasible or not:

$$\mathfrak{F}(p) = \begin{cases} 1 & \text{if } p \text{ is feasible,} \\ 0 & \text{else.} \end{cases} \quad (1.6)$$

However, as explained in Section 1.6, we will usually not work with a parameters set $p \in \mathcal{P}$ directly – because there are too many variables to keep track of – but with a metaparameters set $m \in \mathcal{M}$ and a consumption-syntropy network $(G, A) \in \mathcal{B}_{N_S \times N_R} \times \mathcal{B}_{N_R \times N_S}$ instead. We can define a corresponding *metaparameters set feasibility function* $\mathcal{F} : \mathcal{M} \rightarrow [0, 1] \times \mathcal{B}_{N_R \times N_S}$ which is the probability that a given set of metaparameters $m \in \mathcal{M}$ coupled with binary matrices $B = (G, A)$ gives rise – through the algorithmic procedure \mathcal{A} – to a feasible parameters set:

$$\mathcal{F}(m, B) = \text{Probability} \{ \mathfrak{F}(\mathcal{A}(m, B)) = 1 \}. \quad (1.7)$$

In practice $\mathcal{F}(m, B)$ is estimated numerically by calculating the fraction of feasible systems out of N parameters sets generated from (m, B) :

$$\mathcal{F}(m, B) = \lim_{N \rightarrow \infty} \sum_{i=1}^N \frac{\mathfrak{F}(\mathcal{A}(m, B))}{N} \approx \sum_{i=1}^N \frac{\mathfrak{F}(\mathcal{A}(m, B))}{N} \text{ for } N \gg 1. \quad (1.8)$$

⁵This weak condition should hold only at equilibrium: we allow transition periods where biomass may not be conserved.

1.3.2 Feasibility region

We would like to study feasibility in a mathematically coherent way, and in that purpose we need to define mathematical objects that describe best what we are trying to measure. To quantify feasibility in the metaparameters space, we define for a consumption matrix G and a syntropy adjacency matrix A the x -feasible region $\mathcal{F}_x^{G,A}$ of the metaparameters space \mathcal{M} that will lead to at least a ratio x of feasible systems *i.e.* :

$$\mathcal{F}_x^{G,A} \equiv \{m \in \mathcal{M} : \mathcal{F}(m, (G, A)) \geq x\}. \quad (1.9)$$

It is clear that the whole space of metaparameters is at least 0-feasible: $\mathcal{F}_0^{G,A} = \mathcal{M} \forall G$ and that the size of $\mathcal{F}_x^{G,A}$ should be smaller than the one of $\mathcal{F}_y^{G,A}$ if $x > y$, $\forall (G, A)$. We can similarly define for a set $S = \{(G_1, A_1), (G_2, A_2), \dots, (G_N, A_N)\}$ of N couples of matrices their *common feasibility* region \mathcal{F}_x^S , which is the region of the metaparameters space where feasibility is at least x for every couple in the set:

$$\mathcal{F}_x^S \equiv \bigcap_{(G,A) \in S} \mathcal{F}_x^{G,A}. \quad (1.10)$$

We also define for a matrix set S its critical feasibility $f^*(S)$, which is the largest feasibility we can get while still having a non-empty common feasibility region:

$$f^*(S) \equiv \max_{x \in [0,1]} \{x : \mathcal{F}_x^S \neq \emptyset\}. \quad (1.11)$$

1.4 Dynamical stability

Once we establish which systems are feasible, we may be interested in their reaction to perturbations, *i.e.* their stability. That question has always been of prime importance for ecologists and constitutes a whole scientific field. Many results have been derived, for linear systems [23], Lotka-Volterra systems [27, 28], mutualistic systems [29] or MacArthur's consumer-resource model [30]. As stated above, our ultimate goal is to study equilibria points of the set of coupled differential equations (1.1). In particular we want to know how *stable* a given equilibrium is. However there is no consensual definition of stability: what does it mean exactly that a system is stable under a given perturbation? How is a perturbation even defined? Throughout this Thesis different notions of stability will be tackled: the first is *dynamical stability*. The main idea behind dynamical stability is simple. We want to answer the following question:

Given a feasible equilibrium point $\{R_\mu^, S_i^*\}$, does the system go back to the same positive-valued equilibrium when the consumers and resources abundances are changed? If yes, how much can they be changed?*

1.4.1 Local dynamical stability

We first introduce *local dynamical stability*⁶. A system is said to be *locally dynamically stable* if it goes back to its *initial equilibrium point* $\{R_\mu^*, S_i^*\}$ after R_μ^* and S_i^* have been perturbed by an infinitesimal amount $\{\Delta R_\mu(t_0), \Delta S_i(t_0)\}$ at time t_0 .

More precisely, consider a system which is at equilibrium at time before $t = t_0$. Right after $t = t_0$, we perturb the equilibria abundances $\{R_\mu^*, S_i^*\}$ by an infinitesimal amount $\{\Delta R_\mu(t_0), \Delta S_i(t_0)\}$. We want to know how the perturbations away from equilibrium, written $\{\Delta R_\mu(t), \Delta S_i(t)\}$, and defined as

$$\Delta R_\mu(t) \equiv R_\mu(t) - R_\mu^* \text{ and } \Delta S_i(t) = S_i(t) - S_i^*. \quad (1.12)$$

will evolve qualitatively. Namely, will they go to zero or increase indefinitely as t increases? Perturbation analysis tells us [31] that the quantity which drives the evolution of $\{\Delta R_\mu(t), \Delta S_i(t)\}$ is the *Jacobian matrix of the system at equilibrium* J^* , given by :

$$J^* \equiv J(t_0), \quad (1.13)$$

where $J(t)$ is the *Jacobian* of the system *i.e.* the Jacobian matrix of its temporal evolution (1.1) evaluated at time t . $J(t)$ has a block matrix structure which is given by:

$$J(t) \equiv \begin{pmatrix} \frac{\partial \dot{R}_\mu}{\partial R_\nu} & \frac{\partial \dot{R}_\mu}{\partial S_j} \\ \frac{\partial \dot{S}_i}{\partial R_\nu} & \frac{\partial \dot{S}_i}{\partial S_j} \end{pmatrix} = \begin{pmatrix} \left(-m_\mu - \sum_j \gamma_{j\mu} S_j(t) \right) \delta_{\mu\nu} & -\gamma_{j\mu} R_\mu(t) + \alpha_{\mu j} \\ \sigma_{i\nu} \gamma_{i\nu} S_i(t) & (\sum_\nu \sigma_{i\nu} \gamma_{i\nu} R_\nu(t) - d_i - \sum_\nu \alpha_{\nu i}) \delta_{ij} \end{pmatrix}, \quad (1.14)$$

⁶For the sake of brevity, instead of “local dynamical stability”, we sometimes abbreviate and write “lds”.

where δ is the ubiquitously occurring Kronecker delta symbol defined as:

$$\delta_{ij} = \begin{cases} 1 & \text{if } i = j, \\ 0 & \text{else.} \end{cases} \quad (1.15)$$

J^* is then precisely J with $\{R_\mu, S_i\}$ taken at the considered equilibrium point $\{R_\mu^*, S_i^*\}$, which simplifies its structure. Since we are interested only in positive valued equilibria (*i.e.* $S_i^* > 0 \forall i$), Eq.(1.2b) is equivalent to:

$$\sum_\nu \sigma_{i\nu} \gamma_{i\nu} R_\nu^* - d_i - \sum_\nu \alpha_{\nu i} = 0, \quad (1.16)$$

which means that the lower right block of the Jacobian in Eq.(1.14) will be zero. Hence at equilibrium the Jacobian J^* will have the following block form:

$$J^* = \begin{pmatrix} -D & \Gamma \\ B & 0 \end{pmatrix}, \quad (1.17)$$

where

- $D_{\mu\nu} = \text{diag}(m_\mu + \sum_j \gamma_{j\mu} S_j^*) = \text{diag}\left(\frac{l_\mu + \sum_j \alpha_{\mu j} S_j^*}{R_\mu^*}\right)$ is a positive $N_R \times N_R$ diagonal matrix,
- $\Gamma_{\mu j} = -\gamma_{j\mu} R_\mu^* + \alpha_{\mu j}$ is a $N_R \times N_S$ matrix which does not have entries with a definite sign.
- $B_{i\nu} = \sigma_{i\nu} \gamma_{i\nu} S_i^*$ is a $N_S \times N_R$ matrix with positive entries.

For reasons explained below, we say that a given equilibrium is *locally dynamically stable* if the largest real part of the eigenvalues of J^* is negative.

1.4.2 How to determine local dynamical stability

We stated above that the sign of the largest real part of all the eigenvalues of J^* determines the local dynamical stability. More precisely, we are interested in the real part of λ_1 , which is defined by the following property:

$$\forall \lambda \in \sigma(J^*), \operatorname{Re}(\lambda) \leq \operatorname{Re}(\lambda_1), \quad (1.18)$$

where $\sigma(J^*)$ is the set of eigenvalues of J^* , called the *spectrum* of J^* . Perturbation analysis tells us that the sign of the real part of λ_1 governs the local stability of the system at equilibrium [31]. There are three cases:

- $\operatorname{Re}(\lambda_1) < 0$: any perturbation on the abundances is exponentially suppressed. The system is stable.
- $\operatorname{Re}(\lambda_1) > 0$: any perturbation on the abundances is exponentially amplified. The system is unstable.
- $\operatorname{Re}(\lambda_1) = 0$: a second order perturbation analysis is required to assess the system's local dynamical stability. We call such systems *marginally stable* [32].

1.4.3 The locally dynamically stable region $\mathcal{D}_{L,x}^{G,A}$

Similarly to what was conducted in Section 1.3.2, one can define the *parameters set local dynamical stability function* $\mathfrak{D}_L : \mathcal{P} \rightarrow \{0, 1\}$, which tells us whether a given set of parameters $p \in \mathcal{P}$ is locally dynamically stable or not:

$$\mathfrak{D}_L(p) \equiv \begin{cases} 1 & \text{if } p \text{ is locally dynamically stable,} \\ 0 & \text{else.} \end{cases} \quad (1.19)$$

We require that p is feasible in order to be locally dynamically stable:

$$\mathfrak{D}_L(p) = 1 \implies \mathfrak{F}(p) = 1. \quad (1.20)$$

We also define the *metaparameters set local dynamical stability function* $\mathcal{D}_L : \mathcal{M} \times \mathcal{B}_{N_S \times N_R} \times \mathcal{B}_{N_R \times N_S} \rightarrow [0, 1]$ which tells us, given a set of metaparameters $m \in \mathcal{M}$ and a consumption-syntrophy network $B = (G, A)$ the chance that the procedure $\mathcal{A}(m, B)$ gives a locally dynamically stable set of parameters:

$$\mathcal{D}_L(m, B) \equiv \text{Probability}\{\mathfrak{D}_L(\mathcal{A}(m, B)) = 1\}. \quad (1.21)$$

We also define the x locally dynamically stable region $\mathcal{D}_{L,x}^{G,A}$ by the region of the metaparameters space that gives rise to a percentage of at least x dynamically stable systems:

$$\mathcal{D}_{L,x}^{G,A} \equiv \{m \in \mathcal{M} : \mathcal{D}_L(m, (G, A)) \geq x\}. \quad (1.22)$$

For the same reasons as for the case of feasibility, $\mathcal{D}_{L,0}^{G,A} = \mathcal{M}$, and $\mathcal{D}_{L,x}^{G,A}$ should have a smaller size than $\mathcal{D}_{L,y}^{G,A} \forall x \geq y$. More importantly, Eq.(1.20) implies:

$$\mathcal{D}_{L,x}^{G,A} \subset \mathcal{F}_x^{G,A}. \quad (1.23)$$

We can also define for a set of N couples of matrices $S = \{(G_1, A_1), \dots, (G_N, A_N)\}$ their common x lds-region $\mathcal{D}_{L,x}^S$:

$$\mathcal{D}_{L,x}^S \equiv \bigcap_{(G,A) \in S} \mathcal{D}_{L,x}^{G,A}. \quad (1.24)$$

For such a set S we define also its critical local dynamical stability $d_L^*(S)$ which is the largest local dynamical stability we can achieve while still having a non-empty common lds-region:

$$d_L^*(S) = \max_{x \in [0,1]} \{x : \mathcal{D}_{L,x}^S \neq \emptyset\}. \quad (1.25)$$

1.4.4 Evaluating the size of the basin of attraction

If we establish that a system is locally dynamically stable, we know that it will come back to the same equilibrium after a sufficiently small perturbation of the resources and consumers abundances. The next natural question is:

How much can these equilibria points be perturbed before the system goes to a point where either at least a species has gone extinct or it reaches another positive valued equilibrium $\{\tilde{R}_\mu^, \tilde{S}_i^*\}$ or it simply does not reach a new dynamical equilibrium?*

One way of studying this [29] is to simply take an equilibrium point $\{R_\mu^*, S_i^*\}$ and perturb the abundance of the species and resources at that point by a fixed number Δ_D which allows us to quantify the perturbation:

$$\left\{ \begin{array}{l} R_\mu^* \rightarrow R_\mu(t_0) \equiv R_\mu^* (1 + \Delta_D \nu_\mu), \\ S_i^* \rightarrow S_\mu(t_0) \equiv S_i^* (1 + \Delta_D \nu_i), \end{array} \right. \quad (1.26)$$

$$\left\{ \begin{array}{l} R_\mu^* \rightarrow R_\mu(t_0) \equiv R_\mu^* (1 + \Delta_D \nu_\mu), \\ S_i^* \rightarrow S_\mu(t_0) \equiv S_i^* (1 + \Delta_D \nu_i), \end{array} \right. \quad (1.27)$$

where the $\nu_{\mu,i}$ are random numbers drawn from a uniform distribution between -1 and +1 and t_0 is the time where the previously at equilibrium system is perturbed. The system with the initial values $\{R(t_0), S(t_0)\}$ can then be time evolved from $t = t_0$ until it reaches an equilibrium $\{\tilde{R}^*, \tilde{S}^*\}$ which may be different from the equilibrium $\{R^*, S^*\}$ initially considered. This procedure is essentially a generalized version of local dynamical stability, since we allow the perturbation Δ_D to be non-infinitesimal.

1.4.5 Global dynamical stability

Systems which can be arbitrarily perturbed, *i.e.* for which Δ_D may be arbitrarily large⁷, are said to be *globally stable*. The only way we can prove a system is globally stable is by finding a Lyapunov function (see *e.g.* [33]) for it. In many cases, this cannot be done and one has to explore the basin of attraction numerically with the procedure described above. However, since we cannot numerically try *all* possible perturbations, global stability can never be proved that way.

⁷Of course with the caveat that the perturbed abundances are positive.

1.5 Structural stability

When studying dynamical stability, we investigate what happens when the equilibria abundances $\{R_\mu^*, S_i^*\}$ of a given equilibrium point are perturbed. The question of *structural stability* looks also at the behaviour of a given system when perturbed away from equilibrium. However, structural stability focuses on the perturbations of the parameters of the model i.e. $\{l_\mu, m_\mu, \gamma_{i\mu}, \alpha_{\mu i}, \sigma_{i\mu}, d_i\}$. Namely we will try to answer the following question :

Given a feasible and dynamically stable parameters set, does the microbial community go back to a feasible and dynamically stable parameters set when some of the model parameters are changed? If yes, how much can they be changed before the system evolves in such a way that it does not reach a feasible and dynamically stable point of the parameters space?

Studying how a system responds to the perturbation of the parameters $\{l_\mu, m_\mu, \gamma_{i\mu}, \alpha_{\mu i}, \sigma_{i\mu}, d_i\}$ is a quite difficult and not necessarily appropriate problem. Indeed, in general in this Thesis we do not consider timescales where mutations could happen which means that there is no manifest reason $\gamma_{i\mu}, \alpha_{\mu i}, \sigma_{i\mu}$ or d_i could change. On the contrary, we are interested in environmental perturbations, which occur on far shorter timescales and correspond to a change of l_μ or m_μ . Because m_μ is harder to control experimentally, we will focus on perturbations of the external feeding rate l_μ . More precisely, consider $\Delta_S \in [0, 1]$. We say that a given system $p \in \mathcal{P}$ is *structurally stable* under the perturbation Δ_S , if under the transformation

$$l_\mu \rightarrow \hat{l}_\mu \equiv l_\mu (1 + \Delta_S \nu_\mu) \quad (1.28)$$

the transformed set of parameters $\{\hat{l}_\mu, m_\mu, \gamma_{i\mu}, \alpha_{\mu i}, \sigma_{i\mu}, d_i\}$ gives rise under time evolution to a positive valued-equilibrium $\{\hat{R}_\mu^*, \hat{S}_i^*\}$. In the equation above, ν_μ is a random variable drawn from a uniform distribution of support $[-1, 1]$. In words, we start with an initial parameters set at an equilibrium point, which is constant under time evolution, and see how much we can change the resources external feeding rate until some consumers start to die out as the new system is time-evolved.

Similarly to what was done for feasibility and dynamical stability, we can define the *parameters set structural stability function* $\mathfrak{S} : [0, 1] \times \mathcal{P} \rightarrow \{0, 1\}$ in the following way for $\Delta_S \in [0, 1], p \in \mathcal{P}$:

$$\mathfrak{S}(\Delta_S, p) = \begin{cases} 1 & \text{if } p \text{ is structurally stable under the perturbation } \Delta_S, \\ 0 & \text{otherwise.} \end{cases} \quad (1.29)$$

For a fixed p , we expect $\mathfrak{S}(\Delta_S, p)$ to behave as a step function of Δ_S : we may only perturb the parameters so much before they suddenly become structurally unstable.

The corresponding metaparameters set function, the *metaparameters set structural stability function* \mathcal{S} can also be defined as the function which, given a set of metaparameters and a consumption-syntrophy couple of binary matrices, tells you how probable it is that you draw a system structurally stable under a perturbation Δ_S . Mathematically, $\mathcal{S} : [0, 1] \times \mathcal{M} \times \mathcal{B}_{N_S \times N_R} \times \mathcal{B}_{N_R \times N_S} \rightarrow [0, 1]$ is defined $\forall \Delta_S \in [0, 1], m \in \mathcal{M}, B = (G, A) \in \mathcal{B}_{N_S \times N_R} \times \mathcal{B}_{N_R \times N_S}$:

$$\mathcal{S}(\Delta_S, m, B) = \text{Probability} \{ \mathfrak{S}(\Delta_S, \mathcal{A}(m, B)) = 1 \}. \quad (1.30)$$

Because we expect a step-like drop of \mathfrak{S} as Δ_S increases, we expect also a somewhat sharp drop from $\mathcal{S} \approx 1$ to $\mathcal{S} \approx 0$ (see Section 2.4.1). To quantify this, one can define the *critical structural perturbation* $\Delta_S^*(m, G, A)$ of a consumption-syntrophy network implicitly as :

$$\mathcal{S}(\Delta_S^*(m, G, A), m, G, A) = 0.5 \quad (1.31)$$

Section 2.4.1 below explains how $\Delta_S^*(m, G, A)$ can be estimated numerically.

1.6 Tactics used to simplify the problem

Before jumping right into the matter, it is important to explain how we will study our model. Mainly two different but complementary approaches will be used: analytical and numerical. Note that the lines of code we wrote from scratch and that we use to get the results of Section 3 are available at the address <https://gitlab.ethz.ch/palberto/consumersresources.git>.

1.6.1 Metaparameters

Studying the equilibria of our CRM will lead us to establish and study several relations involving the different *parameters* of the problem. Namely, these are: $l_\mu, m_\mu, \gamma_{i\mu}, \alpha_{\mu i}, \sigma_{i\mu}, d_i, R_\mu^*$ and $S_i^* \forall i = 1, \dots, N_S; \mu = 1, \dots, N_R$. We define the *parameters space* \mathcal{P} as the space that contains all the parameters:

$$\mathcal{P} \equiv \{p : p = (l_\mu, m_\mu, d_i, \gamma_{i\mu}, \alpha_{\mu i}, \sigma_{i\mu}, R_\mu^*, S_i^*)\}. \quad (1.32)$$

Without taking into account the constraints on these parameters, there are $3N_R + 2N_S + 3N_R N_S$ free parameters, so $\mathcal{P} \simeq \mathbb{R}_+^{3N_R + 2N_S + 3N_R N_S}$. Our goal is to study microbial communities with a large number of consumers and resources, typically $N_R, N_S \approx 25, 50, 100, \dots$ i.e. $\mathcal{P} \simeq \mathbb{R}^{>2000}$. It is clear that an exhaustive exploration is unfeasible. Another, simpler, approach is needed. Following previous work [29], we simplify the problem by considering that each variable $q_{i\mu}$ may be written in the following way:

$$q_{i\mu} = \mathfrak{Q} Q_{i\mu} \quad (1.33)$$

where \mathfrak{Q} is a random variable of mean Q_0 and standard deviation σ_Q . $Q_{i\mu}$ is a binary matrix that, if interpreted as an adjacency matrix, tells about the network structure of the quantity $q_{i\mu}$. In order to make computations analytically tractable, we require the standard deviation on the parameters involved in the problem to be small compared to the mean, i.e. not larger than typically 10%. In that regime, every random variable \mathfrak{Q} is well approximated by its average value Q_0 . We call Q_0 a *metaparameter*. While studying things analytically we will hence often come back to the following approximation⁸:

$$\left\{ \begin{array}{ll} l_\mu \approx l_0 & (1.34a) \\ m_\mu \approx m_0 & (1.34b) \\ \gamma_{i\mu} \approx \gamma_0 G_{i\mu} & (1.34c) \\ \alpha_{\mu i} \approx \alpha_0 A_{\mu i} & (1.34d) \\ \sigma_{i\mu} \approx \sigma_0 & (1.34e) \\ d_i \approx d_0 & (1.34f) \\ R_\mu^* \approx R_0 & (1.34g) \\ S_i^* \approx S_0 & (1.34h) \end{array} \right.$$

⁸Note that we do not add any explicit topological structure on $l_\mu, m_\mu, d_i, R_\mu^*, S_i^*$ and $\sigma_{i\mu}$ because we require these to always be larger than zero. In particular, we require positive-valued equilibria [34].

This simplification is mathematically equivalent to collapsing the parameter space \mathcal{P} to a lower dimensional space. Formally that lower dimensional space is the Cartesian product of \mathcal{M} and $\mathcal{B}_{N_S \times N_R} \times \mathcal{B}_{N_R \times N_S}$, where \mathcal{M} is the *metaparameters space*:

$$\mathcal{M} \equiv \{m : m = (l_0, m_0, d_0, \gamma_0, \alpha_0, \sigma_0, R_0, S_0)\} \quad (1.35)$$

and $\mathcal{B}_{N \times M}$ is the set of binary matrices of dimensions $N \times M$. To summarize, we simply designed a *collapsing procedure* $\mathcal{C} : \mathcal{P} \rightarrow \mathcal{M} \times \mathcal{B}_{N_S \times N_R} \times \mathcal{B}_{N_R \times N_S}$ in order to simplify our problem and find analytical solutions.

Of course, collapsing a very high dimensional space to a low-dimensional space makes us lose information. Losing some information – and hence complexity – is desired when doing analytical computations but it is not when we want to produce precise and detailed numerical results: we need to bridge the gap between what we work with analytically, *i.e.* a set of metaparameters and binary matrices, to precise values of quantities defined in our model Eq.(1.1) that we will measure computationally. This is done by defining an algorithmic procedure \mathcal{A} (detailed in Section 2.2.1):

$$\mathcal{A} : \mathcal{M} \times \mathcal{B}_{N_S \times N_R} \times \mathcal{B}_{N_R \times N_S} \rightarrow \mathcal{P} \quad (1.36)$$

which brings us from the collapsed space to the parameter space⁹. Numerically, from a set of metaparameters $m \in \mathcal{M}$ and binary matrices $B = (G, A) \in \mathcal{B}_{N_S \times N_R} \times \mathcal{B}_{N_R \times N_S}$, we produce a (or several) set(s) of parameters $p = \mathcal{A}(m, B) \in \mathcal{P}$ and study properties of it.

1.6.2 Matrix properties

Mathematically, when we do analytical computations, we mostly work in the collapsed space $\mathcal{C}(\mathcal{P})$ because it reduces the number of parameters from $3N_R + 2N_S + 3N_R N_S$ (continuous) to 8 (continuous) + $2N_R N_S$ (binary). For N_R and N_S large, the $2N_R N_S$ degrees of freedom that come from the consumption network G and the syntropy network A are still too many to track individually. To simplify the problem even further, instead of looking at each entry of the binary matrices G and A individually, we will consider only some globally defined quantities of these matrices. Although the conclusions that recent studies of ecological systems draw is sometimes controversial, they have shown that both connectance [12, 13] and nestedness [10, 11, 29] of the matrices of the system play a special role in the dynamics of the system. These two metrics are defined the following way for a matrix M_{ij} :

- **Connectance:** this measure, simply defined as the ratio of non-zero links in a matrix is formally defined for a matrix q_{ij} of size $N \times M$ as:

$$\kappa(q) \equiv \frac{\sum_{ij} Q_{ij}}{NM}, \quad (1.37)$$

where Q is the (binary) network adjacency matrix of q .

⁹Note that since the collapsed space is lower dimensional than the parameters space, \mathcal{A} is not the inverse of \mathcal{C} .

- **Nestedness:** or, for the consumption matrix G only, **ecological overlap**. That quantity measures how “nested” the system is, *i.e.* if there are clusters grouped together¹⁰. It is known [10, 29] that nestedness can play a profound role in the dynamics of ecological communities. Although it is somewhat controversial [36], we will keep the definition of the nestedness $\eta(M)$ of a binary matrix M as it was used in [10]:

$$\eta(M) \equiv \frac{\sum_{i < j} n_{ij}}{\sum_{i < j} \min(n_i, n_j)} \quad (1.38)$$

where the number of links n_i is simply the degree of the i -th row of M

$$n_i \equiv \sum_k M_{ik}, \quad (1.39)$$

and n_{ij} is the overlap matrix defined as

$$n_{ij} \equiv \sum_k M_{ik} M_{jk}. \quad (1.40)$$

Most of the quantities we measure will be studied through these two metrics.

¹⁰In typical Lotka-Volterra models, where only species-species interactions are considered, *e.g.* [35], measuring the nestedness of the γ consumption matrix would be in the same spirit as counting how many niches there are in the community.

1.7 Goals of the Thesis

The previous paragraphs defined many different notions which are so rich that each of them constitutes a whole body of work by itself. This means we need to focus on the specific problems we will address throughout this Thesis.

As explained in Section 1.2.2 we will focus first on feasibility. The goal will be to find a mathematical expression for the feasibility region of each consumption-syntropy network we will consider, which will allow us to explore numerically how syntropy impacts the feasibility of each microbial community, in a certain range of metaparameters (that will be determined in Section 2.1) and with metrics that will hopefully accurately describe what we will observe. We will then move on to local dynamical stability. Similarly to feasibility, our goal will be to mathematically characterize the dynamical stability region and find a regime of parameters that is locally dynamically stable. We aim to study how the largest eigenvalue of the Jacobian depends on both the metaparameters and the shape of the consumption and syntropy matrices. For the sake of brevity and by lack of time, any consideration on the basin of attraction of dynamical stability will be dropped. Finally, because of the knowledge we will have acquired on the dynamical stability of the model, we will be able to move to highly dynamically stable points of the metaparameters space and study how syntropy changes their structural stability. Although most of the time we will work with microbial communities which have the same number of resources and consumers, we will measure some indicators that will allow us to gain hindsight on how the quantities we will study depend on the number of resources and consumers.

2 Methods

2.1 Domain of study

2.1.1 Choice of metaparameters and numerical constants

Feasibility considerations discussed in Section 1.3.1 tell us that we have six metaparameters¹¹ which we can play with: γ_0 , α_0 , l_0 , σ_0 , S_0 and R_0 . Out of simplicity, we will fix three of these six and only γ_0 , S_0 and α_0 will be varied throughout this study. We hence need to fix the value of R_0 , l_0 and σ_0 in a relevant way.

Following the analysis of [26], we notice that our model Eqs.(1.1) still possesses some freedom. Indeed we can choose the set of units we work in to fix the values of some metaparameters. There are two physical quantities at stake here: biomass and time, and we may choose, however we want it, a specific set of units describing both of them. We measure biomass in units of the average resource abundance at equilibrium¹²:

$$\langle R_\mu \rangle = R_0 = 1. \quad (2.1)$$

Similarly, we measure time such that the average external resource uptake rate is one, that is:

$$\langle l_\mu \rangle = l_0 = 1. \quad (2.2)$$

After this manipulation, only the value of σ_0 needs to be fixed. It is difficult to determine which value should be chosen because the efficiency of biomass production varies a lot according to the system in question [37]. However we found analytically that because of physical considerations (Eq.3.3) feasibility depends not exactly on σ_0 but rather on $\min(1 - \sigma_0, \sigma_0)$. This hints at the existence of two regimes, namely $\sigma_0 > 0.5$ and $\sigma_0 < 0.5$. Since in Nature efficiency is usually small [37], it is more realistic to be in the $[0, 0.5]$ regime. We will take the middle of that interval and choose $\sigma_0 = 0.25$.

Note also that when we generate parameters sets from metaparameters through the algorithmic procedure \mathcal{A} (Section 2.2.1), we will take a small relative standard deviation, $\epsilon \approx 4\%$, such that indeed the metaparameters approximation is justified.

As said above, α_0 , γ_0 and S_0 are the only metaparameters we vary throughout this study. Because of that, we sometimes elide the other metaparameters in the notation and will write instead of $m = (\gamma_0, S_0, \alpha_0, \sigma_0, R_0, l_0, d_0, m_0) \in \mathcal{M}$ simply $m = (\gamma_0, S_0, \alpha_0)$. It is explained in Section 3.1.3 which values of α_0 we study. Concerning γ_0 and S_0 , we consider most of the time points $(\gamma_0, S_0) \in [0.01, 1] \times [0.01, 1]$. We sometimes write the square $[0.01, 1] \times [0.01, 1]$ as $[0, 1]^2$ or “the unit square”, where it is understood that points where either γ_0 or S_0 is smaller than 0.01 are not taken into account. In practice we discretize both the γ_0 and the S_0 -axis in N_{points} , which gives us a total of N_{points}^2 different (γ_0, S_0) configurations to study. We use $N_{\text{points}} = 100$ when we study matrices from the set S_{25} (see below) and $N_{\text{points}} = 30$ for the matrices of S_{50} . It was also mentioned that the metaparameters set feasibility and local dynamical stability functions can be estimated

¹¹Indeed, we saw that d_i and m_μ are set by the other parameters, so we cannot freely choose d_0 and m_0 (see Section 1.3.1).

¹²That choice is not completely innocent. Indeed we see in other parts of the manuscript that the matrix $\alpha_{\nu i} - \gamma_{i\nu} R_\nu^*$ is a quantity crucial to the dynamics of the system. Setting $\langle R^* \rangle = 1$ allows us to simply study the impact of γ against α instead of the more complicated γR^* versus α .

numerically using Eq.(1.8), we typically take the number of parameters sets generated $N = 200$. Finally, when we have to perform fitting procedures it is through standard routine functions from the `scipy` Python library. The error on the fitting parameter in question is taken as the square root of the diagonal element of the covariance matrix corresponding to that parameter.

2.1.2 Set of matrices

Throughout this Thesis we consider two sets of consumption matrices. The first one, called G_{25} , is made of sixty full-rank consumption matrices with the dimensions $N_R = N_S = 25$. Except for one matrix with $\eta_G = 0.15$ and $\kappa_G = 0.18$, they are distributed homogeneously among the $\eta_G > \kappa_G$ surface for $\eta_G \in [0.1, 0.6]$ and $\kappa_G \in [0.08, 0.43]$. The second set, called G_{50} , has dimensions $N_R = 50$ and $N_S = 25$ and comprises of forty-one full-rank consumption matrices, also homogeneously distributed among the surface $\eta_G > \kappa_G$ for the same ranges of η_G and κ_G . All the matrices of this set are generated through the general MCMC algorithm¹³ explained in Section 2.3.4. The procedure to produce a matrix G with connectance κ_{target} and nestedness η_{target} is simple. Indeed, by design, the algorithm allows us to choose the connectance of the output matrix and we can reach the desired nestedness by setting the energy as $E(G) = |\eta(G) - \eta_{\text{target}}|$.

It is explained below that for each G -matrix we consider a small number of different A syntropy matrices. We denote a pair of consumption-syntropy network (G, A) sometimes as B , and for each scenario, the set of consumption-syntropy networks (G, A) is denoted¹⁴ as S_{25} when $G \in G_{25}$ and as S_{50} when $G \in G_{50}$. In any case, all the matrices used in this study are available online at the address <https://gitlab.ethz.ch/palberto/consumersresources.git>.

2.1.3 Syntropy scenarios

The general aim of this Thesis is to study how quantities that characterize feasibility and stability change with respect not only to the consumption matrix γ , but also to the syntropy matrix α . As explained above (Section 1.6.1) the large complexity of this task makes us move to a statistical approach, where general matrices are separated in two parts, namely average non-zero link strength (what we call “metaparameter”) and network structure. That led to the definition of the binary syntropy network matrix A . We here will need to simplify our approach even more.

Indeed our goal is to study stability properties of many consumption-syntropy networks (G, A) . We decide to focus on two sets of G -matrices varying two characteristics of G , namely connectance κ_G and nestedness (which, for the case of G , we call ecological overlap) η_G . By symmetry we should also choose a set of A 's with different connectances and nestedness and study every possible pair (G, A) together, making the total number of

¹³Technically that algorithm is designed to obtain an output matrix which is “optimal” for a given input matrix in the sense that it minimizes an energy that depends on both the output and input. By making the energy depend on the output only, we can generate our G -matrices with the same code.

¹⁴To avoid bloating the notation there is no mention of the A -scenario in the matrix set S and it is made clear in the text what scenario of A is chosen when we speak of $(G, A) \in S$.

microbial communities to study equal to the multiplication of the number of consumption networks by the number of syntropy networks. Working that way, although more scientifically thorough, would demand more time than what is allowed for this type of Thesis and is hence not possible. Because we still would like to study the effect of the shape of A , we decide, for each consumption matrix G , to consider four A “scenarios”¹⁵:

- “Fully Connected” (FC): A is filled with ones only, $A_{\mu i} = 1$. This corresponds to a so-called “mean-field” approximation. Every consumer releases every resource at the same intensity (up to some noise) .
- “No Intraspecific Syntropy” (NIS): the structure of A is such that consumers are not allowed to release what they consume, *i.e.* there is no intraspecific syntropy. Apart from that, they release everything else. G -matrices with a small connectance will have an A -matrix with a large connectance (not far away from the FC case) and vice-versa.
- “Low intra-Resource Interaction” (LRI): A is the outcome of the MCMC algorithm described in Section 3.2.2. The purpose of this algorithm is to build an A that minimizes the energy $E(G, A)$ (Eq.3.40), and hence get the A which for a given G , brings the system as close to satisfaction of Eq.(3.24) as possible. The connectance of the A -matrix is taken as the one of the G -matrix.
- “Random Structure” (RS) : A is taken as a random matrix (with the right dimensions), which has the same connectance as the corresponding G but where non-empty links have been randomly placed.

Only these four cases are considered for the feasibility and dynamical stability sections. We consider more scenarios for the study of structural stability. These are described in Section 3.3.2.

¹⁵We talk here about scenarios because, apart from the FC case, A will generally be different for each G . It is important to remember that even though we compare A -matrices “in the same scenario”, those may have a very different shape.

2.2 Feasibility

2.2.1 Building feasible systems

We hereby detail the \mathcal{A} procedure which from a set of metaparameters m and a consumption-syntrophy network (G, A) gives rise to a set of parameters p . It goes like this:

1. We first randomly draw each R_ν^* and S_i^* :

$$R_\nu^* = \mathcal{R} \quad \forall \nu = 1, \dots, N_R \text{ and } S_i^* = \mathcal{S} \quad \forall i = 1, \dots, N_S, \quad (2.3)$$

where \mathcal{R} and \mathcal{S} are random variables coming from a distribution of mean equal to the corresponding metaparameter and relative standard deviation¹⁶ ϵ . In our simulations, we choose uniform distributions :

$$\mathcal{R} \sim \text{Unif}(R_0, R_0\epsilon) \text{ and } \mathcal{S} \sim \text{Unif}(S_0, S_0\epsilon). \quad (2.4)$$

2. The efficiency matrix $\sigma_{i\nu}$ is then drawn similarly, from a distribution with average σ_0 . In order to simplify the problem¹⁷, we take a zero-variance like Butler and O'Dwyer in [34], *i.e.* all species consume resources at the same global efficiency:

$$\sigma_{i\nu} = \sigma_0. \quad (2.5)$$

3. We build the consumption matrix $\gamma_{i\nu}$. Its adjacency matrix G is loaded through a user-provided file. While G gives the structure of γ , *i.e.* if a given $\gamma_{i\nu}$ is zero or not, the actual values of $\gamma_{i\nu}$ need then to be determined. They are drawn from a uniform distribution of mean γ_0 and relative standard deviation ϵ :

$$\gamma_{i\nu} = \text{Unif}(\gamma_0, \gamma_0\epsilon) G_{i\nu}. \quad (2.6)$$

4. We draw the resources external feeding rates, similarly to the other parameters:

$$l_\mu = \text{Unif}(l_0, l_0\epsilon) \quad \forall \mu = 1, \dots, N_R. \quad (2.7)$$

5. The last free parameters are the non-zero elements of the syntropy matrix $\alpha_{\nu i}$, since the d_i and l_μ are determined through the equations of evolution at equilibrium. The adjacency matrix A of α needs then to be specified. The user can either choose one of the scenarios above (Section 2.1.3) or provide directly a matrix with the right dimensions. After the adjacency matrix is loaded, we build α from a uniform distribution of mean α_0 and relative standard deviation ϵ :

$$\alpha_{\nu i} = \text{Unif}(\alpha_0, \alpha_0\epsilon) A_{\nu i}. \quad (2.8)$$

¹⁶By relative standard deviation, we mean the standard deviation measured in units of the average value.

¹⁷Indeed we observed that in general introducing a non uniform $\sigma_{i\nu}$ adds an unnecessary additional layer of complexity, which we would like to avoid.

6. With all of these parameters drawn, we can solve Eqs.(1.4a) for the species death rate d_i and Eqs.(1.4b) for m_ν . All the parameters of the model are now fully determined.
7. We check if the constraints Eqs.(1.4) and (1.5) on the parameters are fulfilled. If they are not, we go back to step 1. Otherwise, a feasible system has been built and the algorithm is successfully exited. We see here the advantage of having input metaparameters that will most likely give rise to a feasible parameter set. If we just give random metaparameters, we run the risk of getting stuck in an unpredictably long loop between steps 1 and 7. If however we are in a region where we know the metaparameters feasibility is high, a feasible system is found much faster.

2.3 Dynamical stability

2.3.1 Master equation for local dynamical stability

In order to get $\text{Re}(\lambda_1)$, which is the quantity that governs local dynamical stability (see Section 1.4.2), we have to get the full spectrum of J^* , denoted $\sigma(J^*)$, since a straightforward application of easier standard techniques like the Perron-Frobenius theorem [38] does not work. The eigenvalues of J^* are obtained through the eigenvalue problem:

$$\det(J^* - \lambda) = 0. \quad (2.9)$$

More explicitly, using Eq.(1.17), we state the *master equation for local dynamical stability*:

$$\det \begin{pmatrix} -D - \lambda & \Gamma \\ B & 0 - \lambda \end{pmatrix} = 0 \quad (2.10)$$

That equation is not trivially solved, which is why we seek regimes where it could be made simpler.

2.3.2 Bounds on the eigenvalues: Gershgorin circle theorem

Gershgorin circle theorem [39] states that every eigenvalue of a $N \times N$ square matrix A is located in one of the N discs \tilde{D}_i defined by:

$$\tilde{D}_i \equiv \left\{ z \in \mathbb{C} : |z - A_{ii}| \leq \sum_{j \neq i} |A_{ij}| \right\}. \quad (2.11)$$

In a more mathematical language:

$$\sigma(A) \subset \bigcup_{i=1}^N \tilde{D}_i, \quad (2.12)$$

where $\sigma(A)$ is the spectrum of A . Intuitively, the circle theorem tells us that the eigenvalues of a matrix deviate from the diagonal elements by a value bounded by the sum of the off-diagonal elements. It is easy to see that if all the discs \tilde{D}_i are located to the left of the imaginary axis (*i.e.* the discs contain only numbers with a negative real part), then the eigenvalues of A are all negative.

2.3.3 Reductio ad absurdum

The strategy we use to solve Eq.(3.17) is inspired by [34]. The strategy is to assume we are in an unstable regime, *i.e.* there exists at least one $\lambda \in \sigma(J^*)$ with $\text{Re}(\lambda) \geq 0$ that satisfies Eq.(3.15) and such that $\text{Re}(\lambda) > 0$. By Eq.(3.17), λ is also an eigenvalue of $S(\lambda)$. If we find conditions under which the real part of the spectrum of $S(\lambda)$ is entirely negative, we will know that $\text{Re}(\lambda) \leq 0$. As this is a contradiction to the hypothesis that the regime is unstable, we must conclude that the regime is stable¹⁸. Hence, the general idea is to find regimes where we know that the spectrum of S will be entirely negative for a positive λ .

¹⁸Indeed, Eq.(3.15) assumes already that either $\text{Re}(\lambda_1) > 0$ or $\text{Re}(\lambda_1) < 0$.

2.3.4 Monte Carlo algorithm for the optimal matrix

We explain how to write a Metropolis-Hastings Markov Chain Monte Carlo (MCMC) method which for an input matrix M_I gives as an output the optimal matrix M_O which minimizes the energy $E(M_I, M_O)$. The procedure follows a traditional Metropolis algorithm:

1. Create a random binary M_O . Its connectance is chosen as the one of the input matrix M_I .
2. Do the following for a given number of steps:
 - Choose a random row or, every other iteration, a column.
 - In that row/column, try to swap a zero and a one while preserving the non-zero degrees of the columns and rows of M_O (a column/row that initially had some non-zero elements cannot end up empty after that step).
 - The swap is accepted, *i.e.* M_O is modified, if the energy difference ΔE is negative or if a random number drawn uniformly between zero and one is smaller than $e^{-\Delta E/T}$ where T is the current temperature. More on ΔE and T below.
3. Return M_O .

A couple comments on this algorithm can be made:

- The algorithm preserves the connectance of M_O but not its nestedness. The question of what connectance to choose is open, but we choose $\kappa(M_O) = \kappa(M_I)$ as a first approach, *i.e.* input and output matrices have the same connectance.
- The temperature T changes dynamically during the simulation. It is obtained in a way close to the spirit of simulated annealing techniques [40]: the temperature T is multiplied by a factor $\lambda = 0.99$ at a fixed frequency (for instance every 1000 steps). We add the requirement that if new moves are rejected during too many consecutive steps, we multiply the temperature by $1/\lambda$.
- The energy difference ΔE between the new proposed M'_O and the old M_O is computed by assigning an energy E to both M'_O and M_O and subtracting them:

$$\Delta E \equiv E(M_I, M'_O) - E(M_I, M_O). \quad (2.13)$$

That algorithm is used not only to generate the G consumption matrices (Section 2.1.2), in that case E only depends on the output G so the input matrix does not matter, but also to find the optimal “LRI” matrix. In that situation, E depends both on the input consumption matrix G and the output syntropy matrix A and is given by Eq.(3.40).

2.4 Structural stability

2.4.1 Numerical estimate of the critical structural perturbation

As explained in Section 1.5, the critical structural perturbation of a set of metaparameters m and a consumption-syntrophy network (G, A) is the point where we shift from structural stability to instability. In that sense, $\Delta_S^*(m, G, A)$ is a measure of how good (m, G, A) respond to structural perturbation and can be interpreted geometrically as the radius of a sphere of “tolerance” around the metaparameters m . It turns out that Δ_S^* can be estimated numerically quite easily.

Indeed, to decide whether a system is structurally stable or not, one can simply perturb the parameters of the system, let it time-evolve until it reaches a new equilibrium and count how many of the original consumers are still present at the new equilibrium. By repeating this procedure many times one gets a good estimate of the *probability of observing an extinction* $P_E(\Delta_S, m, G, A)$ after a structural perturbation Δ_S and it is clear that

$$\mathcal{S}(\Delta_S, m, G, A) = 1 - P_E(\Delta_S, m, G, A). \quad (2.14)$$

So $\Delta_S^*(m, G, A)$ can be found by computing $P_E(\Delta_S, m, G, A)$ over the Δ_S -range $[0, 1]$ and finding at which point it is equal to 0.5:

$$P_E(\Delta_S^*(m, G, A), m, G, A) = 0.5. \quad (2.15)$$

Section 1.5 explains that we choose that specific value of 0.5 because we expect \mathcal{S} (and hence P_E) to have a typical sigmoidal shape which would go from 1 to 0 (or from 0 to 1 for P_E) in a very abrupt way as a function of Δ_S . Figure 2.4.1 shows that the expected behaviour is indeed observed: the transition between $P_E = 0$ and $P_E = 1$ is sharp compared to the size of the interval $[0, 1]$ where Δ_S^* lies and the rest of the curve saturates at either 0 or 1. We exploit that property to write an algorithm that solves Eq.(2.15). It works in the following way:

1. Through the help of a standard solver from the `GSL` library, find a “high” Δ_H for which $P_E(\Delta_H)$ is very close to 1 but smaller, typically $P_E(\Delta_H) \approx 0.99$. Then find a “low” $\Delta_L < \Delta_H$, very close to 0 but larger.
2. Compute $P_E(\Delta_S)$ for N_{points} points Δ_S homogeneously spread in the interval $[\Delta_L, \Delta_H]$.
3. Because the $P_E(\Delta_S)$ computed at the previous step typically form a sigmoidal shape, fit these points with a sigmoidal function $S_f(\Delta_S)$. We choose:

$$S_f(\Delta_S) \equiv \frac{1}{1 + e^{-C_1(\Delta_S - C_2)}}, \quad (2.16)$$

where the constants C_1, C_2 precisely are estimated through the fitting procedure.

4. $\Delta_S^*(m, G, A)$ is obtained by solving analytically $S_f(\Delta_S^*) = 0.5$. For the choice of Eq.(2.16), this is trivial : $\Delta_S^* = C_2$. Indeed $S_f(C_2) = 1/(1 + 1) = 0.5$. We take the error on C_2 obtained through the standard fitting routine from the `GSL` library as the “error” on Δ_S^* .

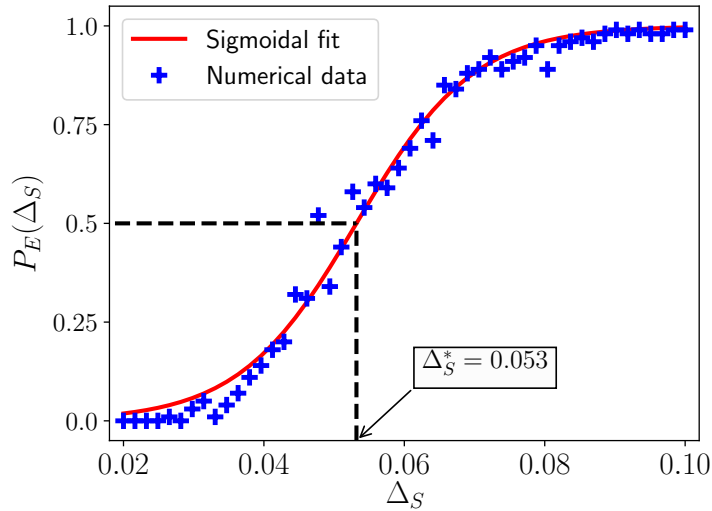


Figure 2.4.1: Typical probability of finding one extinction when structurally perturbing the system with a magnitude Δ_S . The critical structural perturbation is easily estimated with a sigmoidal fit.

Finally, it is worth mentioning that $P_E(\Delta_S, m, G, A)$, which again is the probability to observe *at least* one extinction when structurally perturbing a parameters set $\mathcal{A}(m, G, A)$ by Δ_S , is estimated numerically through the following procedure:

1. Create a parameters set $\mathcal{A}(m, G, A)$.
2. Structurally perturb it by an amount Δ_S .
3. Time evolve the parameters set until an equilibrium is reached. Compute $p_E \in \{0; 1\}$, which is 0 if no extinction has been observed, and 1 if at least one extinction occurred.
4. Repeat steps 1–3 N_{sys} times. $P_E(\Delta_S)$ is the average value of p_E .

For the figures of Section 3.3, we used $N_{\text{points}} = 125$ and $N_{\text{sys}} = 50$. We observed (although did not have the time to quantify it properly) that increasing N_{points} reduces the error on Δ_S^* faster than increasing N_{sys} .

3 Results

3.1 Feasibility

As explained in Section 1.3, before addressing the question of the stability of a system, be it dynamical or structural, it is important to study whether that system is *feasible*. In short we must answer the question: “does it make sense to talk about this system? What are the restrictions on the parameters of a microbial community in order for it to exist?”. In the following section we provide an analytical estimate of the fully feasible region $\mathcal{F}_1^{G,A}$ and study numerically the impact of syntropy on feasibility.

3.1.1 Estimating the fully feasible region $\mathcal{F}_1^{G,A}$

We would like to know what regions of the metaparameters space lead to fully feasible systems. As explained in Section 1.3.1, we impose two conditions that characterize the set of feasible parameters: conservation of biomass and positivity of parameters. We use them as a starting point to get corresponding metaparameters equations that describe $\mathcal{F}_1^{G,A}$. Biomass conservation is equivalent to fulfilling Eq.(1.5), which we rewrite here:

$$\sum_{\nu} (1 - \sigma_{i\nu}) \gamma_{i\nu} R_{\nu}^* \geq \sum_{\nu} \alpha_{\nu i} \quad \forall i = 1, \dots, N_S. \quad (3.1)$$

Additionally, the consumers death rates d_i and the resources diffusion rates m_{ν} have to be positive. This implies Eq.(1.4), which may be recast as :

$$\left\{ \begin{array}{l} d_i = \sum_{\nu} (\sigma_{i\nu} \gamma_{i\nu} R_{\nu}^* - \alpha_{\nu i}) > 0 \quad \forall i = 1, \dots, N_S \\ m_{\mu} = \frac{l_{\mu} - \sum_j (\gamma_{j\mu} R_{\mu}^* - \alpha_{\mu j}) S_j^*}{R_{\mu}^*} > 0 \quad \forall \mu = 1, \dots, N_R \end{array} \right. \quad (3.2a)$$

$$\left\{ \begin{array}{l} d_i = \sum_{\nu} (\sigma_{i\nu} \gamma_{i\nu} R_{\nu}^* - \alpha_{\nu i}) > 0 \quad \forall i = 1, \dots, N_S \\ m_{\mu} = \frac{l_{\mu} - \sum_j (\gamma_{j\mu} R_{\mu}^* - \alpha_{\mu j}) S_j^*}{R_{\mu}^*} > 0 \quad \forall \mu = 1, \dots, N_R \end{array} \right. \quad (3.2b)$$

Section 5.2.1 explains how to use our formalism to translate these three conditions on the parameters set into corresponding conditions on metaparameters. After some computations, we find that the fully feasible region $\mathcal{F}_1^{G,A}$ is characterized by the inequalities:

$$\max_i \left\{ \frac{\deg(A, i)}{\deg(G, i)} \right\} \alpha_0 \lesssim \min(1 - \sigma_0, \sigma_0) \gamma_0 R_0 \lesssim \min(1 - \sigma_0, \sigma_0) \min_{\nu} \left\{ \frac{l_0}{\deg(G, \nu) S_0} + \frac{\deg(A, \nu)}{\deg(G, \nu)} \alpha_0 \right\} \quad (3.3)$$

The biological implications of that equation are discussed below.

3.1.2 The feasibility region in the absence of syntropy

We start with the “null” case and study feasibility in the absence of syntropy. A first order approximation of the fully feasible volume $\mathcal{F}_1^{G,A}$ is given by Eq.(3.3). In the absence of syntropy $\alpha_0 = 0$, it becomes:

$$\gamma_0 R_0 \lesssim \frac{l_0}{\max_{\nu} \{\deg(G, \nu)\} S_0}. \quad (3.4)$$

That relation provides a lot of biological insight about how the different metaparameters of actual microbial communities should be linked together.

- Given a feasible system, for a fixed consumption interaction (*i.e.* constant γ_0 and G) and average consumers abundance S_0 , increasing the average resource equilibrium abundance R_0 implies that, in order to maintain feasibility, the external resource input rate also has to be increased. This is completely expected: since the microbes feed on a part of the resources, more available resources that are not consumed can only come from outside in the absence of syntropy. Similarly, at fixed G , S_0 and R_0 , increasing the consumption rate requires increasing the input of external resources.
- For a fixed consumption network G , resources abundance R_0 and resource input rate l_0 , a higher consumption rate γ_0 past a certain threshold is only possible if the consumers abundance S_0 is decreased. Since there are fewer consumers, they can individually feed on more of the available resources.
- For every metaparameter except γ_0 fixed, arranging the shape of G such that few consumers feed on the same resources¹⁹ increases the range of possible consumption rates. If the total amount of resources is fixed, consumers can individually feed more on it if they do not have to share it!

Equation (3.4) can be confronted to simulations. The first step is to note that for all the matrices in the set G_{25} (see Section 2.1.2), there exists a fully feasible zone, *i.e.* $\mathcal{F}_1^{G,0}(\alpha_0 = 0) \neq \emptyset \forall G$. There exists an overlap between all these regions $\mathcal{F}_1^{S_{25}}(0) \equiv \bigcap_{G \in G_{25}} \mathcal{F}_1^{G,0} \neq \emptyset$, such that the critical feasibility $f^*(S) = 1$ (see Eq.(1.11)).

Figure 3.1.1 shows the typical proportion of feasible systems without syntropy for two consumption matrices G_1 and G_2 in the set G_{25} . We generally observe two distinct zones in the (γ_0, S_0) space: full feasibility (\mathcal{F} as defined in Eq.(1.7) is equal to 1, blue part of Fig.3.1.1) and full unfeasibility ($\mathcal{F} = 0$, red part). These two zones are separated by a narrow region of partial feasibility $0 < \mathcal{F} < 1$. Since that region is very thin, we can define the “boundary” line between feasibility and unfeasibility as the level²⁰ $\mathcal{F} = 0.5$. Theoretically, that sharp transition between feasibility and unfeasibility happens when both sides of the inequality (3.4) are equal, *i.e.* at $\gamma_0 R_0 = l_0 / \max_\nu \{\deg(G, \nu)\} S_0$. Hence we expect the boundary measured above to be well characterized by the curve $S_0 = K \gamma_0^{-1}$ with $K = l_0 / (R_0 \max_\nu \{\deg(G, \nu)\})$.

For G_1 , the theoretical expectation is $S_0 = 0.125 \gamma_0^{-1}$ and a fit on the numerical results gives $S_0 = (0.124 \pm 3 \times 10^{-8}) \gamma_0^{-1}$ so the theoretical estimate is very accurate. For G_2 , we expect $S_0 = 0.077 \gamma_0^{-1}$. A fit gives $S_0 = (0.076 \pm 7 \times 10^{-9}) \gamma_0^{-1}$. Again, the theoretical value is very close to the numerical measurement. However, the numerical estimate does not always match the theoretical value that well. Figure 3.1.2 shows the relative error $\Delta_K = 1 - K_{\text{theoretical}} / K_{\text{fit}}$. We see that in general $\Delta_K < 0$, *i.e.* the theoretical expectation tends to overestimate the fully feasible region. This is probably due to noise (*i.e.* coming from the difference between the metaparameters and the parameters) in the actual systems and the topology of the consumption matrix G . Figure 3.1.2 shows that the lower the ecological overlap or connectance of G , the worse the theoretical estimate. Finding a more accurate

¹⁹Indeed, $\deg(G, \nu)$ is the number of species that consume resource ν . Reducing the number of species that consume from the same resources reduces $\max \deg(G, \nu)$ in Equation (3.4).

²⁰Numerically because of the possible noise, we take as part of the boundary every (γ_0, S_0) such that $0.4 < \mathcal{F} < 0.6$.

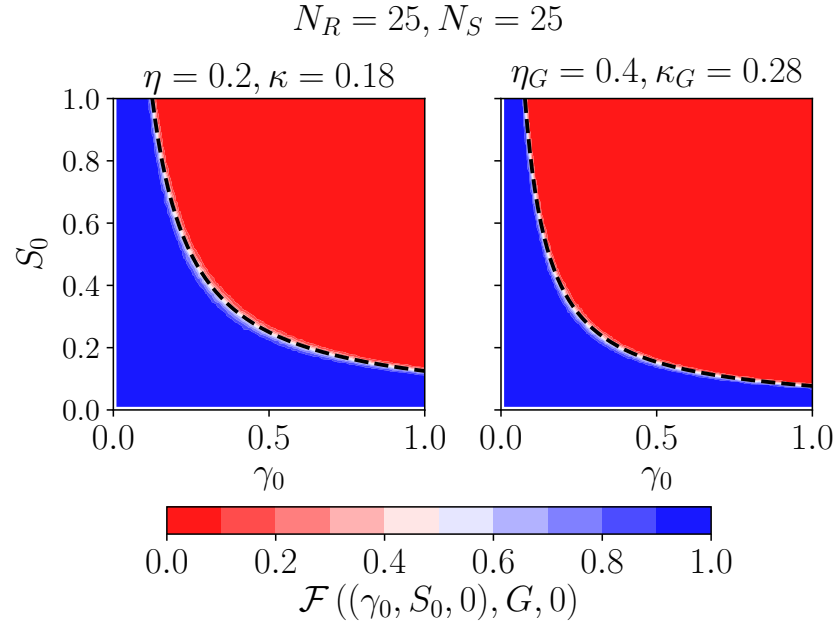


Figure 3.1.1: Plot of the feasibility region in the absence of syntropy. The color curve indicates the feasibility function $\mathcal{F}((\gamma_0, S_0, \alpha_0 = 0), G, 0)$ for G_1 , which has a connectance $\kappa_G = 0.18$ and ecological overlap $\eta_G = 0.2$ (left) and G_2 with $\kappa_G = 0.28$ and $\eta_G = 0.4$ (right). We observe a steep descent which marks a very clear transition from a totally feasible regime to a totally unfeasible regime, which allows us to precisely get the boundary of $\mathcal{F}_1^{G,0}$. The dashed lines indicate the theoretical predictions.

approximation which takes into account the deviations away from the metaparameters and the topology of G remains a challenge for future studies.

We can similarly measure the common fully feasible volume in the absence of syntropy (depicted in Fig.3.1.3). According to Eq.(3.4), its boundary is inversely proportional to the largest maximal row degree of the matrix set. For the set S_{25} , this yields in theory: $S_0 = 0.053\gamma_0^{-1}$. A fit on the points at the edge yields the critical boundary $S_0 = (0.042 \pm 10^{-8})\gamma_0^{-1}$, which is $\sim 21\%$ away from the theoretical prediction. The discrepancy is probably due to the difference between the way we estimate the boundary numerically and analytically.

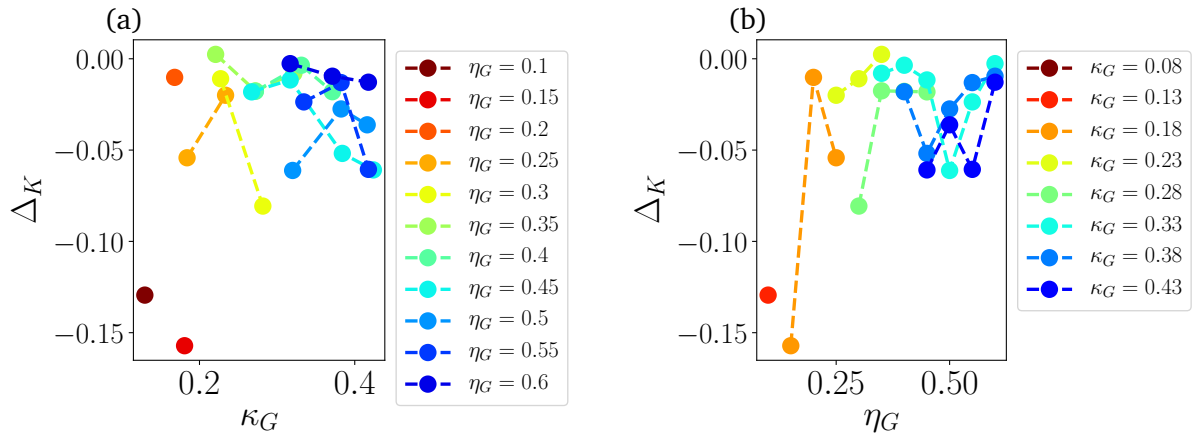


Figure 3.1.2: Relative error in the determination of the boundary of $\mathcal{F}_1^{G,0}$. The curious reader may easily show that this is also the relative error on the area of $\mathcal{F}_1^{G,0}$. (a) varying connectance at fixed ecological overlap and (b) varying ecological overlap at fixed connectance. The theoretical prediction tends to overestimate the measured value. The larger the ecological overlap or connectance, the better the estimate.

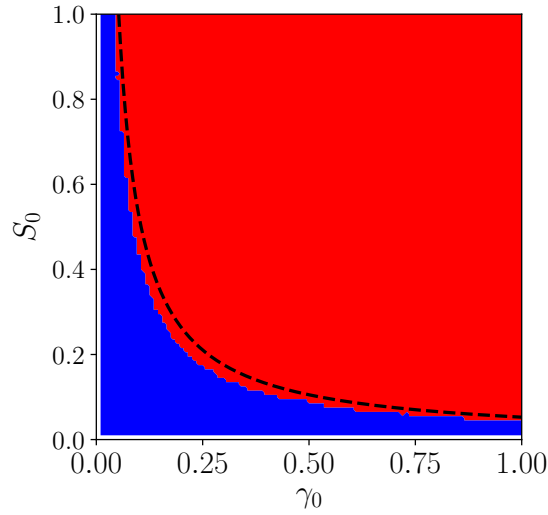


Figure 3.1.3: Plot of the common feasibility region in the absence of syntropy. The blue area indicates the common feasibility volume, computed numerically, while the dashed line shows the analytical prediction. Although the match is not as good as before, the relative error is only of the order of 20%. The red part is the area where not all matrices are fully feasible.

3.1.3 Impact of syntropy on the feasible region

Above we computed feasible volumes when there is no syntropy *i.e.* $\mathcal{F}_1^{G,0}$. Because there was no syntropy, we did not need to specify what the structure of A was. The next naturally arising question is then: what happens to the feasible region of a community with a given consumption matrix G when we add a syntrophic interaction, *i.e.* a syntrophic network A of average interaction strength α_0 ? More precisely, how does the shape of $\mathcal{F}_1^{G,A}$ change as a function of A and α_0 ?

A layer of complexity arises on top of the problem discussed above: apart from the structure of the consumption matrix G , we now have to think about both the topology of A and α_0 . As explained in Section 2.1, performing a detailed numerical study of the topology of A would lead to a combinatorially unfeasible exploration, so we focus on the four A cases enunciated above: “fully connected” (FC), “no intraspecific syntropy” (NIS), “LRI matrix” (LRI), and “random structure” (RS). Concerning the question of α_0 , we would like to be “fair” among all networks and study syntropy strengths that are feasible for all the consumption-syntropy networks considered $(G, A) \in S_{25}$. The largest syntropy compatible with full feasibility for all the networks considered, which we will refer to as *the largest common fully feasible syntropy* α_C^F is the value of α_0 such that $\mathcal{F}_1^{G,A} \neq \emptyset \forall (G, A) \in S_{25}$. It can be estimated with the help of Eq.(3.3):

$$\alpha_0 \lesssim \frac{\min(1 - \sigma_0, \sigma_0) R_0}{\max_{(G,A)\gamma_0 \in S} \left\{ \max_i \left\{ \frac{\deg(A,i)}{\deg(G,i)} \right\} \right\}} \gamma_0 \approx 0.01 \gamma_0 \leq 0.01. \quad (3.5)$$

We will hence investigate the impact of α_0 evaluated at ten different values from 0 to 0.015. Since we do not change α_0 in a continuous way but instead focus on different “ α_0 -slices” of $\mathcal{F}_1^{G,A}$, the object of our attention is the set of (γ_0, S_0) such that $(\gamma_0, S_0, \alpha_0) \in \mathcal{F}_1^{G,A}$. We will refer to it as $\mathcal{F}_1^{G,A}(\alpha_0)$:

$$\mathcal{F}_1^{G,A}(\alpha_0) \equiv \left\{ (\gamma_0, S_0) : (\gamma_0, S_0, \alpha_0) \in \mathcal{F}_1^{G,A} \right\}. \quad (3.6)$$

Because Equation (3.3) depends on the structure of G and of A , we expect $\mathcal{F}_1^{G,A}(\alpha_0)$ to depend heavily on the topology of both the consumption and syntropy matrices.

The influence of matrix topology

Figure 3.1.4 shows that indeed $\mathcal{F}_1^{G,A}(\alpha_0)$ changes significantly not only with syntropy α_0 but also with the network structure of the consumption matrix G . We observe a general trend among all matrices: as syntropy increases, the fully feasible region in the unit square shrinks towards high γ_0 . This can be explained with the LHS of Eq.(3.3) which provides a lower bound to γ_0 when $\alpha_0 > 0$:

$$\gamma_0 \gtrsim \frac{\max_i \left\{ \frac{\deg(A,i)}{\deg(G,i)} \right\}}{\min(1 - \sigma_0, \sigma_0) R_0} \alpha_0. \quad (3.7)$$

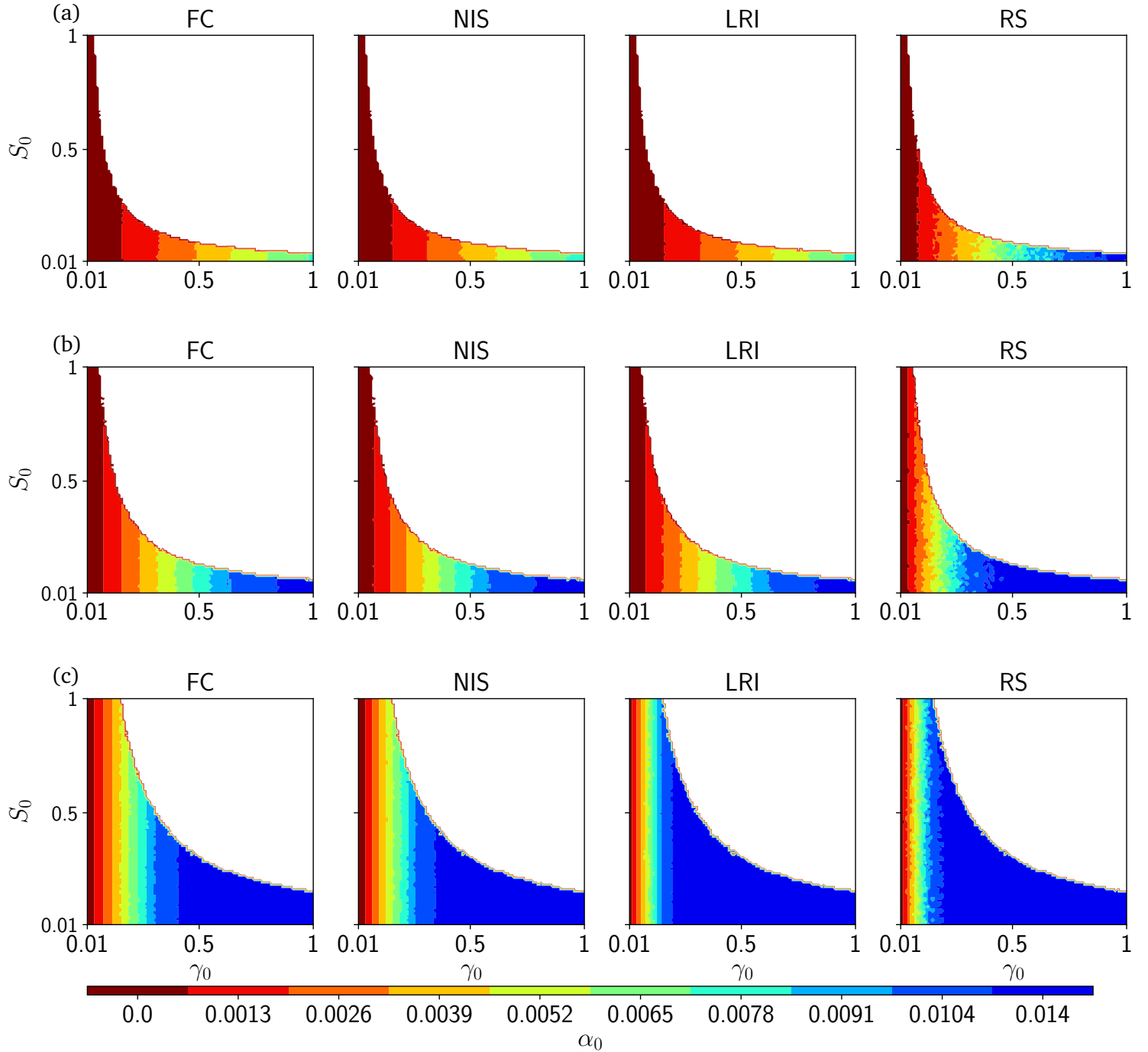


Figure 3.1.4: Fully feasible region in the $(\gamma_0, S_0) \in [0, 1]^2$ unit square as a function of syntropy for different consumption matrices G : (a) $\eta_G = 0.6$, $\kappa_G = 0.33$, (b) $\eta_G = 0.35$, $\kappa_G = 0.23$ and (c) $\eta_G = 0.15$, $\kappa_G = 0.18$. The white zone corresponds to points that are never fully feasible. The colour of a given point tells until which syntropy that point is fully feasible, e.g. a light blue point is fully feasible for $0 \leq \alpha_0 \leq 9.1 \times 10^{-3}$. The size of the feasibility regions depends heavily on the topology of the matrix, which makes the problem far from trivial.

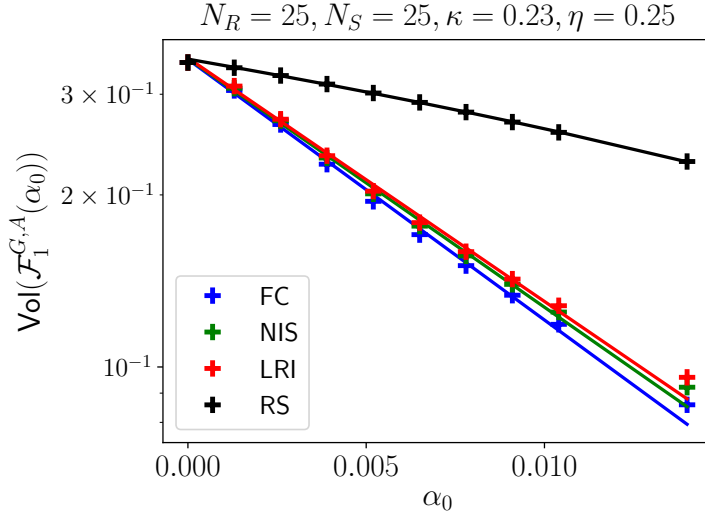


Figure 3.1.5: Decay of the volume of the fully feasible region $\mathcal{F}_1^{G,A}(\alpha_0)$ for a matrix consumption G with ecological overlap $\eta_G = 0.25$ and connectance $\kappa_G = 0.23$ on a logarithmic scale. The solid lines represent the exponential fit explained in the main text. The four different colors represent the four different structures considered for the syntropy matrix. The decay of $\text{Vol}(\mathcal{F}_1^{G,A}(\alpha_0))$ seems well approximated by an exponential decay. A random syntropy matrix (RS scenario) allows for a larger feasibility volume.

The abundance of consumers S_0 still has an upper bound provided by the RHS of Eq.(3.3) which goes as something close to²¹ γ_0^{-1} :

$$\gamma_0 R_0 \lesssim \min_{\nu} \left\{ \frac{l_0}{\deg(G, \nu) S_0} + \frac{\deg(A, \nu)}{\deg(G, \nu)} \alpha_0 \right\}. \quad (3.8)$$

So in general, as syntropy increases, systems with a high consumption rate and a low consumers abundance at equilibrium will remain feasible, while other simply will not exist.

Because of that shift to the right, $\mathcal{F}_1^{G,A}(\alpha_0)$ shrinks in size²²: as syntropy is increased, the set of possible consumption rates and average consumers abundances is more restricted. Figure 3.1.5 shows that typically the feasibility volume $\text{Vol}(\mathcal{F}_1^{G,A}(\alpha_0))$, formally defined in Section 5.1.1, decays in an exponential-like fashion as α_0 increases. This is a simple translation of the biological hindsight that, because of the physical considerations (conservation of biomass and positivity of the parameters) discussed above, the number of systems that can sustain a given syntrophic interaction strength decreases with that interaction strength, *i.e.* no system can support an arbitrarily large syntropy. The shrinkage of the feasibility volume can be quantified by defining the *feasibility decay rate* d_F , which is

²¹Mathematically the difficulty is that we cannot split the two terms of the RHS of (3.8). If we assume $\deg(A, \nu)$ is small, then $S_0 \lesssim \gamma_0^{-1}$.

²²Note that when we talk about the size of $\mathcal{F}_1^{G,A}(\alpha_0)$, it is understood relatively to the $(\gamma_0, S_0) \in [0, 1]^2$ unit square. In fact we expect that new points also appear to the right of the $\gamma_0 = 1$ axis as can be seen by inspecting Eq.(3.3). However, because the larger the γ_0 , the smaller the range of feasible S_0 , this newly added feasible area should vanish quickly as γ_0 increases.

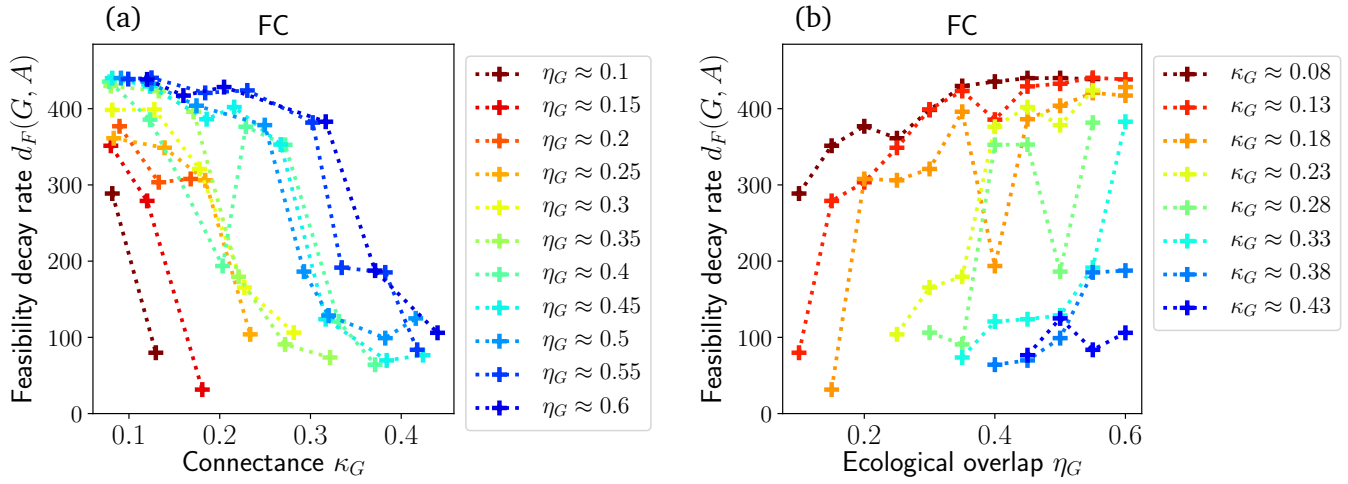


Figure 3.1.6: Feasibility decay rate $d_F(G, A)$ for A fully connected and $(G, A) \in S_{25}$. (a) d_F as a function of the connectance of G for different fixed ecological overlaps and (b) d_F as a function of the ecological overlap η_G for fixed different connectances. A strong trend may be seen: at fixed ecological overlap, d_F decreases with connectance and at fixed connectance it increases with ecological overlap. Since a small d_F allows to sustain a larger syntropy, microbial communities where syntrophic interactions play a large role will tend to have a high connectance of the consumption matrix and a low ecological overlap.

obtained by performing a non-linear regression to find the coefficients $c_1, c_2, d_F \in \mathbb{R}^+$ that satisfy best:

$$\text{Vol} \left(\mathcal{F}_1^{G,A}(\alpha_0) \right) \approx c_1 \exp(-d_F \alpha_0) - c_2. \quad (3.9)$$

The value of $d_F(G, A)$ tells us how fast the feasible volume shrinks for a given consumption-syntropy couple (G, A) . In that sense $d_F(G, A)$ provides a measure of how good (G, A) can sustain an increase in syntropy. If d_F is low then the system can bear an increase of syntropy and stay feasible. On the opposite, if d_F is high, if syntropy is increased too much, the microbial community will have to fundamentally change (e.g. move to a (G, A) configuration with a lower d_F) or it will become unfeasible, i.e. at least one species will get extinct.

Figure 3.1.6 shows how $d_F(G, A)$ changes as a function of the structure of G , for A fully connected, and Figure 3.1.7 shows how d_F changes when the structure of A changes.

A systematic trend can be observed as a function of the consumption matrices: for a given connectance κ_G , d_F is increased if the ecological overlap η_G is increased and for a given ecological overlap, d_F decreases if the connectance is increased. In biological terms, systems where there is a small ecological overlap (i.e. small competition) but a lot of links in the food consumption network will be favoured. Microbial communities where consumers on average feed on a lot of different resources (i.e. each their own) can sustain a larger syntrophic interaction than others. The shape of the syntropy matrix changes the feasibility decay rate in a non-trivial way. An NIS structure strongly (we observe up to a 50% percent difference) decreases d_F ; the improvement is better for larger κ_G and

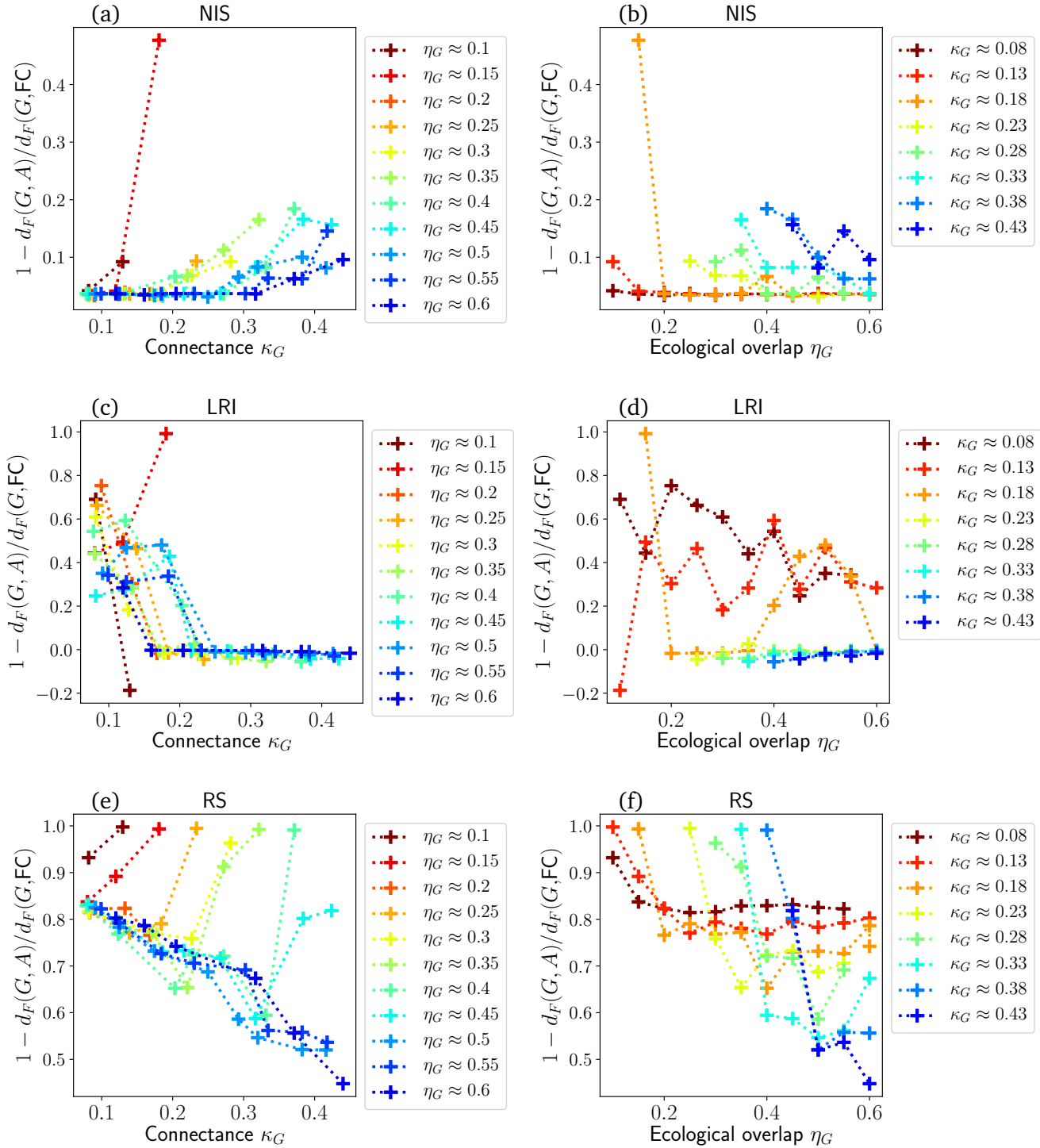


Figure 3.1.7: Relative difference of the feasibility decay rate for the considered A scenario compared to the FC null case (Fig.3.1.6) for $N_R = 25$ and $N_S = 25$. Plots on the first column (a)-(c)-(e) show how that quantity changes with connectance for a given ecological overlap, while plots on the second column (b)-(d)-(f) show how it evolves when ecological overlap is changed and connectance is kept fixed. Different structures of the A matrix are considered: (a)-(b) NIS, (c)-(d) LRI (e)-(f) RS. A positive y-coordinate means that for the feasibility decay rate of the current syntropy scenario is smaller than for the FC case, i.e. the system sustains syntropy better with the considered A-structure compared to fully connected. The FC scenario is always outperformed by the other scenarios, especially the random structure (RS) case.

lower η_G . The LRI scenario has a surprising effect: for low κ_G , d_F is lowered a lot (almost by 100% in the best case) but for $\kappa_G > 0.23$, there is no improvement. Finally the RS scenario offers the best improvement: d_F is improved by at least 50% for all networks. Note that the underlying trend is very regular: for a fixed connectance κ_G , the improvement is almost 100% at low ecological overlap. As η_G increases, the improvement decreases until it saturates and stays constant. The saturation value is larger when κ_G is smaller. The regularity of such results suggests an underlying analytical explanation that has yet to be derived.

Common fully feasible volume

After studying the effect of syntropy on each consumption-syntropy network (G, A) , we can focus on the overlap of all the fully feasible regions: the common fully feasible region $\mathcal{F}_1^{S_{25}} \equiv \bigcap_{(G,A) \in S_{25}} \mathcal{F}_1^{G,A}$. Similarly to above, we slightly abuse notation and write:

$$\mathcal{F}_1^{S_{25}}(\alpha_0) \equiv \{(\gamma_0, S_0) : (\gamma_0, S_0, \alpha_0) \in \mathcal{F}_1^{S_{25}}\}. \quad (3.10)$$

Figure 3.1.8 shows the evolution of $\mathcal{F}_1^{S_{25}}(\alpha_0)$ as syntropy increases. In accordance to what was observed individually for each matrix before, the RS scenario allows for a larger syntropy: at a given α_0 , there are more feasible (γ_0, S_0) points if A has a random structure. The three other scenarios do not offer a significant difference and at $\alpha_0 = 9.1 \times 10^{-3}$ there are no more (γ_0, S_0) that are fully feasible for all matrices. This means that the largest common fully feasible syntropy respects $7.8 \times 10^{-3} < \alpha_C^F \leq 9.1 \times 10^{-3}$ for those three scenarios, which puts the estimate $\alpha_C^F \approx 0.01$ of Eq.(3.5) not far from the numerical bounds.

Without surprise, $\text{Vol}(\mathcal{F}_1^{S_{25}}(\alpha_0))$ also decays in an exponential-like fashion as is shown by Figure 3.1.9. An exponential fit allows to find the feasibility decay rates of each scenario: for the FC case, $d_F = 480 \pm 42$ (in units of syntropy α_0); for NIS, $d_F = 463 \pm 43$; for LRI, $d_F = 450 \pm 42$ and finally for RS, $d_F = 139 \pm 33$. The FC, NIS and LRI scenarios of A do not produce a significant difference in feasibility. However a random A -matrix (RS scenario) allows for a 3 times smaller feasibility decay rate and hence at a given syntropy α_0 , for many more pairs of common feasible (γ_0, S_0) . Again we observe the same shift of $\mathcal{F}_1^{S_{25}}$ towards points with a high γ_0 and consequently a small S_0 . Overall, independently of the consumption-syntropy network structure, microbial communities which have a low abundance and high uptake rates can sustain a larger syntropy than others. Among these, the ones which have a random syntropy network are the most “compatible” with even larger syntrophic interactions.

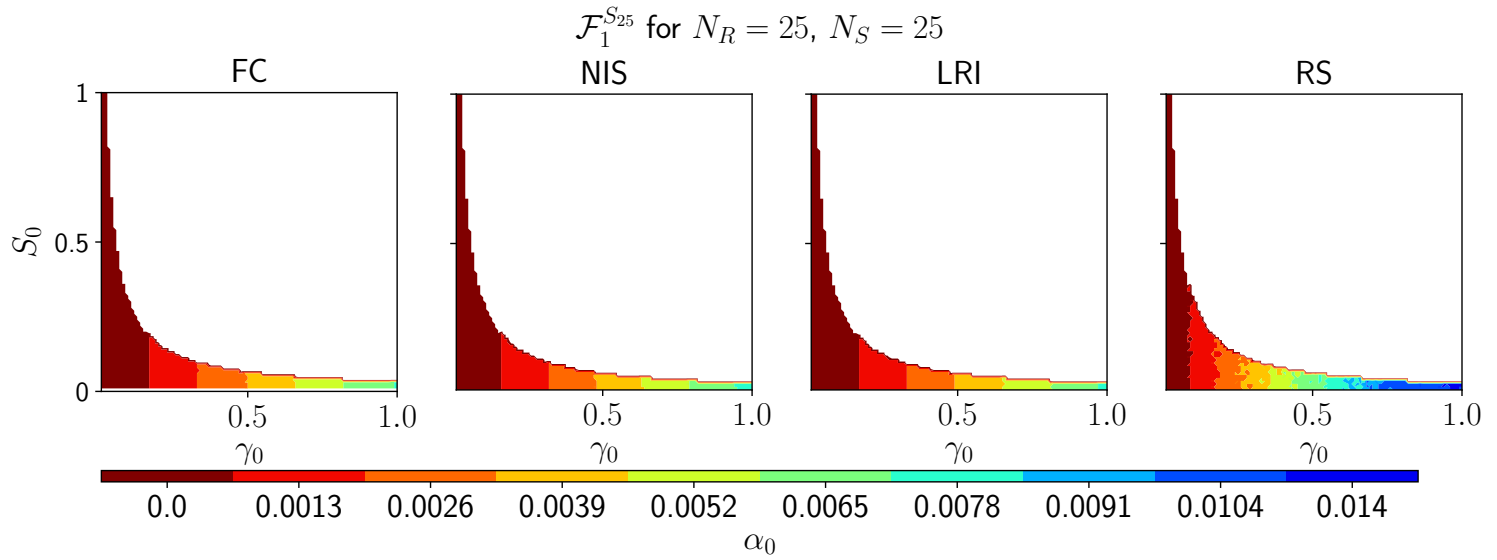


Figure 3.1.8: Surface plot of the fully feasible volume $\mathcal{F}_1^{S_{25}}(\alpha_0)$. The color bar on the side indicates the value of α_0 to which the surface corresponds. The white part of the plot corresponds to points that never are fully feasible. Note that even though it is not very clear on the figure $\mathcal{F}_1^{S_{25}}(\alpha_0^+) \subset \mathcal{F}_1^{S_{25}}(\alpha_0^-) \forall \alpha_0^+ > \alpha_0^-$, i.e. the common fully feasible region of higher syntropy is included in the one of lower syntropy. The different subplots correspond to the different structures of the syntropy matrix.

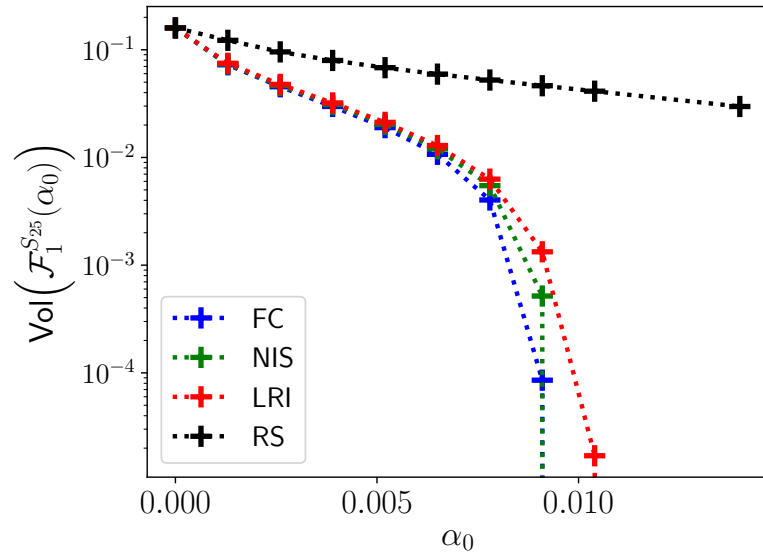


Figure 3.1.9: Volume of the common feasibility region $\mathcal{F}_1^{S_{25}}(\alpha_0)$ as a function of syntrophic interaction strength α_0 (plotted on logarithmic scale). While the FC, NIS and LRI cases offer similar results, the RS scenario outperforms all of them. An exponential fit (Eq.3.9) allows to measure a global d_F for each of the four scenarios. The global decay feasibility rate of the RS scenario is 3 times smaller than the others.

The influence of the matrix dimensions

We focused above on microbial communities with the same number of consumers and resources: $N_R = N_S = 25$. But such systems lie at what has been referred to in the literature as May's stability bound [32], which is defined as an ecological community where the number of resources is equal to the number of species. According to the defenders of the competitive exclusion principle²³, an ecological system which has as many resources as consumers is the limiting case where coexistence, *i.e.* feasibility in the terms used here, starts to exist. In a way, the study conducted before can be seen as a borderline case and it can be very fruitful to investigate the behaviour of systems where the number of resources has been increased to $N_R = 50$.

Figure 3.1.10 shows the common feasibility region $\mathcal{F}_1^{S_{50}}$ of the $N_R = 50$ matrix set S_{50} , which is to be compared with the common feasibility region for $N_R = 25$ (Fig.3.1.8). It seems that, independently of the structure of the A -matrix, a lesser common maximal syntropy can be attained when the number of resources is doubled.

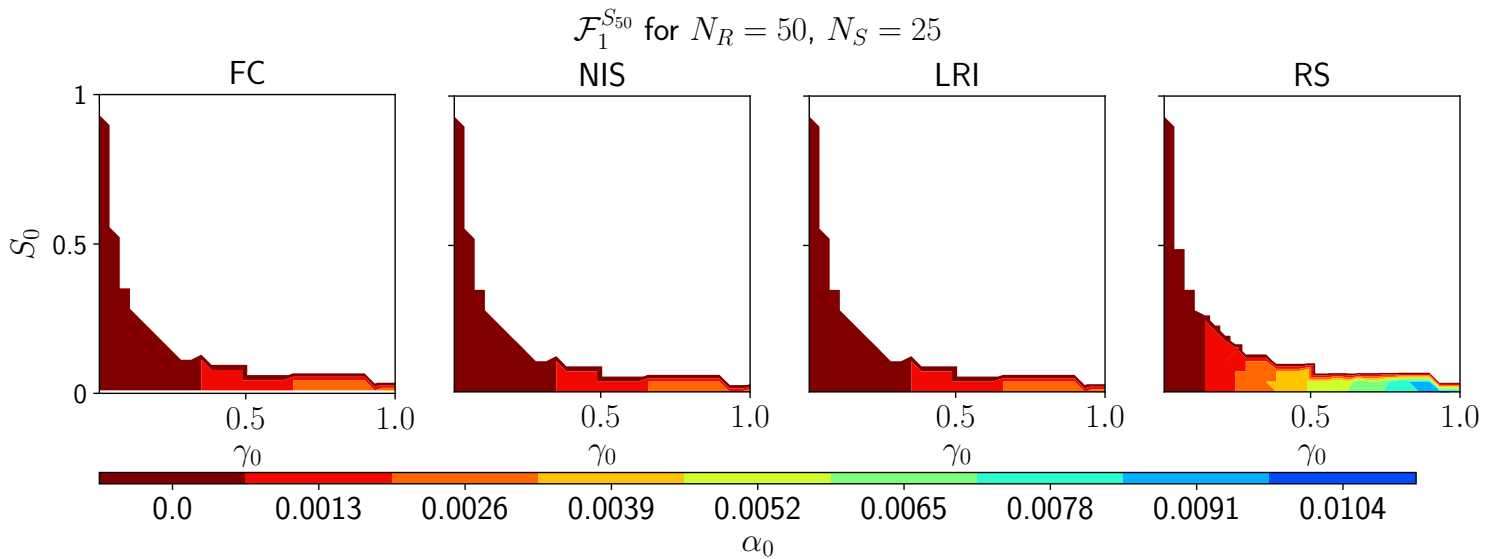


Figure 3.1.10: Common feasibility region $\mathcal{F}_1^{S_{50}} (\alpha_0)$ for $N_R = 50$ and $N_S = 25$, to compare with 3.1.8. We considered four different structures of the syntropy matrix: FC, NIS, LRI and RS. As the number of resources increases, the feasibility volume for a given α_0 decreases.

This might be the indication that changing N_R modifies feasibility in a non-trivial way: the fact that the common feasibility region is different implies that the feasibility regions $\mathcal{F}_1^{G,A}$ change for all networks (G, A) when $N_R = 50$. To quantify the effect on each individual consumption-syntropy network, we may compute the decay feasibility rate and compare it to its counterpart when $N_R = 25$. Figure 3.1.11 shows that there is no clear pattern on how d_F evolves when the number of resources is changed. Overall, the average ratio of the decay rates among the networks is equal to ~ 1 : one could say that doubling the resources

²³The heavily debated and often misunderstood [41] *competitive exclusion principle*, also known as Gause's principle, states that "Complete competitors cannot coexist" [41], or more generally that "the number of consumer species in steady coexistence cannot exceed that of resources" [42].

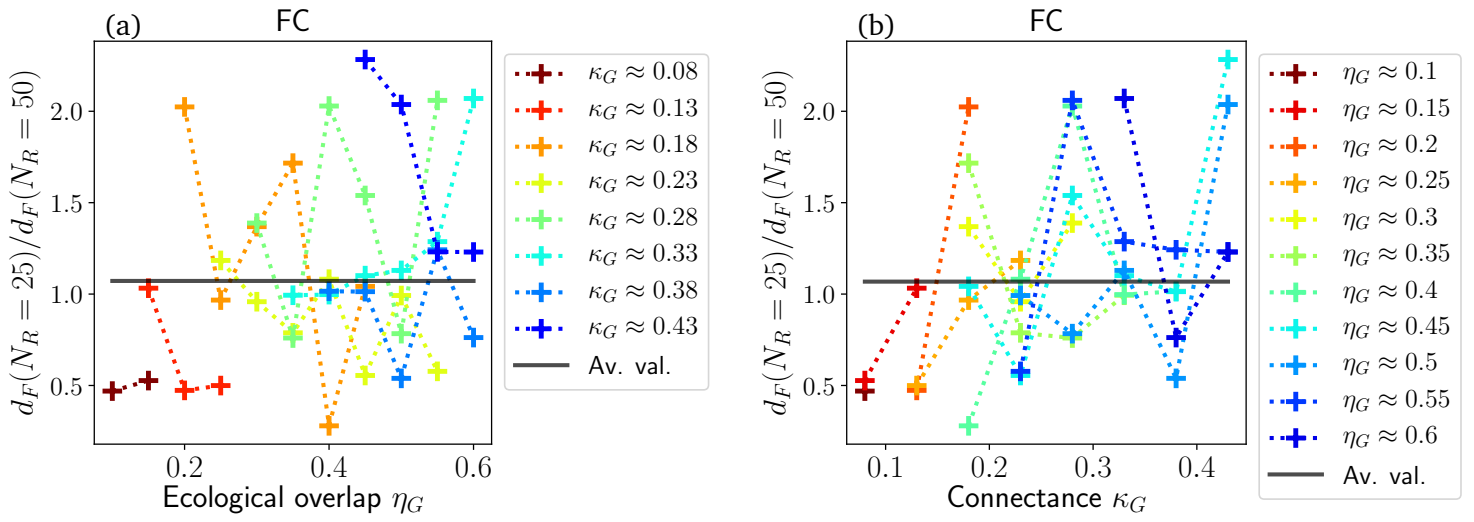


Figure 3.1.11: Ratio of the feasibility decay rates at $N_R = 25$ and at $N_R = 50$ as a function of the consumption matrix properties. A y -axis larger than 1 means $d_F(N_R = 25)$ is larger than $d_F(N_R = 50)$, which means the system endures the addition of syntrophic interaction better at $N_R = 50$. We considered the four usual A scenarios (a)-(b) FC, and on the page below, (c)-(d) NIS, (e)-(f) LRI and (g)-(h) RS. Increasing the number of resources in the system does not allow microbial communities to be “more feasible” as syntropy increases: on average d_F is unchanged by doubling the number of resources. A detailed trend on how the consumption matrix properties or the A-scenario precisely modify the improvement is difficult to draw from this data.

has on average no effect. Keep in mind that this conclusion should be carefully dealt with: although the matrices generated indeed do have the same connectance and ecological overlap, they may be different according to a measure that we have not monitored but which could be relevant biologically. This would mean that comparing the networks at $N_R = 50$ and $N_R = 25$ may not be fair. In the end, the parameter that controls how feasibility changes when the number of resources is modified is still unknown.

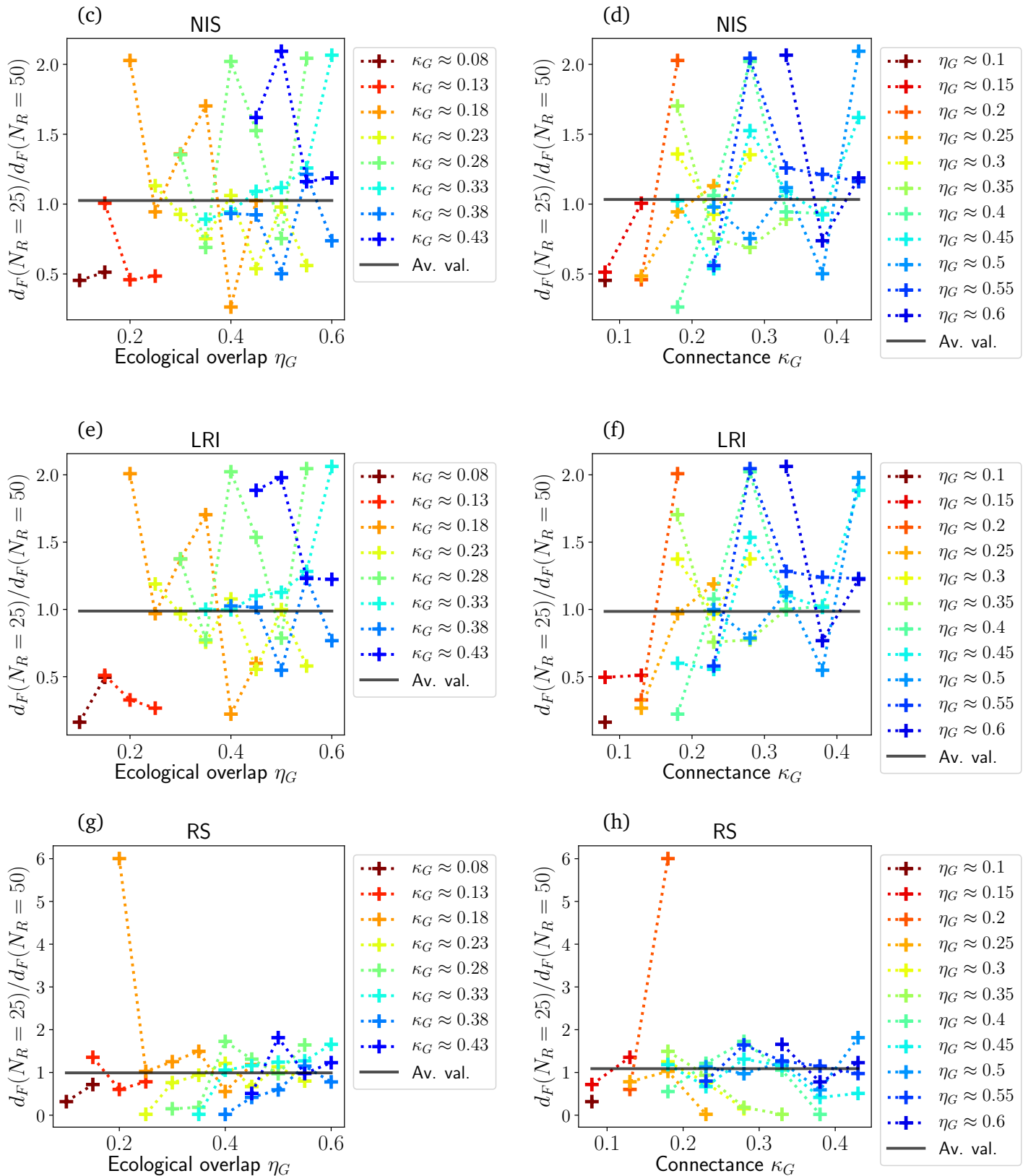


Figure 3.1.11: Continuation of the Figure above.

3.2 Dynamical stability

We discovered in the previous section that we expect microbial communities where a large syntrophic interaction is observed to have a large consumption rate γ_0 and a small abundance of consumers at equilibrium S_0 . It is time to work with feasible microbial communities and investigate their local dynamical stability. In short, we want to investigate the behaviour of systems when their populations (of both resources and microbes) at equilibrium are perturbed.

In the next section we will discover and discuss a special regime of parameters designed to shape more dynamically stable systems. We will then move on to study the dynamical stability of microbial communities by examining the shape of their fully dynamically stable regions, looking in what case feasibility implies dynamical stability and checking how the largest eigenvalue changes with the shape of the consumption-syntropy network. Finally we will investigate what happens when the number of resources in the community is changed.

3.2.1 The quest for dynamical stability

Section 2.3.1 establishes the master equation whose solutions govern the dynamical stability of our model. We rewrite it here:

$$\det \begin{pmatrix} -D - \lambda & \Gamma \\ B & 0 - \lambda \end{pmatrix} = 0. \quad (3.11)$$

That equation is very difficult to solve for λ . Our goal now is to find a special regime of parameters where we know dynamical stability is ensured. To achieve this, the first step is to make Eq.(3.11) simpler. In general there are many paths to obtain an approximate version of the dynamics. One of them, for instance, is building an effective Lotka-Volterra model. Although we do not study it here, we explicitly compute it in Section 5.2.2. We choose here a different way and obtain an exact equation when certain assumptions on the spectrum of the Jacobian can be made.

Simplifying the master equation

Equation (3.11) may be simplified if we assume that:

$$\lambda \neq 0. \quad (3.12)$$

Indeed²⁴, a non-zero λ implies

$$\det(\lambda \mathbb{I}_{N_S}) \neq 0, \quad (3.13)$$

where \mathbb{I}_{N_S} stands for the $N_S \times N_S$ identity matrix. One can use this condition to simplify Eq.(3.11) using the properties of block matrices [43]:

$$\det \begin{pmatrix} -D - \lambda \mathbb{I}_{N_R} & \Gamma \\ B & 0 - \lambda \mathbb{I}_{N_S} \end{pmatrix} = \det(-\lambda \mathbb{I}_{N_S}) \det \left(-D - \lambda \mathbb{I}_{N_R} + \frac{1}{\lambda} \Gamma B \right). \quad (3.14)$$

²⁴Section 5.2.2 elaborates on when that condition is fulfilled.

Hence Eq.(3.11) becomes:

$$\det(\lambda^2 \mathbb{1}_{N_R} + D\lambda - \Gamma B) = 0. \quad (3.15)$$

The complexity here is already reduced because we go from the determinant of a $N_R + N_S$ square matrix to a N_R square matrix. We see from the previous expression that the dynamics is essentially dictated by the ΓB N_R -dimensional square matrix, which is given by:

$$(\Gamma B)_{\mu\nu} = \sum_i \Gamma_{\mu i} B_{i\nu} = \sum_i (\alpha_{\mu i} - \gamma_{i\mu} R_\mu^*) \sigma_{i\nu} \gamma_{i\nu} S_i^*. \quad (3.16)$$

Using standard properties of determinants, we can rewrite Eq.(3.15) as²⁵:

$$\det(-D^{-1}) \det(-D^{-1}\lambda^2 - \lambda + D^{-1}\Gamma B) = 0 \iff \det(S(\lambda) - \lambda) = 0 \quad (3.17)$$

with

$$S(\lambda) = D^{-1}\Gamma B - D^{-1}\lambda^2, \quad (3.18)$$

or, component-wise:

$$S_{\mu\nu} = \frac{1}{D_\mu} \left[\left(\sum_i \Gamma_{\mu i} B_{i\nu} \right) - \lambda^2 \delta_{\mu\nu} \right]. \quad (3.19)$$

Bound on the eigenvalues of the Jacobian

In order to find a dynamically stable regime – *i.e.* conditions on the parameters that will guarantee that $\text{Re}(\lambda_1) < 0$ (why this matters is detailed in Section 1.4.2) – we need to know more about the eigenvalues of the Jacobian. Our most powerful tool in that quest is the Gershgorin circle theorem [39] which allows us to find a bound on the modulus of every eigenvalue of the Jacobian. More precisely, Section 5.2.2 shows that:

$$|\lambda| \leq R_C \quad \forall \lambda \in \sigma(J^*), \quad (3.20)$$

where we defined the *critical radius* R_C as:

$$R_C \equiv \max \left\{ \max_i \left\{ \sum_\nu |B_{i\nu}| \right\}, \max_\mu \left\{ \sum_j |\Gamma_{\mu j}| + D_\mu \right\} \right\}. \quad (3.21)$$

This gives us an estimation of how big the eigenvalues can get: we know that all the eigenvalues *have* an absolute value smaller than or equal to the critical radius R_C . The next step is to estimate R_C in terms of metaparameters, so that we can get a qualitative insight on how the eigenvalues change when the metaparameters are changed. Section 5.2.2 shows that after a few computations, one finds:

$$R_C \approx \max \left\{ \max_i (\deg(G, i)) \sigma_0 \gamma_0 S_0, \right. \\ \left. \max_\mu \left\{ \deg(G, \mu) \gamma_0 R_0 + \deg(A, \mu) \left(1 + \frac{\alpha_0 S_0}{R_0} \right) + \frac{l_0}{R_0} \right\} \right\}. \quad (3.22)$$

Note that R_C depends not only on all metaparameters but also on the structure of both A and G . In particular, R_C increases when the largest degrees of A or G increase.

²⁵We can do this because since $m_\mu > 0$, we know D will always be invertible.

3.2.2 LRI regime

Analytical expression

The bound on the spectrum of the Jacobian Eq.(3.20) is a step in the right direction to find a dynamically stable regime. It is however not sufficient alone. Once again, the Gershgorin circle theorem comes to our rescue and allows us to enunciate the following lemma, which puts an upper bound on the real part of the spectrum²⁶ of any square matrix.

Lemma 1. *If a N -dimensional square matrix A verifies the equations:*

$$\operatorname{Re}(A_{ii}) + \sum_{j \neq i} |A_{ij}| < 0, \forall i = 1, \dots, N, \quad (3.23)$$

then $\operatorname{Re}(\lambda) < 0 \quad \forall \lambda \in \sigma(A)$.

The interested reader may find its proof in Section 5.2.2. That lemma plays a pivotal role: combined with the “Reductio ad absurdum” strategy described in Section 2.3.3, it allows us to get the following theorem.

Strong LRI regime

Theorem 1. *Let p be a parameter set with a Jacobian at equilibrium J^* . If 0 is not an eigenvalue of J^* and the equations*

$$(\Gamma B)_{\mu\mu} < - \sum_{\nu \neq \mu} |(\Gamma B)_{\mu\nu}| - R_C^2 \quad \forall \mu, \quad (3.24)$$

are verified, then p is dynamically stable.

Proof. We assume

$$(\Gamma B)_{\mu\mu} < - \sum_{\nu \neq \mu} |(\Gamma B)_{\mu\nu}| - R_C^2 \quad \forall \mu. \quad (3.25)$$

This implies:

$$(\Gamma B)_{\mu\mu} + R_C^2 < - \sum_{\nu \neq \mu} |(\Gamma B)_{\mu\nu}| \quad \forall \mu. \quad (3.26)$$

Using Eq.(3.20) and $\operatorname{Im}(\lambda)^2 \leq |\lambda|^2$, we get:

$$(\Gamma B)_{\mu\mu} + \operatorname{Im}(\lambda)^2 < - \sum_{\nu \neq \mu} |(\Gamma B)_{\mu\nu}| \quad \forall \mu. \quad (3.27)$$

It is not difficult to prove that for any complex number:

$$\operatorname{Im}(c)^2 \geq -\operatorname{Re}(c^2) \quad \forall c \in \mathbb{C}. \quad (3.28)$$

²⁶We denote the spectrum of a matrix M with the symbol $\sigma(M)$.

Using this result and dividing Eq.(3.27) by²⁷ D_μ , we get:

$$\frac{1}{D_\mu} \left[\left(\sum_i \Gamma_{\mu i} B_{i\mu} \right) - \operatorname{Re}(\lambda^2) \right] < - \sum_{\nu \neq \mu} \left| \frac{\sum_i \Gamma_{\mu i} B_{i\nu}}{D_\mu} \right| \forall \mu. \quad (3.29)$$

Looking at Eq.(3.19), we see that Eq.(3.29) is equivalent to:

$$\operatorname{Re}(S_{\mu\mu}) + \sum_{\nu \neq \mu} |S_{\mu\nu}| < 0 \forall \mu. \quad (3.30)$$

Lemma 1 implies that all the eigenvalues of $S(\lambda)$ have a negative real part. Using the “Reductio ad absurdum” reasoning from Section 2.3.3, that means that if $\operatorname{Re}(\lambda_1) \geq 0$ in Eq.(3.18) (unstable or marginally stable regime), then $\operatorname{Re}(\lambda_1) < 0$, which leads to a contradiction. This then implies that the equilibrium is dynamically stable. \square

Theorem 1 is a strong statement but it also demands strong constraints on the parameters set, namely ΓB must have diagonal elements that are “very negative”, which imposes severe conditions especially on the α and γ matrices. That is why we do not expect to find many parameters sets which would be in such a regime. We need to find another more relaxed regime in which more parameters sets could be.

Weak LRI regime Another version of Theorem 1 can be stated. Its proof is in Section 2. Its assumptions are less restrictive, but that comes with a price : its statement is weaker.

Theorem 2. *Let p be a parameter set with a Jacobian at equilibrium J^* . If 0 is not an eigenvalue of J^* and the equations*

$$(\Gamma B)_{\mu\mu} < - \sum_{\nu \neq \mu} |(\Gamma B)_{\mu\nu}| \forall \mu, \quad (3.31)$$

are verified, then the real eigenvalues of J^ are negative.*

Biological interpretation of the theorems

We observe that the key feature of both of these regimes is that the diagonal element of the ΓB matrix is small compared to the opposite of the sum of the absolute value of the off-diagonal elements. What is the biological interpretation behind this?

Let us consider two different resources labelled ν and μ and a species i (Fig.3.2.1). That species consumes an amount of biomass $\gamma_{i\nu} S_i^* R_\nu^*$ from resource ν . Out of this, only $\sigma_{i\nu} \gamma_{i\nu} S_i^*$ is dedicated to the growth of species i . However species i contributes through syntrophy to the growth of resource μ . Indeed, resource μ receives biomass from species i : $(\alpha_{\mu i} - \gamma_{i\mu} R_\mu^*) S_i^*$. If species i receives less biomass from resource ν , S_i^* will decrease and resource μ gets less biomass from species i . Overall the term:

$$(\alpha_{\mu i} - \gamma_{i\mu} R_\mu^*) \sigma_{i\nu} \gamma_{i\nu} S_i^* \quad (3.32)$$

²⁷That step is valid because $D_\mu > 0, \forall \mu$.

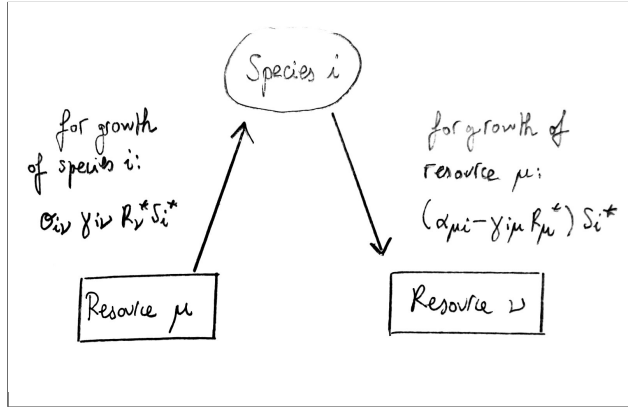


Figure 3.2.1: Biomass flux from resource ν to resource μ through species i .

can be regarded as the impact of resource ν on resource μ through species i (normalized by the abundance of resource ν). If it is positive, when resource ν increases, resource μ also increases. However if it is negative resource μ decreases when resource ν increases. The total impact of resource ν on resource μ is obtained by summing over all the species:

$$\sum_i (\alpha_{\mu i} - \gamma_{i\mu} R_\mu^*) \sigma_{i\nu} \gamma_{i\nu} S_i^* = (\Gamma B)_{\mu\nu}. \quad (3.33)$$

The ΓB matrix may then be seen as an *effective interaction matrix* between the resources. Coming back to the question initially asked, this means that Theorems 1 and 2 correspond to a regime where each resource has a very negative impact on its own growth: this is the reason we call it the *low intra-resource interaction* (LRI) regime. It is no surprise that such a regime is dynamically stable: if the growth of a resource encouraged its own growth, any small perturbation could lead to either an asymptotic explosion or decay of resources.

LRI regimes in terms of metaparameters

So we found that if a system has parameters that respect Eq.(3.24) then it is dynamically stable. A naturally arising question is then to ask how that equation is translated in terms of metaparameters – since our ultimate goal is to find what combination of metaparameters and consumption-syntrophy network (G, A) lead to dynamical stability. The path is simple : we need to find a metaparameters approximation of the resource interaction matrix $(\Gamma B)_{\mu\nu}$, which will allow us to get such a “metaparameters-version” of Eq.(3.24) and to know what part of the metaparameters space leads for sure to dynamically stable systems. Using the metaparameters approximations Eqs.(1.34), Eq.(3.16) can be simplified as:

$$(\Gamma B)_{\mu\nu} \approx \sigma_0 \gamma_0 S_0 \left(\alpha_0 \sum_i A_{\mu i} G_{i\nu} - \gamma_0 R_0 \sum_i G_{i\mu} G_{i\nu} \right) \equiv \sigma_0 \gamma_0 S_0 (\alpha_0 O_{\mu\nu} - \gamma_0 R_0 C_{\mu\nu}), \quad (3.34)$$

where we defined the *syntropy overlap matrix* $O_{\mu\nu}$ and the *consumption overlap matrix* $C_{\mu\nu}$ as:

$$O_{\mu\nu} \equiv (AG)_{\mu\nu} \text{ and } C_{\mu\nu} \equiv (G^T G)_{\mu\nu}. \quad (3.35)$$

The opposite effects of syntropy and consumption is translated by the opposite sign these two binary matrices have in Eq.(3.34). These matrices essentially build the dynamics of our model and an intuitive understanding of them can be very helpful. The syntropy overlap matrix $O_{\mu\nu}$ is defined as:

$$O_{\mu\nu} \equiv \sum_k A_{\mu k} G_{k\nu}. \quad (3.36)$$

Although A and G are binary, O does not have to and usually will not be. A given consumer k contributes to $O_{\mu\nu}$ if and only if both $A_{\mu k}$ and $G_{k\nu}$ are non zero, that is if consumer k releases resource μ and consumes resource ν . Hence $O_{\mu\nu}$ essentially tells how many species effectively “link” resource μ to resource ν through the indirect interaction of the species consumption. Similarly, the consumption overlap matrix is defined as:

$$C_{\mu\nu} = \sum_k G_{k\mu} G_{k\nu}. \quad (3.37)$$

Like O , C usually is not binary. The intuition behind $C_{\mu\nu}$ is straightforward: it counts how many species consume both resources μ and ν . We then find a lower bound for the RHS of Eq.(3.24):

$$-\sum_{\nu \neq \mu} |\Gamma B|_{\mu\nu} \geq -\sum_{\nu \neq \mu} \max_{\nu \neq \mu} |\Gamma B|_{\mu\nu} \geq -\deg(\mu, O - C) \max_{\nu \neq \mu} |\Gamma B|_{\mu\nu}. \quad (3.38)$$

Combining Eqs.(3.38), (3.34) and (3.24), we get an approximative strong LRI regime condition on the metaparameters:

$$\alpha_0 O_{\mu\mu} - \gamma_0 R_0 C_{\mu\mu} \lesssim -\deg(\mu, O - C) \max_{\nu \neq \mu} |\alpha_0 O_{\mu\nu} - \gamma_0 R_0 C_{\mu\nu}| - \frac{R_C^2}{\sigma_0 \gamma_0 S_0} \quad \forall \mu. \quad (3.39)$$

The corresponding equation for the weak LRI regime is the same without the R_C term. Since R_C gets smaller as the largest degree of G decreases (see Eq.3.22) we only expect systems with a low connectance food consumption adjacency matrix to be able to achieve an LRI state.

Let us recap what we accomplished since the start of this Section: we simplified the Master Equation (3.11) from a $N_R + N_S$ -dimensional to a N_R -dimensional polynomial. We then found with the help of the Gershgorin circle theorem a condition on the parameters of a system which guarantees its dynamical stability, which we called (strong) LRI regime. Finally we derived the equivalent of that condition in terms of metaparameters (Eq.3.39). What we would like to do now is to be able to look at that equation and say directly what metaparameters and (G, A) we should choose to obtain parameters in an LRI configuration. That task is however difficult, mainly because Eq.(3.39) is very complicated and mixes the A and G -matrices in a far from trivial way. Our strategy then is to design an algorithm which, for a given set of metaparameters and a consumption matrix G , gives us back the syntropy matrix A such that Eq.(3.39) is as close to being satisfied as possible. We discuss below how this can be achieved.

Monte Carlo Markov Chain algorithm for the optimal syntropy matrix

Given a consumption network G and fixed metaparameters, Eq.(3.39) is more likely satisfied if the syntropy matrix A is such that the LHS of Eq.(3.39) is minimal and its RHS is maximal:

- The LHS is minimized if $O_{\mu\mu} = (AG)_{\mu\mu}$ is set to its lowest possible value for every μ , that is zero. Because $(AG)_{\mu\mu} = \sum_{i=1}^{N_S} A_{\mu i} G_{i\mu}$ corresponds to the number of species that both consume and release resource μ , we expect the algorithm to yield A -matrices that minimize intraspecific syntropy.
- On the other hand, if we neglect the R_C term out of simplicity²⁸, the RHS is maximal if $\alpha_0(AG)_{\mu\nu} \approx \gamma_0 R_0 (G^T G)_{\mu\nu} \forall \nu \neq \mu$. The sum of the off-diagonal elements of $|\alpha_0 AG - \gamma_0 R_0 G^T G|$ is minimized. This means that outside the diagonal, we should have $\frac{\alpha_0}{\gamma_0 R_0} AG \approx G^T G$. A direct ecological interpretation is harder to draw. For a couple of different resources (μ, ν) , $(AG)_{\mu\nu} = \sum_{i=1}^{N_S} A_{\mu i} G_{i\nu}$ is the number of species that at the same time consume resource ν and release resource μ and $(G^T G)_{\mu\nu} = \sum_{i=1}^{N_S} G_{i\mu} G_{i\nu}$ is the number of consumers that feed on both ν and μ .

Intuitively, we want an algorithm that finds the syntropy matrix A such that AG is zero on the diagonal and $AG \approx \frac{\gamma_0 R_0}{\alpha_0} G^T G$ outside the diagonal. We take inspiration from standard Computational Physics techniques and look at the A -matrix we are searching for as the matrix which minimizes an “energy” – which remains to be determined. Considering the problem from that angle allows us to use standard, well-known minimization tools. Namely we choose to find the optimal syntropy matrix through a Metropolis-Hastings Monte Carlo Markov Chain (MCMC) algorithm, explained in Section 2.3.4.

But what function $E(G, A)$ should we use as the energy that has to be minimized? Since our goal is to build systems in the LRI regime, we use the simplest and most natural function that is compatible with the intuitively expected characteristics of A explained above (*i.e.* AG is zero on the diagonal and equal to $\frac{\gamma_0 R_0}{\alpha_0} G^T G$ outside of it):

$$E(G, A) \equiv \sum_{\mu} \left(|\alpha_0(AG)_{\mu\mu}| + \sum_{\nu \neq \mu} |(\alpha_0 AG - \gamma_0 R_0 G^T G)_{\mu\nu}| \right). \quad (3.40)$$

The energy function and hence the optimal syntropy adjacency matrix A depend on the ratio $\frac{\alpha_0}{\gamma_0 R_0}$. Note first that $R_0 = 1$ is fixed so we do not have to think about it. Because the energy only depends on the ratio $\frac{\alpha_0}{\gamma_0 R_0}$, we also may fix $\gamma_0 = 0.2$. The most rigorous way to proceed would be to compute the optimal A -matrix for each different α_0 and G we consider. However, out of simplicity, we assume that the optimal A does not depend too strongly on α_0 and we choose one fixed value of α_0 . We take the theoretical largest feasible syntropy, which is given by Eq.(5.33): $\alpha_0 = \min(1 - \sigma_0, \sigma_0) \gamma_0 R_0 N_R$. Fixing α_0 allows us to obtain a syntropy matrix A that only depends on²⁹ σ_0 and G . Because σ_0 is kept fixed throughout

²⁸We saw *a posteriori* that this decision may have non negligible consequences. More on that in the following Sections.

²⁹Technically, A also depends on N_R but N_R is completely determined by the shape of G .

this study, we only need to compute one optimal A -matrix for each consumption matrix G . Finally, the algorithm we use needs to have the connectance of its output matrix as an input; so we choose that the optimal A -matrix has the connectance of G . For each consumption matrix G , the specific A obtained through that MCMC minimization procedure will be referred to as the “LRI matrix” of G or similar expressions.

Outcome of the MCMC algorithm

As explained above, the LRI MCMC algorithm should give us a syntropy matrix that both limits intraspecific syntropy and such that for every couple of different resources (μ, ν) , the number of species that consume both μ and ν is proportional to the number of species that consume μ and release ν . Since the connectance and the dimensions of A are fixed, the number of links of A is already decided and the algorithm simply determines how to optimally distribute them. Figure 3.2.2 shows that typically the algorithm will put links in a cell (μ, i) if (i, μ) is zero, meaning that not only intraspecific syntropy tries to be avoided but also species that consume a lot of resources will tend to release few of them and vice-versa.

Figure 3.2.3 shows that indeed we obtain for a given G matrix a syntropy matrix A such that the two requirements above are satisfied as best as possible. As expected, the algorithm works better for matrices with a low connectance. It is worth noticing that this procedure produces highly nested syntropy matrices (Fig.3.2.4) where only a few species produce most of the syntrophic flow. The obtained matrices have an even larger nestedness if we increase the number of resources.

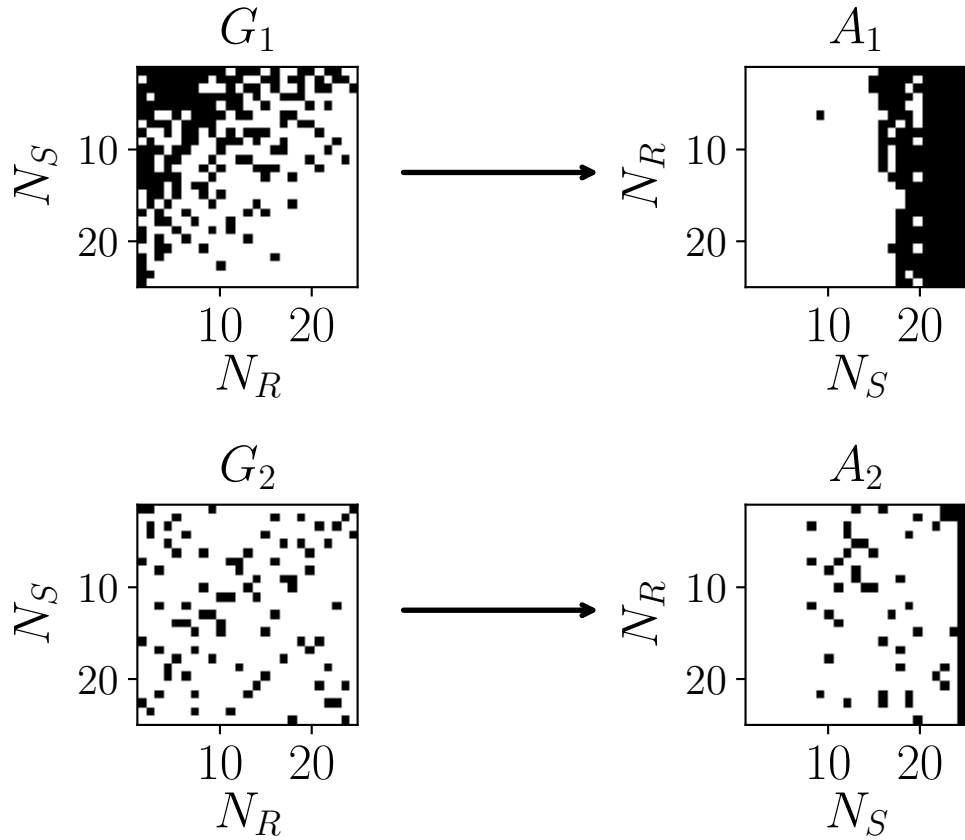


Figure 3.2.2: Typical shape of the consumption G_i and syntropy A_i matrices for $i = 1, 2$ systems. The white cells symbolize a zero matrix element and the black cells, a one. A_i here is the outcome of the LRI MCMC algorithm described in Section 3.2.2. The first row has a consumption matrix with $\eta_1 = 0.6$ and $\kappa_1 = 0.32$, the algorithm gives rise to a syntropy matrix with same connectance and ecological overlap ≈ 0.85 . The second row has G_2 with $\eta_2 = 0.1$ and $\kappa_2 = 0.13$ and the corresponding syntropy matrix A_2 has ecological overlap ~ 0.43 . We observe that under this optimization, species that consume few resources end up releasing many and the other way around.

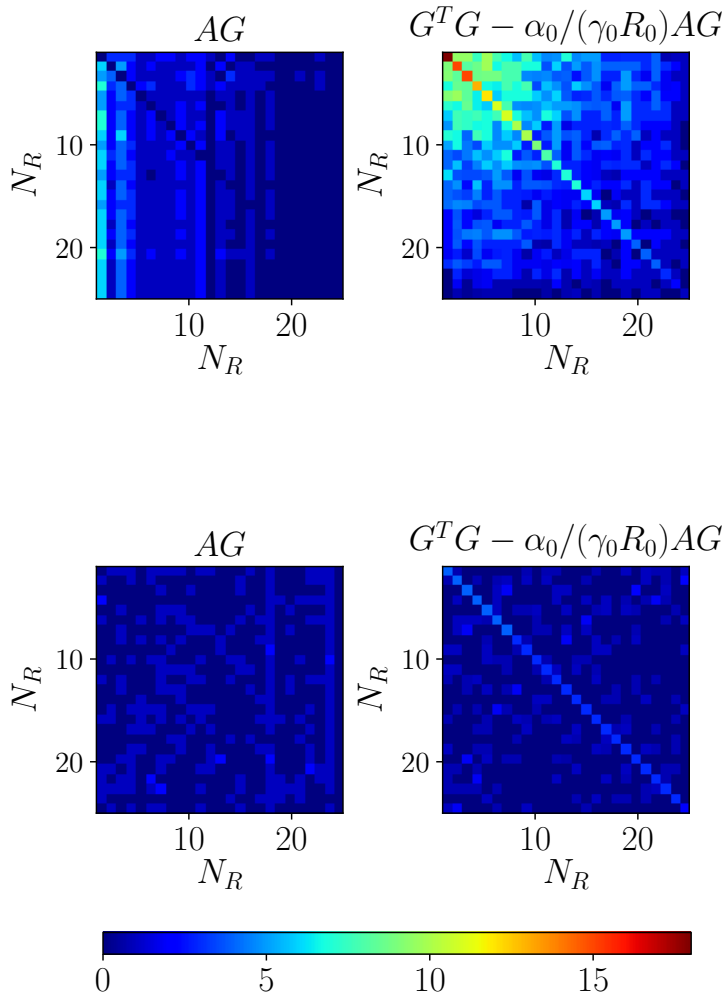


Figure 3.2.3: Plotting of AG and $G^T G - \alpha_0 / (\gamma_0 R_0) AG$. The A and G matrices of the first and second rows correspond to the respective A and G of Figure 3.2.2. As expected, we obtain an A such that intraspecific syntrophy is limited (the diagonal of AG is roughly zero) and, outside the diagonal, $G^T G - \alpha_0 / (\gamma_0 R_0) AG \approx 0$. The algorithm tries to minimize as much as it can the off-diagonal elements of $G^T G - \alpha_0 / (\gamma_0 R_0) AG$, even though this is not always possible (probably because the connectance of A is fixed). Both relations are better satisfied for consumption (and hence syntropy) matrices with a low connectance.

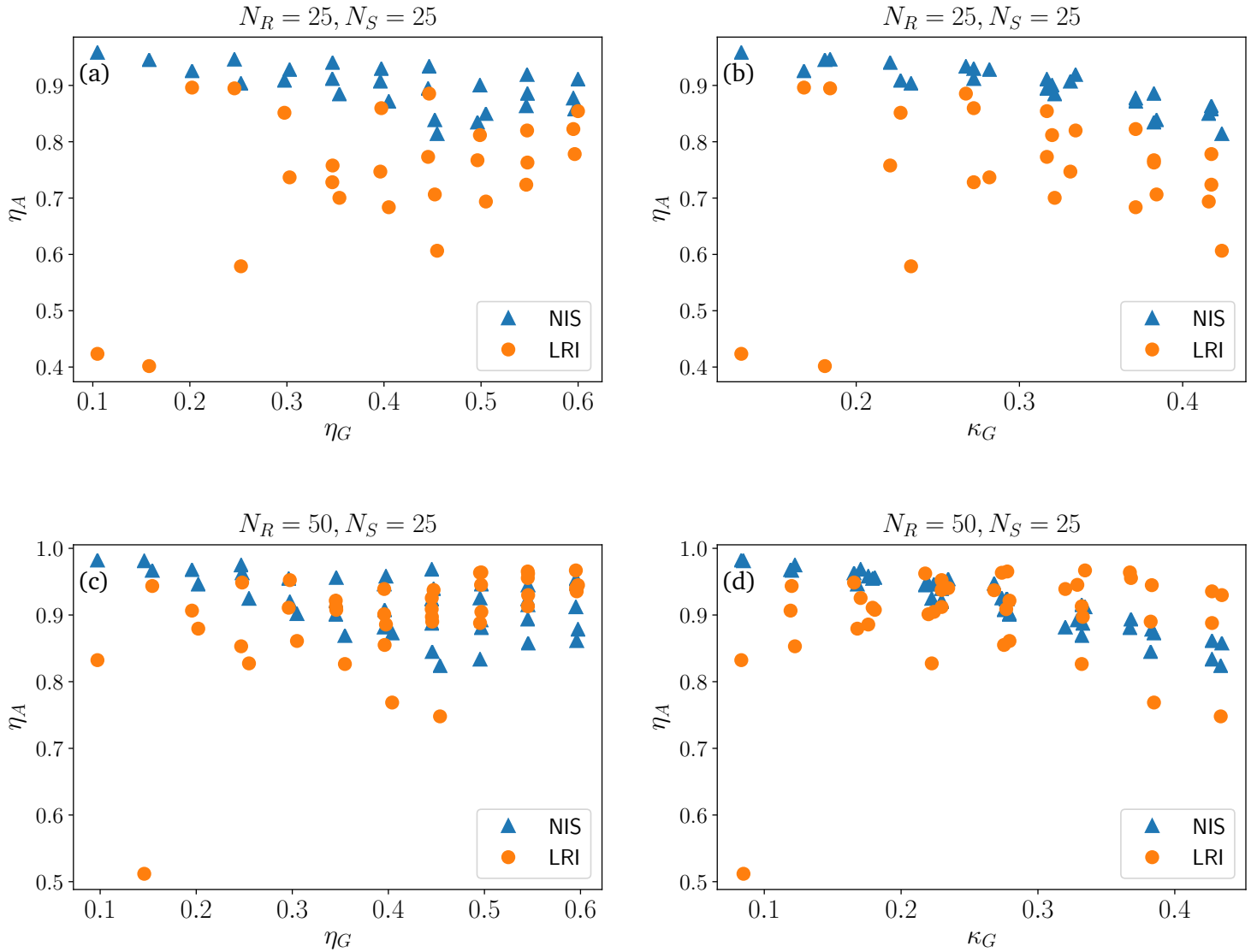


Figure 3.2.4: Properties of the syntropy matrix against the consumption matrix in the LRI regime. (a)-(c) Ecological overlap of A as a function of the ecological overlap of G for $N_S = 25$ and $N_R = 25$ (a) or $N_R = 50$ (c). (b)-(d) Ecological overlap of A as a function of the connectance of G for $N_S = 25$ and $N_R = 25$ (b) or $N_R = 50$ (d). The nestedness of the NIS regime is also plotted as a matter of comparison. As η_G or κ_G increases, the two results will give matrices with similar properties.

3.2.3 General numerical observations

We observed in Section 3.1.2 that, for all $(G, A) \in S_{25}$, at fixed α_0 the metaparameters feasibility function $\mathcal{F}(m, G, A)$ has a typically sharp transition from fully feasible ($\mathcal{F} = 1$) to fully unfeasible ($\mathcal{F} = 0$) regimes in the (γ_0, S_0) plane. Figure 3.2.5 shows that a similar although more complicated behaviour is observed in the case of the dynamical stability function $\mathcal{D}_L((\gamma_0, S_0, \alpha_0), G, A)$. On one hand, the (γ_0, S_0) plane is split in two distinct zones, which are also separated by a very narrow boundary. The first zone is characterized by complete dynamical instability, *i.e.* $\mathcal{D}_L = 0$. On the other hand, the second zone is not described by full dynamical stability, but rather *almost* full dynamical stability: \mathcal{D}_L is very close to but not always exactly equal to 1. The consequence is that the fully dynamically stable region $\mathcal{D}_{L,1}^{G,A}$ will be very patchy (Fig.3.2.7).

That patchiness could come from purely numerical effects: \mathcal{D}_L is estimated by generating parameters sets and counting the proportion that is dynamically stable, which inevitably leads to an uncertainty on \mathcal{D}_L that could explain the patchiness. This conjecture would hint that most of the points are almost dynamically stable – for the ones where $\mathcal{D}_L = 1$, we simply would not have run enough systems to observe the very rare unstable ones. However that explanation would not justify *why* we do not have full dynamical stability.

It has been shown for other models [32] that the regime $N_R = N_S$ leads to critical phenomena in communities, which may be linked to ongoing debates about the competitive exclusion principle mentioned above. We here also have the same number of consumers and resources and therefore think that the fact that we observe systems very close to full dynamical stability is an indicator of a similar underlying criticality of our model. That is the reason why we focus our attention on such points.

3.2.4 Fully dynamically stable region

The same way we studied the fully feasible volume $\mathcal{F}_1^{G,A}(\alpha_0)$, we investigate now the behaviour of its special subset, the locally fully dynamically stable region $\mathcal{D}_{L,1}^{G,A}(\alpha_0)$, which is defined³⁰ as

$$\mathcal{D}_{L,1}^{G,A}(\alpha_0) \equiv \left\{ (\gamma_0, S_0) : (\gamma_0, S_0, \alpha_0) \in \mathcal{D}_{L,1}^{G,A} \right\}. \quad (3.41)$$

Intuitively, $\mathcal{D}_{L,1}^{G,A}(\alpha_0)$ corresponds to the set of all (γ_0, S_0) such that $\mathcal{A}((\gamma_0, S_0, \alpha_0), G, A)$ is a feasible, locally dynamically stable parameters set with probability 1. Since we require $\mathcal{A}((\gamma_0, S_0, \alpha_0), G, A)$ to be feasible, it is clear that $\mathcal{D}_{L,1}^{G,A}(\alpha_0)$ is indeed a subset of $\mathcal{F}_1^{G,A}(\alpha_0)$.

As a naive approach, one could take a look at the *common fully locally dynamically stable region* $\mathcal{D}_{L,1}^{S_{25}}$, which is the intersection of the $\mathcal{D}_{L,1}^{G,A}(\alpha_0) \forall (G, A) \in S_{25}$ (Figure 3.2.6). However, as said before, because of the patchy and heterogeneous nature of each $\mathcal{D}_{L,1}^{G,A}(\alpha_0)$, we observe a very fractured and small common fully locally dynamically stable region, which is the same for all structures of A considered. It has a non-zero volume for $\alpha_0 = 0$, but for the next point investigated $\alpha_0 = 1.3 \times 10^{-3}$, no point is fully locally dynamically stable for every matrix considered, which means that the critical common syntropy is

³⁰A formal definition of $\mathcal{D}_{L,1}^{G,A}$ is provided in Section 1.4.3.

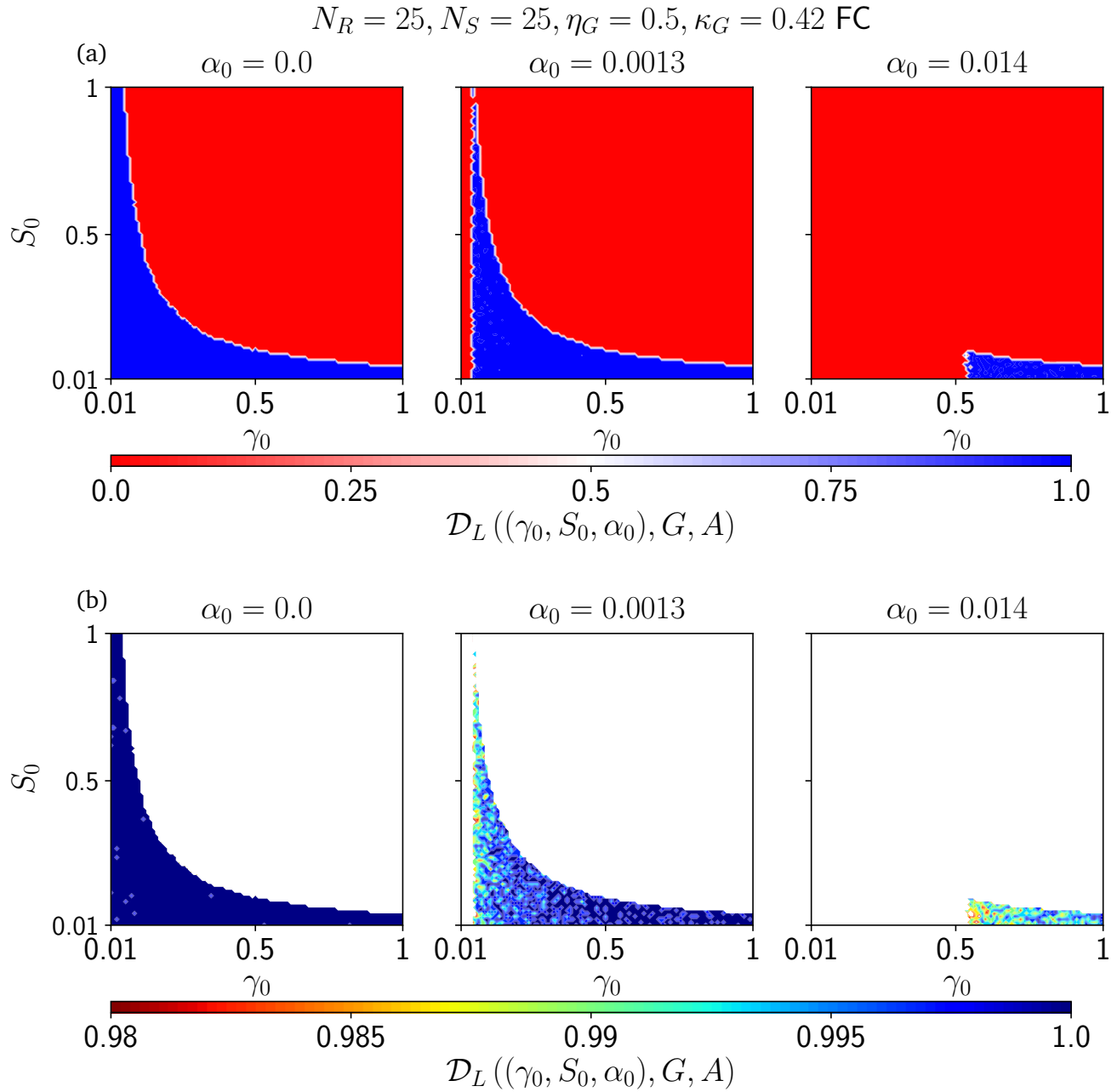


Figure 3.2.5: Typical color plot local dynamical stability metaparameters function \mathcal{D}_L . for microbial communities with $\eta_G = 0.5$ and $\kappa_G = 0.42$. The color bar indicates the value of $\mathcal{D}_L ((\gamma_0, S_0^0, \alpha_0), G, A)$ with A fully connected. Although at first sight, the plane is divided in two zones, one where $\mathcal{D}_L = 0$ and another where $\mathcal{D}_L \approx 1$ (the red and blue regions, respectively, in (a)), upon further notice (b), it turns out the $\mathcal{D}_L \approx 1$ region is very patchy: we observe many $(\gamma_0, S_0^0, \alpha_0)$ configurations for which \mathcal{D}_L is very close but not exactly equal to 1. These points are almost fully dynamically stable.

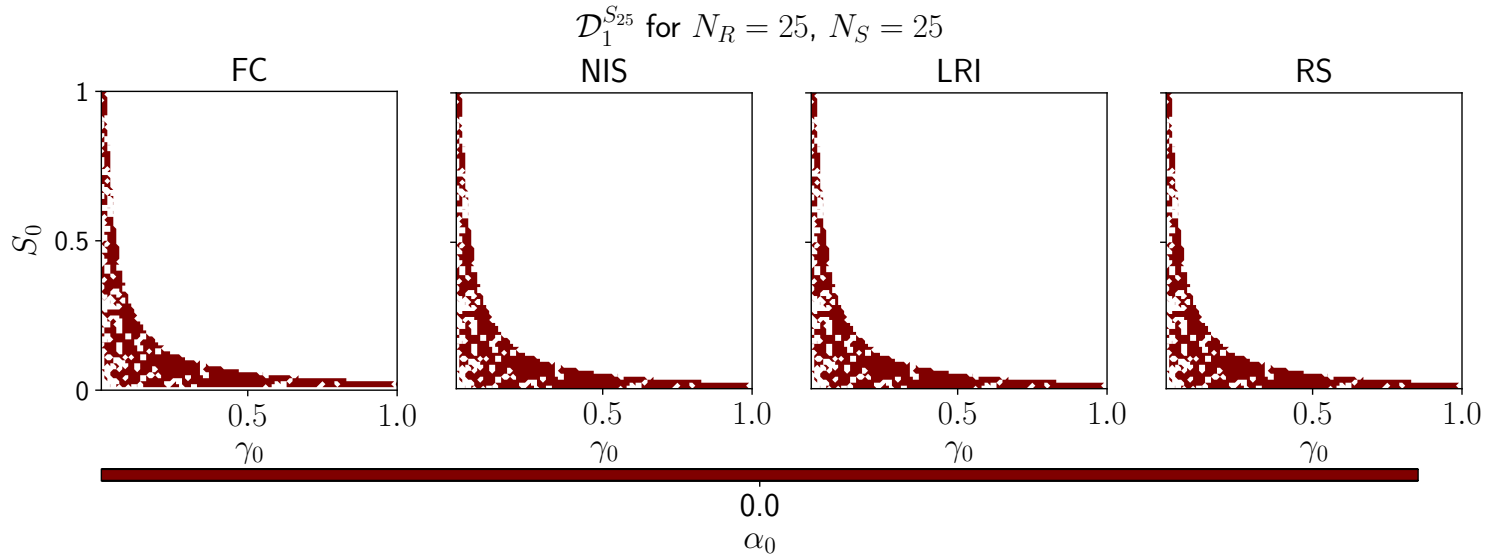


Figure 3.2.6: Common full local dynamical stability volume for the four different A structures considered. The points colored in dark red give rise to locally dynamically stable systems with probability 1 for all the matrices considered. Very few spots verify this property when there is no syntrophic interaction, and no point gives rise to a fully dynamically stable system for $\alpha_0 = 1.3 \times 10^{-3}$. This is independent of the structure of A that we chose. The white points never give rise to fully dynamically stable systems.

smaller than this. This means that we have to consider the impact of syntropy on each consumption-network individually.

As we saw, $\mathcal{D}_{L,1}^{G,A}(\alpha_0)$ is geometrically more complex than $\mathcal{F}_1^{G,A}(\alpha_0)$ (Figure 3.2.7) because of the *almost* fully dynamically stable points. It may sometimes have holes, even without syntropy, and sometimes not, even for matrices that are topologically very close. Compare for instance Fig.3.2.7a with Fig.3.2.7c, these two networks have the same ecological overlap, but even though their connectance is very similar, their fully locally dynamically stable regions have a very different shape: one of them can sustain only a tiny bit of syntropy before becoming dynamically unstable (Fig.3.2.7a) while the second can endure basically any feasible syntrophic interaction (Fig.3.2.7c).

However, we can still note a general trend among matrices: points with a larger γ_0 and a smaller S_0 tend to remain dynamically stable as shows Figure 3.2.8. As an aside, note that on this figure the sudden drop of $\langle\gamma_0\rangle_D$ (and rise of $\langle S_0 \rangle_D$) at $\alpha_0 = 9.1 \times 10^{-3}$ is a finite-size effect. Indeed we only monitor points in the unit square $[0, 1]^2$, such that the (G, A) for which the center of $\mathcal{D}_{L,1}^{G,A}(\alpha_0)$ leave that zone at $\alpha_0 = 9.1 \times 10^{-3}$ do not contribute to $(\langle\gamma_0\rangle_D, \langle S_0 \rangle_D)$ anymore. Only the (G, A) which previously had a lower, resp. higher, contribution to $\langle\gamma_0\rangle_D$, resp. $\langle S_0 \rangle_D$, are taken into account, which results in that strange behaviour. The fact that $\langle\gamma_0\rangle_D$ continues to increase (and $\langle S_0 \rangle_D$ to decrease) after that point corroborates that reasoning.

The question is then: why do other points lose their dynamical stability? Is it because they become unfeasible, or do they remain feasible but become dynamically unstable? To answer that question, we quantify for each network $(G, A) \in S_{25}$ the *probability of being dynamically stable when feasible*, denoted $\text{Prob}(\mathcal{D}_L | \mathcal{F})(G, A, \alpha_0)$. That quantity, for-

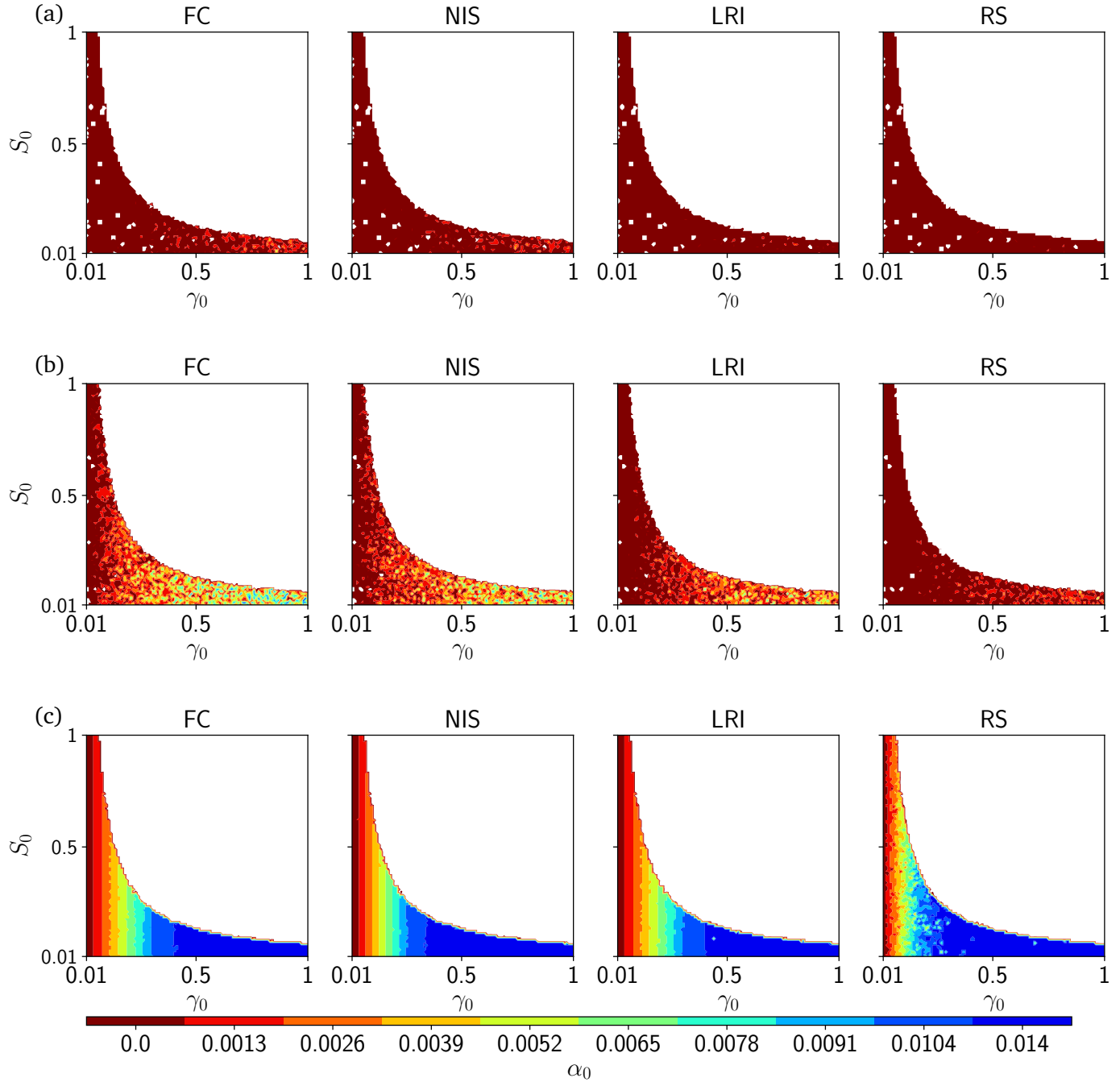


Figure 3.2.7: Fully locally dynamically stable region $\mathcal{D}_{L,1}^{G,A}$ as a function of syntropy for different matrices G and the four scenarios of A . The white zone corresponds to points that are never fully locally dynamically stable. The colour of a given point tells until which syntropy that point is fully locally dynamically stable, e.g. a green point is fully locally dynamically stable for $0 \leq \alpha_0 \leq 6.5 \times 10^{-3}$. Row (a) corresponds to G with $\eta_G = 0.35$ and $\kappa_G = 0.23$, (b) has $\eta_G = 0.35$ and $\kappa_G = 0.33$ and (c) $\eta_G = 0.35$ and $\kappa_G = 0.28$. Even at fixed ecological overlap, different connectances of G give rise to systems which can have very different fully dynamically stable regions.

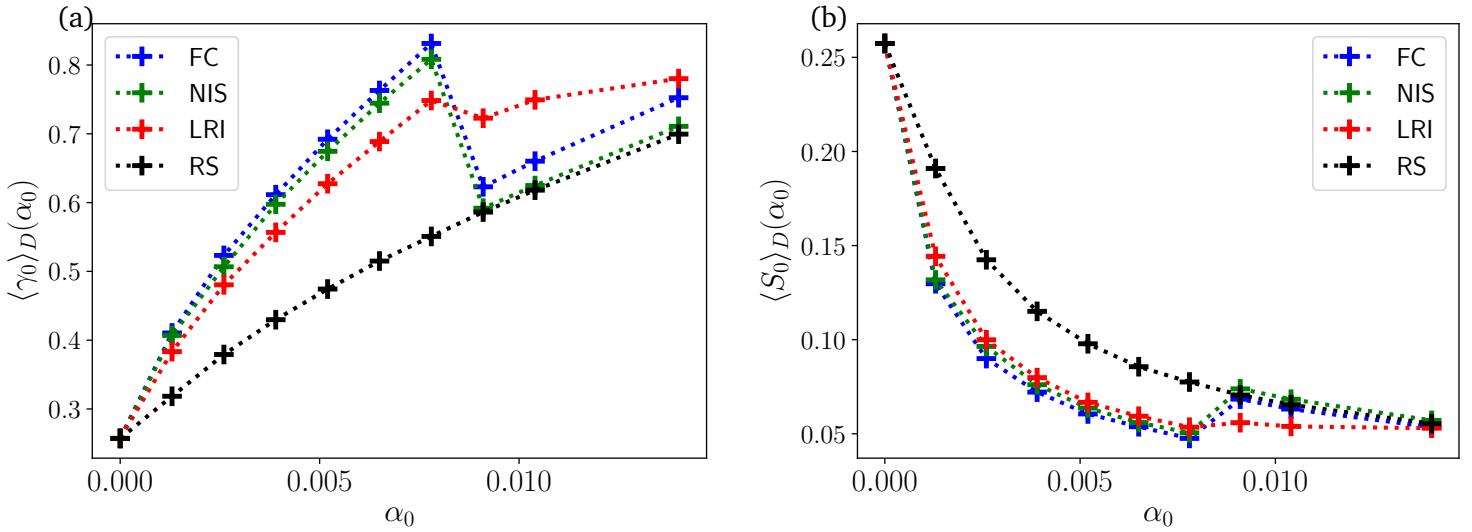


Figure 3.2.8: (a) Average consumption rate $\langle \gamma_0 \rangle_D(\alpha_0)$ and (b) average resource abundance equilibrium $\langle S_0 \rangle_D$ as a function of syntropy (α_0). A formal definition of $(\langle \gamma_0 \rangle_D, \langle S_0 \rangle_D)$ is provided in Section 5.1.1). Intuitively, $(\langle \gamma_0 \rangle_D, \langle S_0 \rangle_D)$ represents the center (γ_0, S_0) point of $\mathcal{D}_{L,1}^{G,A}(\alpha_0)$, averaged over all matrices $(G, A) \in S_{25}$, or as we call it the “center of dynamical stability”. As syntropy increases, only points with a large consumption rate and a small resource abundance at equilibrium remain dynamically stable.

mally defined in Section 5.1.1, has a straightforward interpretation: if for a certain (G, A) , $\text{Prob}(\mathcal{D}_L | \mathcal{F})(G, A, \alpha_0) = x$, then a feasible $(\gamma_0, S_0, \alpha_0)$ has on average a chance x to be dynamically stable³¹. Figure 3.2.9 shows that $\text{Prob}(\mathcal{D}_L | \mathcal{F})(G, A, \alpha_0) < 1 \forall (G, A) \in S_{25}$ and $\forall \alpha_0 \geq 0$. That result has a very important biological consequence: there is no consumption-syntropy network which guarantees that all feasible systems are dynamically stable, *i.e.* there can always exist feasible but dynamically unstable microbial communities³².

Similarly to what was done for feasibility in Section 3.1.3, we can measure the local dynamical stability volume (see Section 5.1.1) $\text{Vol}(\mathcal{D}_{L,1}^{G,A}(\alpha_0))$ of each consumption-syntropy network (G, A) . $\text{Vol}(\mathcal{D}_{L,1}^{G,A}(\alpha_0))$ tells us what proportion of the unit square is occupied by dynamically stable (γ_0, S_0) points and is therefore an indicator of how well communities can sustain an increase of average syntrophic strength α_0 . Figure 3.2.10 shows that the dynamically stable volume typically decays in an exponential-like fashion. We follow the same line of reasoning as Section 3.1.3, and, to quantify that decay, define the *dynamical stability decay rate* $d_D(G, A)$ of a consumption-syntropy network (G, A) . It is obtained numerically by finding through a non-linear regression the coeffi-

³¹More precisely, there is a chance x that a parameters set $\mathcal{A}((\gamma_0, S_0, \alpha_0), G, A)$, which we know is feasible, is also dynamically stable.

³²This does not mean they will survive, of course, since they may vanish at any small perturbation. However it means that there is no physical law that hinders their existence: they can exist, and could appear *e.g.* through random mutations.

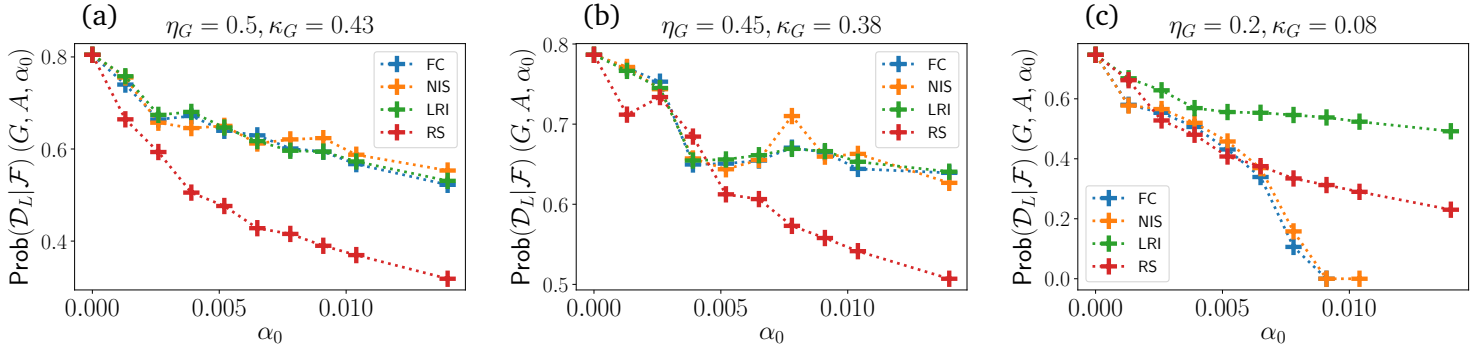


Figure 3.2.9: Plot of the probability that a feasible microbial community is dynamically stable for different consumption-syntropy networks (G, A) . The different lines on the same subplot show the four different A -scenarios. The results differ with the consumption matrix considered: (a) $\eta_G = 0.5$, $\kappa_G = 0.43$, (b) $\eta_G = 0.45$, $\kappa_G = 0.38$ and (c) $\eta_G = 0.2$, $\kappa_G = 0.08$.

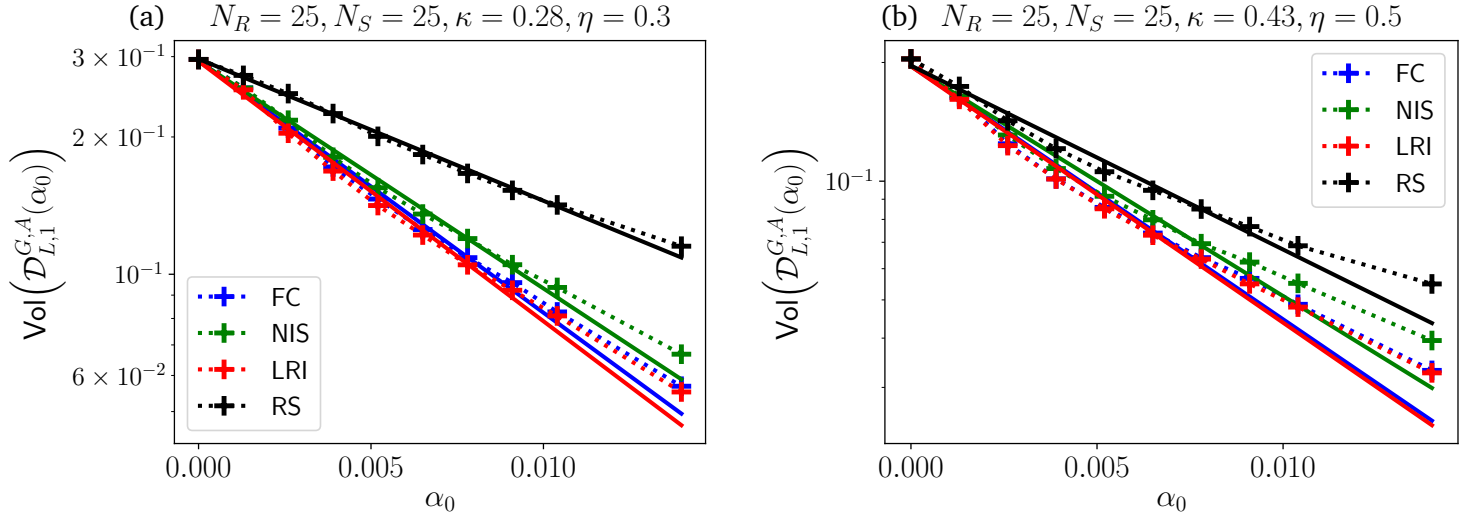


Figure 3.2.10: Evolution of the dynamically stable volume $\text{Vol}\left(\mathcal{D}_{L,1}^{G,A}(\alpha_0)\right)$ (see Section 5.1.1) with α_0 for different $(G, A) \in S_{25}$ (plotted on a logarithmic scale). (a) $\eta_G = 0.3$ and $\kappa_G = 0.28$, (b) $\eta_G = 0.5$ and $\kappa_G = 0.43$. The cross-shaped points indicate the data as measured numerically while the solid lines are the corresponding exponential fit (see main text). The four colors indicate the four A -scenarios considered. Independently of the (G, A) network, fewer points are dynamically stable as syntropy increases.

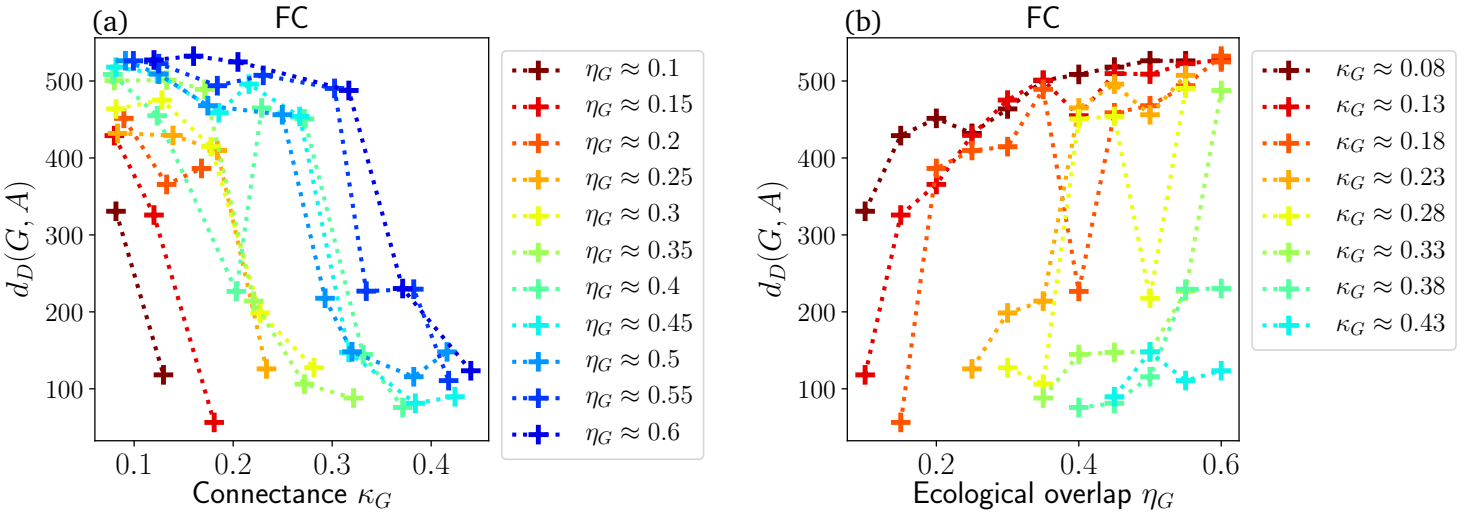


Figure 3.2.11: Dynamical stability decay rate $d_D(G, A)$ for the A -matrix fully connected (FC scenario) and every $G \in G_{25}$, (a) as a function of connectance κ_G for fixed ecological overlap η_G and (b) as a function of ecological overlap for fixed connectance. The trend confirms previous observations: at fixed ecological overlap, a microbial community with a more connected consumption matrix will sustain a larger syntropy (i.e. have a smaller decay rate) and at fixed connectance, systems with a small ecological overlap remain dynamically stable as syntropy grows.

cients $c_1, c_2, d_D \in \mathbb{R}^+$ that satisfy best the relation:

$$\text{Vol} \left(\mathcal{D}_{L,1}^{G,A}(\alpha_0) \right) \approx c_1 \exp(-d_D \alpha_0) - c_2. \quad (3.42)$$

Much like for the corresponding discussion in the case of feasibility, $d_D(G, A)$ is an indicator of how well a consumption-syntropy network (G, A) can sustain syntropy while remaining dynamically stable: a smaller $d_D(G, A)$ indicates a more robust network (it will take a larger syntropy to find unstable points), a larger $d_D(G, A)$ shows the network is weak against an increase in syntrophic interaction. Figure 3.2.11 shows how $d_D(G, A)$ changes as a function of the characteristics of the consumption matrix G , $\forall G \in G_{25}$, when the syntropy matrix is fully connected. A clear trend may be seen: in order to avoid losing dynamical stability when syntropy is increased, a microbial community should either increase the number of average resources eaten by each consumer (i.e. increase the connectance of the consumption matrix) or decrease its ecological overlap, which means that consumers should stop eating from the same resources. Figure 3.2.12 shows how $d_D(G, A)$ changes for each matrix as different syntropy regimes are considered. The following comments can be made³³:

- The NIS scenario slightly lowers the dynamical stability decay rate. It decreases it by $\sim 5 - 15\%$, except in the case $\kappa_G = 0.18, \eta_G = 0.15$, where $d_D(G, A)$ is decreased by $\sim 30\%$.
- The LRI scenario improves ($>\sim 50\%$) the dynamical stability for consumption matrices with a very low connectance. On average, the lower the connectance, the greater

³³In the following, we use terms like “is better”, “outperforms” or “improves the dynamical stability” as a way of saying “lowers the dynamical stability decay rate compared to the FC case”.

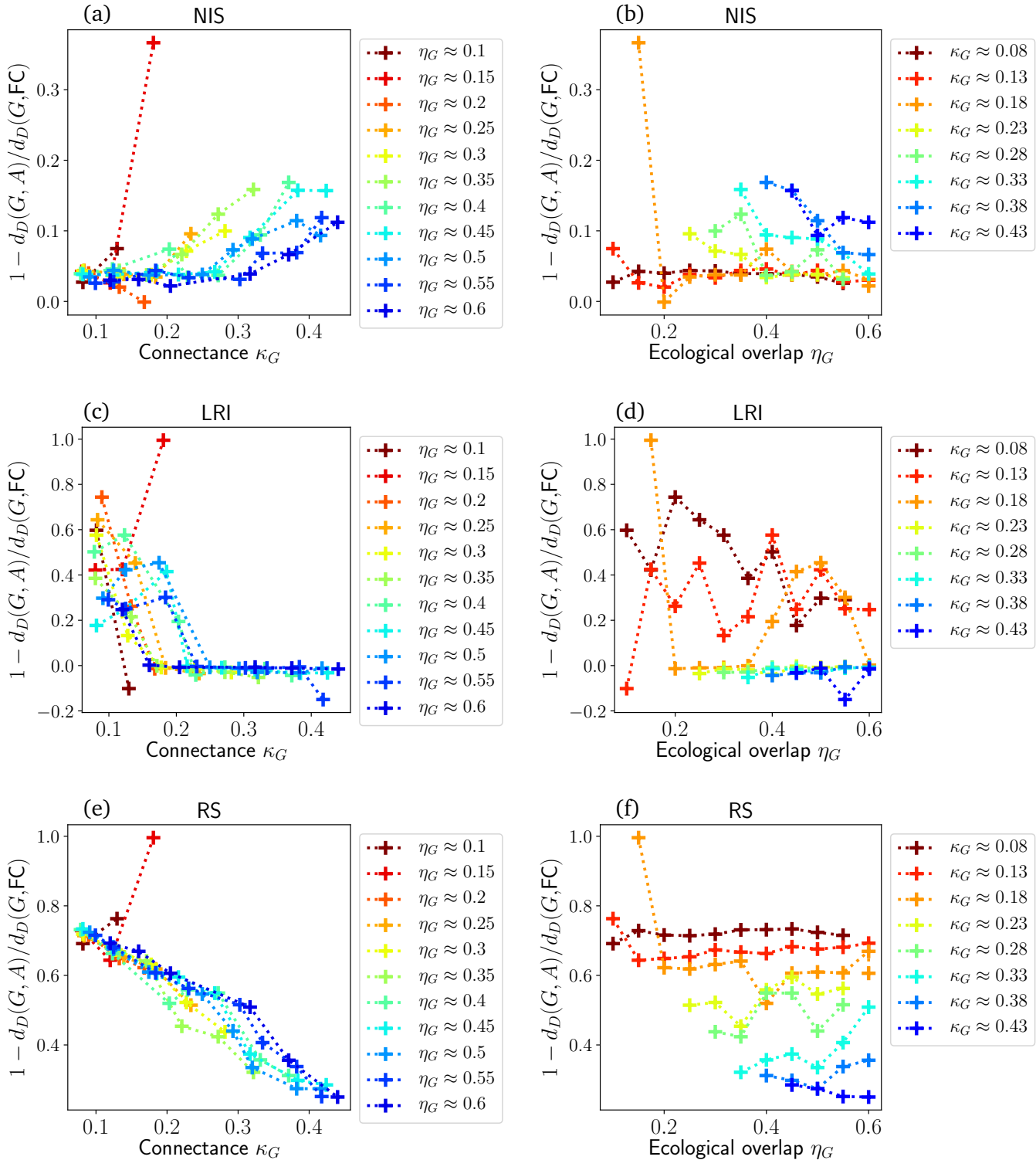


Figure 3.2.12: Relative difference of the dynamical stability decay rate between the FC scenario and the NIS (Figs. a and b), LRI (c and d) and RS (e and f) scenarios. Positive y-values indicate a smoother decay for the considered scenario compared to the FC case. It therefore can sustain higher syntropy values while remaining dynamically stable.

the improvement. However, for larger connectances, it does not change $d_D(G, A)$ in any way.

- The RS scenario offers the best improvement: any consumption matrix we considered got a considerably better result (at least $>\sim 20\%$). At fixed connectance, the improvement is the same for every ecological overlap considered and the lower the connectance the better the improvement.

Overall, dynamical stability follows the same trend as feasibility – compare the striking similarity between Figure 3.1.7 and 3.2.12. Note that the LRI and RS scenarios offer a more significant improvement the lower the connectance of the consumption matrix. Because both have a syntropy matrix whose connectance is equal to the one of the consumption matrix, this suggests that microbial communities which have very few syntrophic interactions (*i.e.* A has a low connectance) can remain dynamically stable with a larger average syntrophic interaction than others. Because the random structure (RS) scenario is, for a given matrix, a better improvement than LRI, we think that the syntropy matrix should also have a lower syntrophic overlap, *i.e.* a low nestedness³⁴.

3.2.5 Largest eigenvalue of the Jacobian

By studying the very simplified case of a microbial community where both G and A are fully connected and there is no variance in the parameters, we may find after long computations detailed in Section 2 a condition on the metaparameters that promotes dynamical stability:

$$4N_R\sigma_0\gamma_0S_0(\alpha_0 - \gamma_0R_0) + \frac{l_0^2}{R_0^2} + \frac{2N_S\alpha_0S_0l_0}{R_0^2} + \frac{N_S^2\alpha_0^2S_0^2}{R_0^2} \ll 1. \quad (3.43)$$

The smaller the LHS of Eq.(3.43), the smaller the non-zero real parts of the spectrum of the Jacobian, so the greater the dynamical stability. Although strictly speaking that relation is only valid for the case where both G and A are fully connected, we expect it to work too when G and A are *not too far away* from the fully connected case. It tells us that in order to get more local dynamically stable systems we should³⁵:

- Decrease N_S or α_0 .
- If $\alpha_0 - \gamma_0R_0 < 0$, increase N_R , σ_0 and γ_0 .
- Be careful in how S_0 is handled: Section 2 shows that at very low syntropy, we should increase S_0 but decrease it when α_0 becomes very large. Since in practice the observed feasible α_0 are fairly low, we should increase S_0 as much as possible.

Combining these considerations with the feasibility conditions Eq.(3.3) we expect that – for all other metaparameters fixed – systems get more and more locally dynamically stable as γ_0 is increased and S_0 is taken at its largest feasible value. In short, points at the upper border of $\mathcal{D}_{L,1}^{G,A}(\alpha_0)$ should have a lower $\text{Re}(\lambda_1)$ as γ_0 increases. Figure 3.2.14 shows that indeed that trend is observed. This tells us that if we keep the consumption flux $N_S\gamma_0S_0$

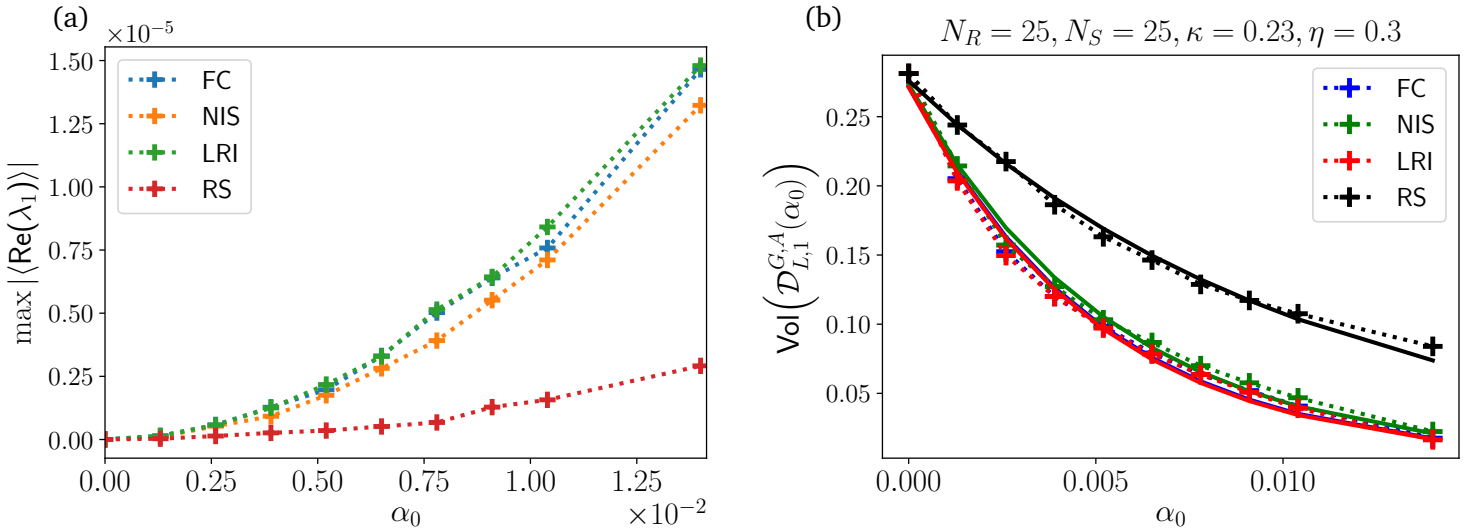


Figure 3.2.13: For a consumption matrix G with $\eta_G = 0.3$ and $\kappa_G = 0.23$. (a) Evolution of the maximal $|\langle \text{Re}(\lambda_1) \rangle|$ observed in the $(\gamma_0, S_0) \in [0, 1]^2$ region. The maximal eigenvalue increases in magnitude, making the system more dynamically stable, as syntropy increases. That trend is observed for all matrices we considered. (b) Volume of $\mathcal{D}_{L,1}^G(\alpha_0)$. As syntropy increases, fewer and fewer points become fully dynamically stable. The different structures of the syntropy matrix are indicated with different colours.

constant, increasing γ_0 (and hence decreasing S_0) will give rise to more stable systems in the sense that they will recover from changes in the abundance of resources and consumers quicker. Notice that contrarily to the prediction made above, increasing α_0 does not decrease stability but increases the maximal $|\text{Re}(\lambda_1)|$ observed as shows Fig.3.2.13a. That is coupled with the already discussed shrinkage of the fully locally dynamically stable volume seen on Fig.3.2.13b. This means that overall increasing syntropy makes the system *more stable* but at *fewer points*. This hints that systems in a high syntrophic regime, where consumers produce a lot of resources, should be very fine tuned and occur for very specific consumption strength and average abundance of consumers.

³⁴Indeed, the LRI regime has a significantly more nested syntropy matrix compared to RS (Fig.3.2.4). At equal connectance, A with the lower nestedness provides a better improvement.

³⁵We do not focus on how R_0 and l_0 should be changed because they are always equal to 1 for our study of feasibility and local dynamical stability.

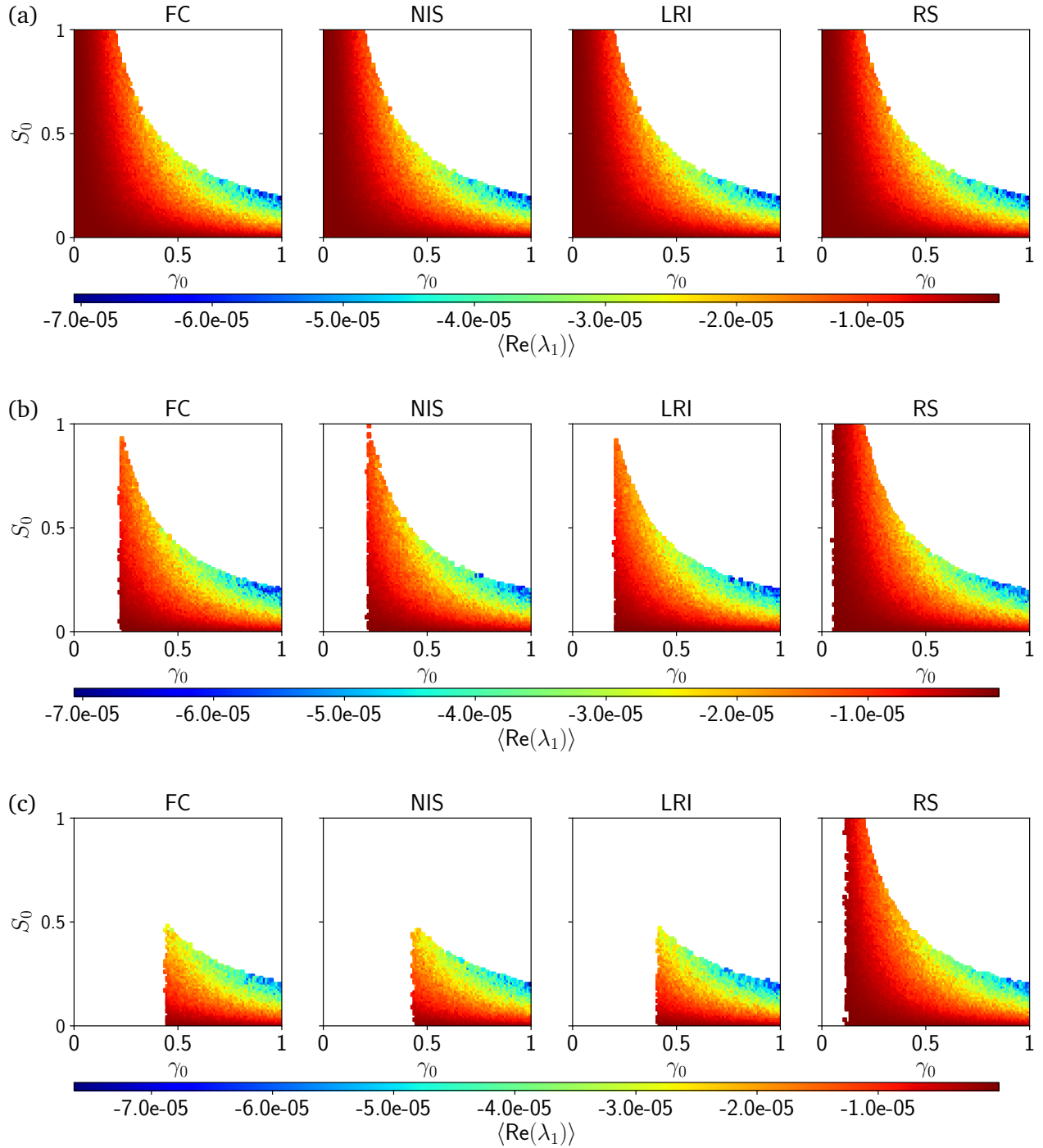


Figure 3.2.14: Largest real eigenvalue $\text{Re}(\lambda_1)$ averaged over 200 realizations for each (γ_0, S_0) points for the consumption matrix G with consumers overlap $\eta_G = 0.1$ and connectance $\kappa_G = 0.13$. The white points correspond to not fully dynamically stable systems. Each row corresponds to a different syntropy value (a) $\alpha_0 = 0$ (no syntrophic interaction), (b) $\alpha_0 = 3.9 \times 10^{-3}$ and (c) $\alpha_0 = 7.8 \times 10^{-3}$. The different columns correspond to the different A scenarios considered. As expected, the points close to the $S_0 \sim \gamma_0^{-1}$ boundary curve are the most stable in every situation. Points with a large γ_0 are the most stable of the unit square.

3.2.6 The influence of the matrix dimensions

As said above, because of Eq.(3.43), we expect dynamical stability to improve when the number of resources is increased and the number of consumers is kept fixed. It is therefore worth briefly studying what happens when the number of resources is doubled $N_R = 25 \rightarrow N_R = 50$ and every other metaparameter, as well as the number of consumers, keeps the same value as before.

Figure 3.2.15 shows that the effect of adding resources can be quite dramatic on the stability of the system. For that specific matrix for instance, adding resources allowed for a way larger $\mathcal{D}_{L,1}^{G,A}(\alpha_0)$ at each α_0 . This however does not hold for all networks. Figure 3.2.16 shows the difference in dynamical stability decay rates between the case $N_R = 50$ and $N_R = 25$. Doubling the number of resources has a very different effect on each matrix. On average the ratio between the two decay rates is 1 and it is not clear which parameter of the matrix topology decides whether stability will be improved or not.

We can also observe on Figure 3.2.15, that adding more resources seems to take away the patchiness of $\mathcal{D}_{L,1}^{G,A}(\alpha_0)$. We think that this effect happens for all matrices because the common fully locally dynamically stable region has a radically different shape. Indeed $\mathcal{D}_{L,1}^{S_{50}}(\alpha_0)$ is smoother than $\mathcal{D}_{L,1}^{S_{25}}(\alpha_0)$ and can sustain a non-zero syntropy (see the striking difference between Figure 3.2.6 and Figure 3.2.17). Recall that for $N_R = 25$, the critical common syntropy was between 0 and 1.3×10^{-3} . It is greatly improved for $N_R = 50$: up until between 1.04×10^{-2} and 1.4×10^{-2} (in the RS scenario). This supports the theory stated above that the patchiness of the system of the system observed at $N_R = N_S = 25$ is the effect of an underlying criticality that does not appear when the number of resources is larger than the number of consumers.

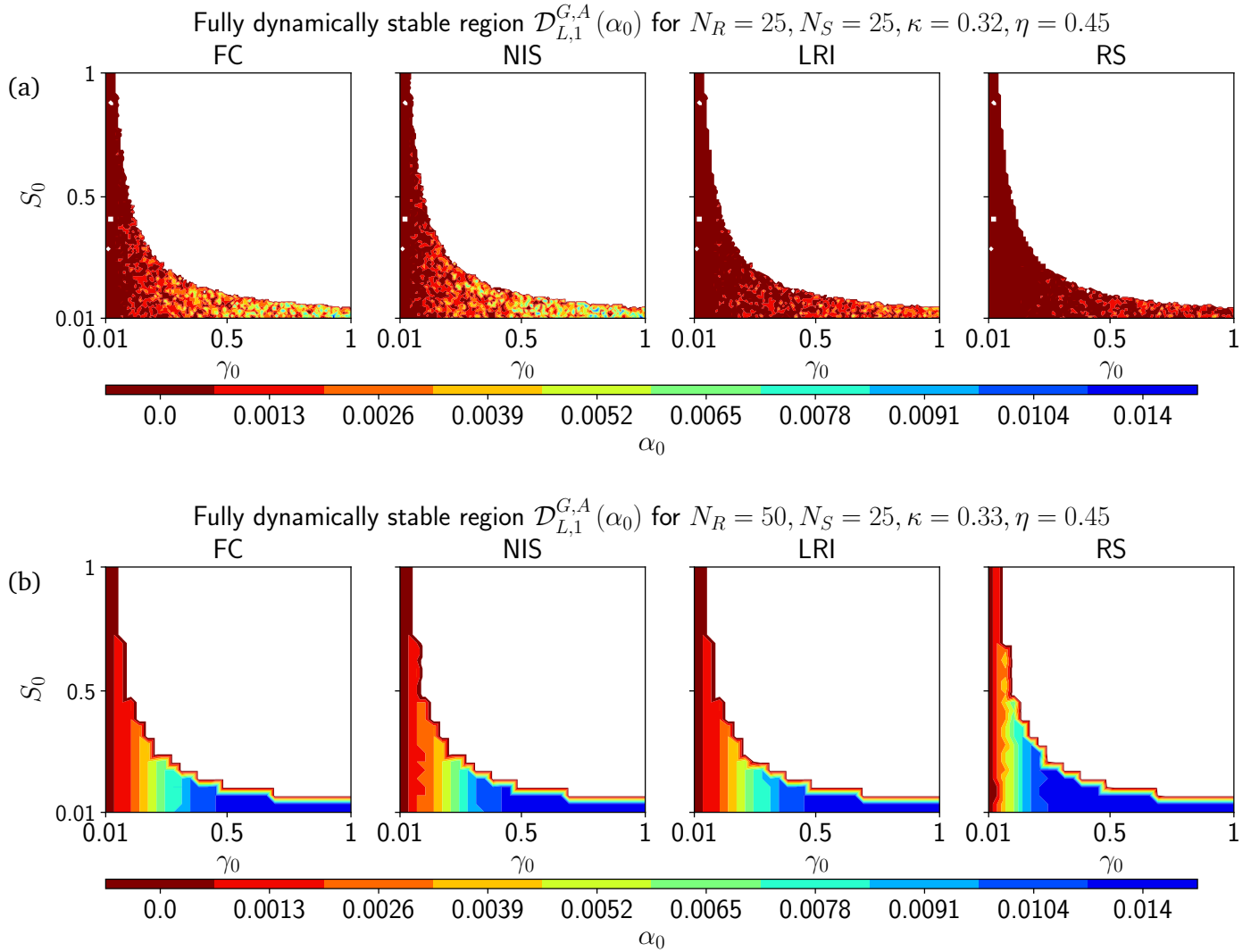


Figure 3.2.15: Fully dynamically stable region $\mathcal{D}_{L,1}^{G,A}$ with the four different structures of A considered. The two matrices considered have the same ecological overlap and connectance, only the number of resources changes. (a) G has $N_R = 25, N_S = 25$ and $\kappa_G = 0.33$ and $\eta_G = 0.45$. (b) G has $N_R = 50, N_S = 25$ and $\kappa_G = 0.33$ and $\eta_G = 0.45$. At $N_R = 50$, the typical fully dynamically stable region seems less disconnected. More points can sustain an increased syntropy for most of the matrices of the set.

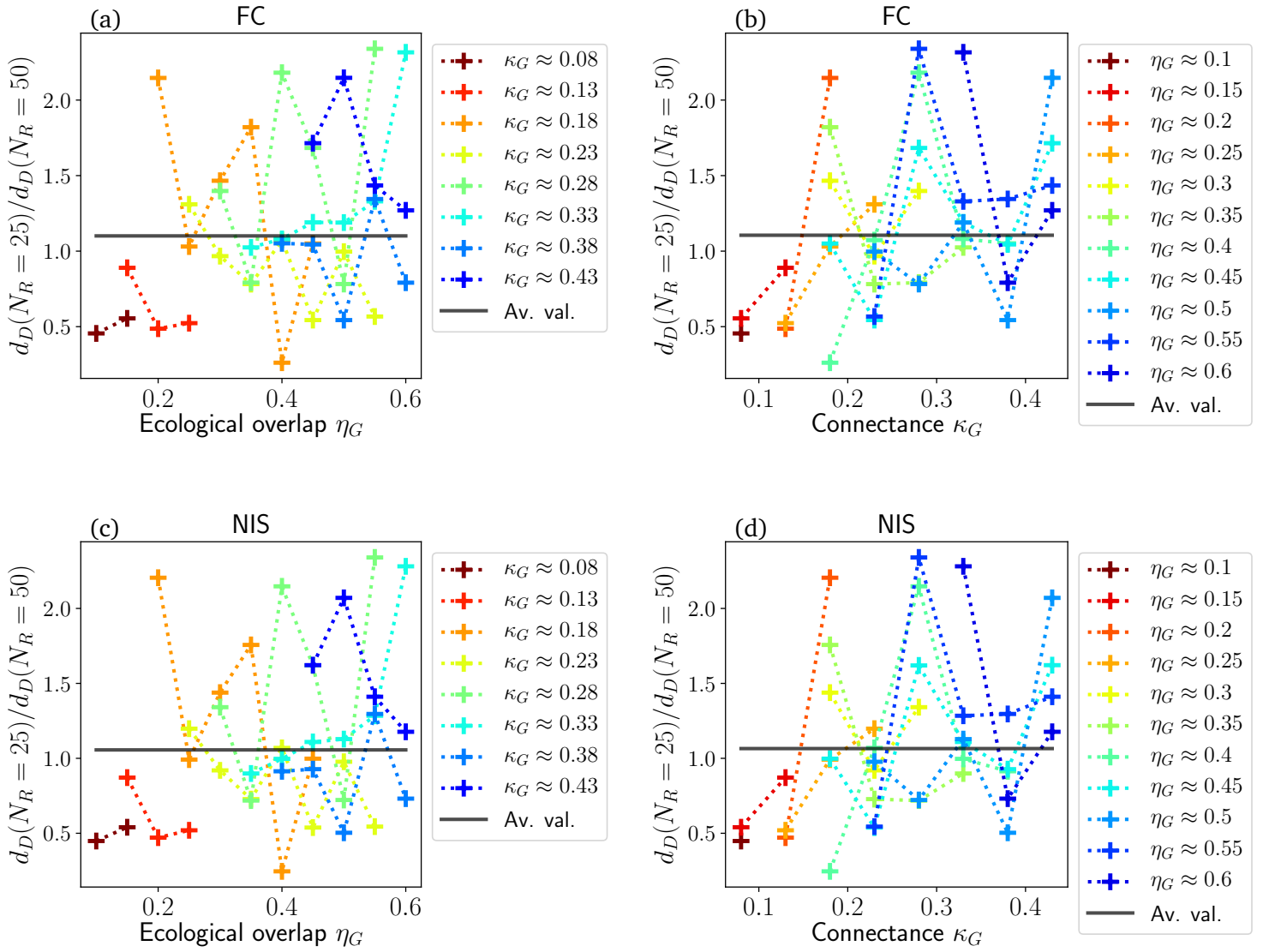


Figure 3.2.16: Ratio of the dynamical stability decay rates at $N_R = 25$ and at $N_R = 50$ as a function of the consumption matrix properties. A y -axis larger than 1 means $d_D(N_R = 25)$ is larger than $d_D(N_R = 50)$, which means the system remains “more” dynamically stable as syntrophic interaction is added at $N_R = 50$ compared to $N_R = 25$. We considered the four usual A scenarios (a)-(b) FC, (c)-(d) NIS, (e)-(f) LRI and (g)-(h) RS. Increasing the number of resources in the system does not allow microbial communities to be “more dynamically stable”, on average, as syntropy increases. Indeed the average ratio between the dynamical stability decay rates is very close to 1.

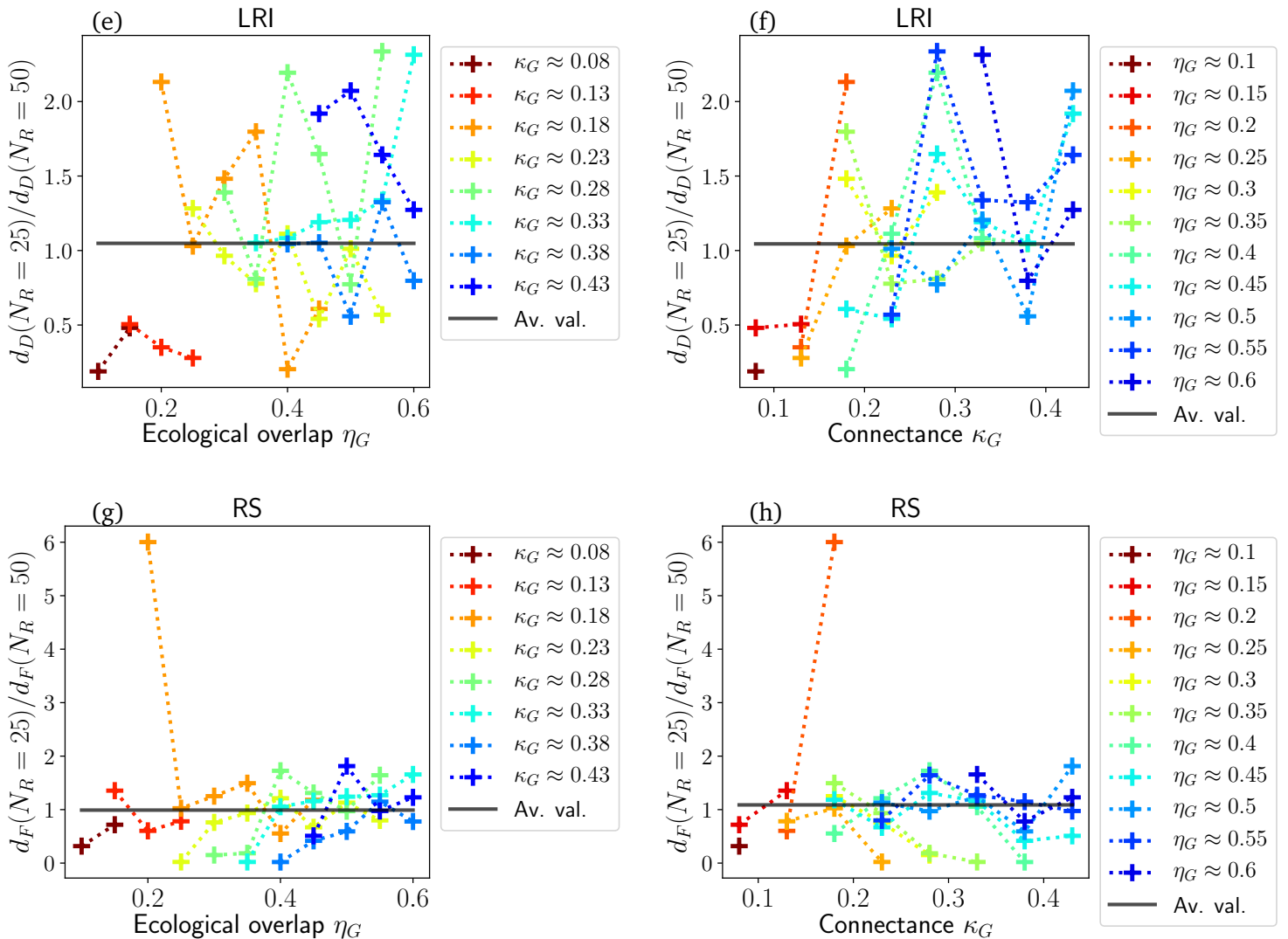


Figure 3.2.16: Continuation of Figure above.

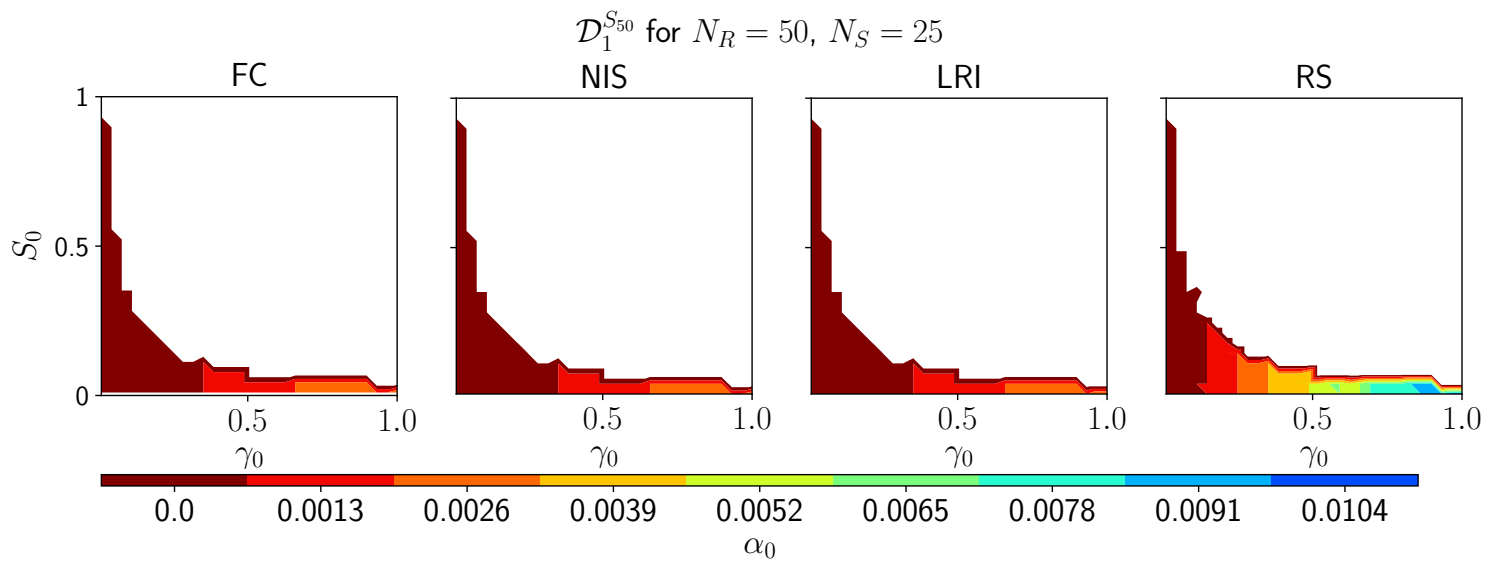


Figure 3.2.17: Common fully dynamically stable volume of the S_{50} matrix set, which comprises of matrices with dimensions $N_R = 50$ and $N_S = 25$. This figure is the $N_R = 50$ version of Figure 3.2.6. At a given syntropy, we observe a larger zone that is fully dynamically stable for all matrices when the number of resources is doubled.

3.3 Structural stability

We deal here with the last question of this Thesis, which is the one of *structural stability*. We follow the path opened by Bastolla et al. in the Supplementary Material of [10] and later explored by Rohr, Saavedra, and Bascompte in [11]. The latter defined the question of structural stability as “*asking how large is the range of parameter values that are compatible with the stable coexistence of all species*” [11]. Their analysis was done in the context of the study of plants-pollinators networks. For microbial communities, apart from incipient considerations found in [44, 45], only Butler and O’Dwyer fully considered that question [34] and even found a sufficient condition for structural stability of their model under some special assumptions³⁶.

In the following, we study a quantity called critical structural perturbation, which allows to investigate how much the rate of supply of external resources l_μ can be perturbed until extinctions are observed in the community. That measure is computed for systems which we know are feasible and dynamically stable for a given set of metaparameters m . We aim to find what topologies (G, A) and metaparameters $(\gamma_0, S_0, \alpha_0)$ lead to systems that can sustain the largest perturbations.

3.3.1 Domain of analysis

Section 2.4.1 explains the numerical algorithm we designed to determine $\Delta_S^*(m, G, A)$. Although this algorithm always converges, it is computationally demanding: it typically takes on the order of ~ 1 hour to provide its result. This means we cannot analyze in detail the whole fully dynamically stable domain $\mathcal{D}_{L,1}^{G,A}(\alpha_0)$ studied earlier and we need to focus on specific points.

As explained before, in order to assess the structural stability of a given parameters set p , we require that p is locally dynamically stable. Hence we need to work with metaparameters m that are in a highly dynamically stable region. To make different systems comparable, we need to choose m in a region that is very dynamically stable for *all consumption-syntropy networks*, e.g. the common fully dynamically stable domain. However, we cannot pick any random point of that domain. Indeed we saw above that the value of α_0 changes the shape of said domain. Because our goal is to study the impact of α_0 only, while keeping other metaparameters fixed, we need to choose (γ_0, S_0) such that they are indeed highly dynamically stable for all values of α_0 and all networks we consider. The idea is of course to take α_0 as large as possible.

We saw above that the structure of the dynamically stable domains was complicated for the case $N_R = N_S = 25$ (see e.g. the common fully dynamically stable region on Figure 3.2.6). In fact, doubling the number of resources led to a smoother profile of dynamical stability for all networks as shows for instance Figure 3.2.17. Overall a larger syntropy could be attained without losing dynamical stability for any of the networks. These considerations make us focus our analysis on systems with dimensions $N_R = 50$ and $N_S = 25$,

³⁶The model they consider in [34] differs slightly from ours (e.g. resources are not removed from the system $m_\mu = 0$) and the sufficient condition they found assumes fully specialist consumers i.e. $N_R = N_S$ and $\gamma = \gamma_0 \mathbb{1}_{N_S}$.

i.e. on matrices from the set S_{50} . Looking at Figure 3.2.17, we see that points with $\gamma_0 \gtrapprox 0.7$ can sustain the largest syntropy while remaining fully dynamically stable for all matrices. In consequence we choose $(\gamma_0, S_0) = (0.75, 0.05)$ and keep these fixed until the end of this section.

Now that we chose γ_0, S_0, N_R and N_S such that we can work with a fairly high syntropy, we still need to decide for which values of α_0 we compute $\Delta_S^*(m, G, A)$. For a fixed γ_0, S_0, G and A , we define the *critical dynamical syntropy* $\alpha_C^D(\gamma_0, S_0, G, A)$ as:

$$\alpha_C^D(\gamma_0, S_0, G, A) \equiv \max_{\alpha_0} \{ \alpha_0 : \mathcal{D}_{L,1}((\gamma_0, S_0, \alpha_0), G, A) = 1 \}. \quad (3.44)$$

In words, $\alpha_C^D(\gamma_0, S_0)$ is the largest syntropy for which we are sure that a system built with the procedure \mathcal{A} is locally dynamically stable. So, it is basically the largest syntropy at which we can measure structural stability. As is explained in the next section, $\alpha_C^D(\gamma_0, S_0)$ depends heavily on both the structure of G and A and it definitely cannot be approximated as the same for all matrices considered.

Since we want syntropy to have noticeable effects on $\Delta_S^*(m, G, A)$, we will compute the critical structural perturbation for each network at its individual critical syntropy. To add another point of comparison, we will also compute it for each at the lowest critical syntropy found, which is the largest syntropy which leads to fully dynamically stable systems for all networks. Finally, we will compare these two Δ_S^* with the one obtained when there is no syntropy, i.e. $\alpha_0 = 0$, which will act as a null model.

3.3.2 Critical dynamical syntrophies

Figure 3.3.1 shows how $\alpha_C^D(\gamma_0, S_0, G, A)$ evolves for the case of A fully connected as a function of connectance κ_G and ecological overlap η_G of the consumption matrix. We observe a clear trend, in accordance with prior results: at fixed ecological overlap, networks with a larger connectance can attain more syntropy while remaining dynamically stable and at fixed connectance, networks with a larger ecological overlap become unstable faster as syntropy increases. Apart from the four A structures considered since the beginning of this Thesis (FC, NIS, LRI, RS), we include three additional A -topologies:

- Restricted Random Structure matrix (RS-R); A is random, except that no intraspecific syntropy is allowed. Its connectance is taken as the connectance of G . This is more or less a “lower connectance version” of the NIS scenario.
- LRI matrix with NIS Connectance (LRI-NIS); A is the outcome of the LRI MCMC procedure described in Section 3.2.2, except that in contrast to the LRI scenario where $\kappa_A = \kappa_G$, the connectance of A is taken as the one of A in the NIS scenario.
- Random Structure with NIS Connectance (RS-NIS); A has a completely random structure. Its connectance is chosen as the connectance of A in the NIS regime.

Figure 3.3.2 shows how α_C^D changes as a function of the topology of A . The RS-R and RS cases outperform the other scenarios for every consumption matrix considered. Both the FC and NIS cases have κ_A larger than the RS scenario, which hints that systems where

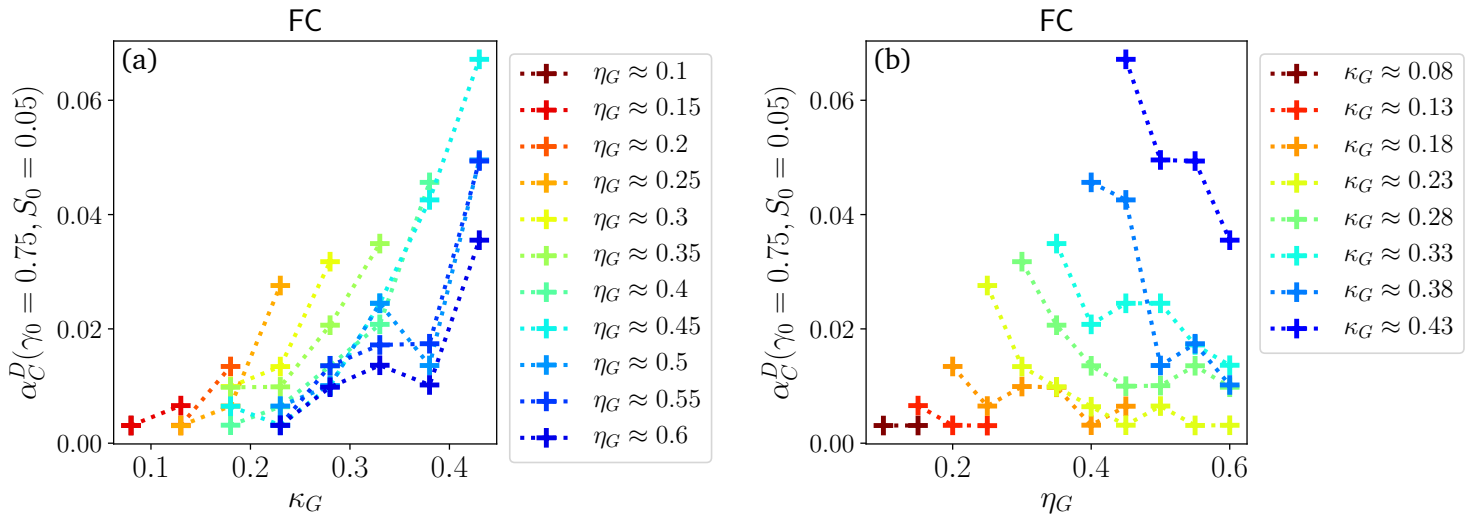


Figure 3.3.1: Critical dynamical syntropy α_C^D for all the consumption matrices G in the set S_{50} (with a fully connected syntropy matrix) (a) as a function of the connectance of G for fixed ecological overlap and (b) as a function of the ecological overlap of G for fixed connectance. For a fixed ecological overlap, systems with a larger connectance can attain larger syntropies. For a fixed connectance, a small ecological overlap is needed to get a large critical dynamical syntropy.

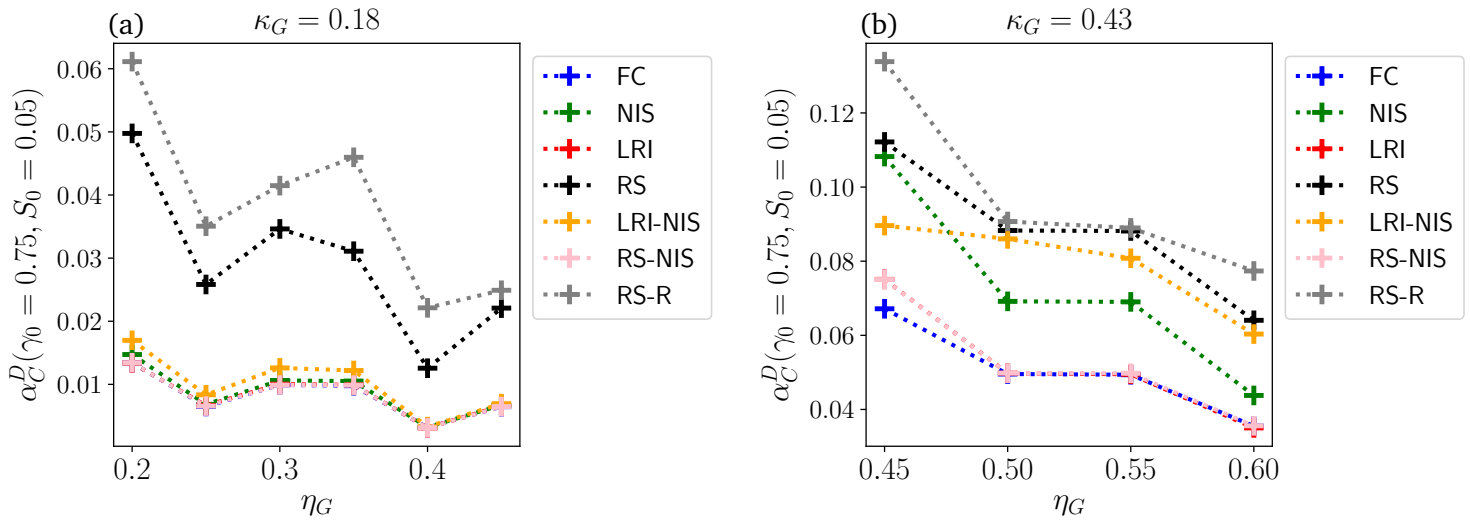


Figure 3.3.2: Critical dynamical syntropy $\alpha_C^D(\gamma_0 = 0.75, S_0 = 0.05, G, A)$ as a function of the ecological overlap of the consumption matrix G for fixed connectance (a) $\kappa_G = 0.18$ and (b) $\kappa_G = 0.43$. The different lines symbolize the different structures of the syntropy matrix A : FC, NIS, LRI, RS but also RS-R, LRI-NIS, and RS-NIS (which are explained in the main text). A higher critical dynamical syntropy is achieved when A has a random structure. The LRI curve is the same as the FC curve.

many syntrophic interactions take place (*i.e.* A has a large connectance) can sustain an overall smaller maximal syntrophic strength. The main difference between the LRI and the RS-R/RS regimes, since their respective syntropy matrix have the same connectance, is their *syntrophic overlap*, *i.e.* the nestedness of A , as is shown by Figure 3.2.4. Note that RS-R is slightly better than RS. Although RS-R and RS both have the same connectance and an approximately similar syntrophic overlap, the main difference is that RS-R does not allow intraspecific syntropy. In the end it seems like dynamical stability is favoured – in the sense that a higher syntropy can be attained while remaining dynamically stable – by the following three factors concerning the syntropy matrix: low connectance of A , low syntrophic overlap of A and prohibition of intraspecific syntropy. Microbial communities where consumers do not release too many resources – and if they do, in separate niches – can achieve a larger average syntropy than others while remaining dynamically stable.

3.3.3 Critical structural perturbation

Now that we calculated the critical dynamical syntrophies of each consumption-syntropy network, we compare their critical structural perturbation $\Delta_S^*(m, G, A)$. As a “null model”, we first compute Δ_S^* when there is no syntropy at play. Figure 3.3.3 shows that structural stability confirms the trend hitherto observed: for a given ecological overlap η_G , Δ_S^* increases as the connectance κ_G increases and for a given κ_G , Δ_S^* decreases as η_G increases. In short, microbial communities where microbes consume a lot of different resources but do not share them resist best to environmental perturbations. These results coincide well with the stability trend hitherto observed.

We now focus on what happens when the system is syntrophic, *i.e.* $\alpha_0 > 0$. Figure 3.3.4 shows that, surprisingly, for the FC, LRI, RS, RS-R, LRI-NIS and RS-NIS scenarios we observe no significant deviation away from the “no syntropy” case. Whether $\Delta_S^*(m, G, A)$ is computed at each individual α_C^D or at $\min\{\alpha_C^D\}$, it seems like syntropy does not influence much the structural stability of the system, at least not in a clearly decidable way. The only scenario where a clear effect (at most 15%) is observable is when Δ_S^* is computed at the critical dynamical syntropy in the NIS regime as show Figure 3.3.5 and 3.3.6. Again, the larger the connectance of the consumption matrix, the greater the improvement and the larger the ecological overlap the smaller the improvement. As a consequence of that behaviour, here also appears an interesting phenomenon. On one hand, we obtain the largest critical dynamical syntropy when A has a random structure, so in a sense a larger dynamical stability. On the other hand, that A structure does not allow the system to reach a larger structural stability, even when evaluated at its critical dynamical syntropy. To attain the largest structural stability, A must be in the NIS scenario, where the critical dynamical syntropy is lower. We observe a trade-off in the structure of the syntropy matrix: the structure of A that allows a system to be at its maximum syntropy (RS-R) while remaining dynamically stable is not the one that allows to improve structural stability. On the opposite the A -configuration in which syntropy can increase structural stability (NIS) does not allow to reach the largest possible syntrophic strength while remaining dynamically stable.

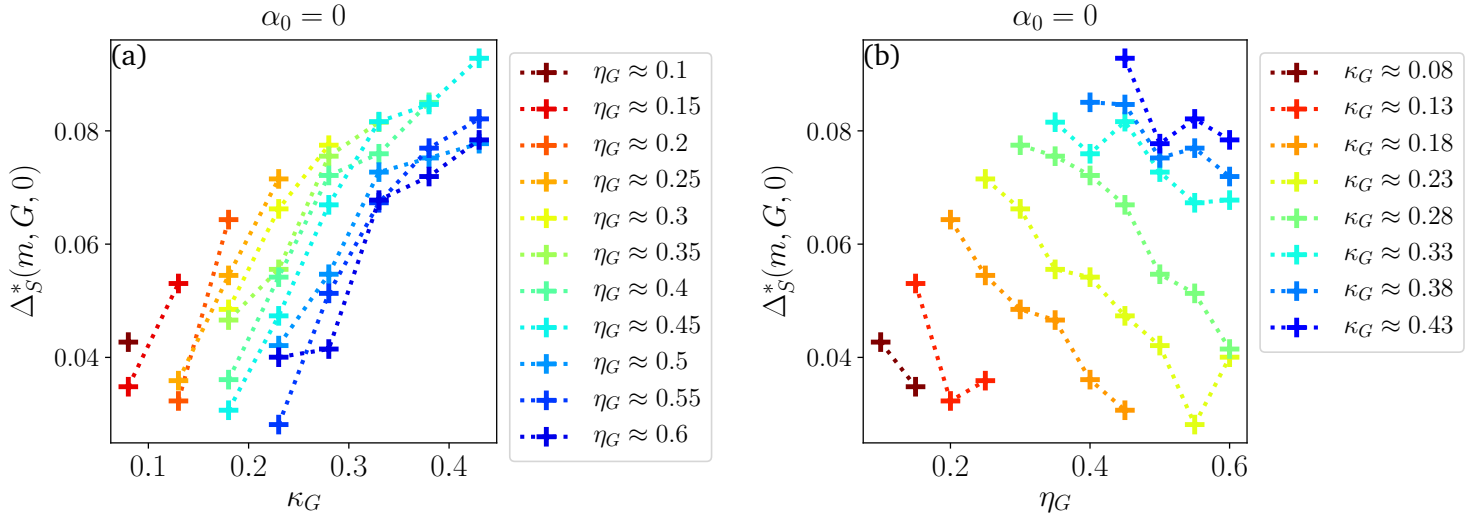


Figure 3.3.3: Critical structural perturbation without syntropy $\Delta_S^*(m, G, A = 0)$ (a) as a function of ecological overlap with fixed connectance and (b) as a function of connectance for a fixed ecological overlap. We look at matrices with $N_R = 50$ and $N_S = 25$ at one of the points in the metaparameters space that are the most dynamically stable for all the matrices (see Fig. 3.2.17), namely $(\gamma_0, S_0) = (0.75, 0.05)$. A clear trend may be observed, which is coherent with trends hitherto observed: for a given connectance, communities with a large ecological overlap are structurally less stable. Similarly, for a given ecological overlap, microbial communities with a consumption matrix with a larger connectance are more structurally stable.

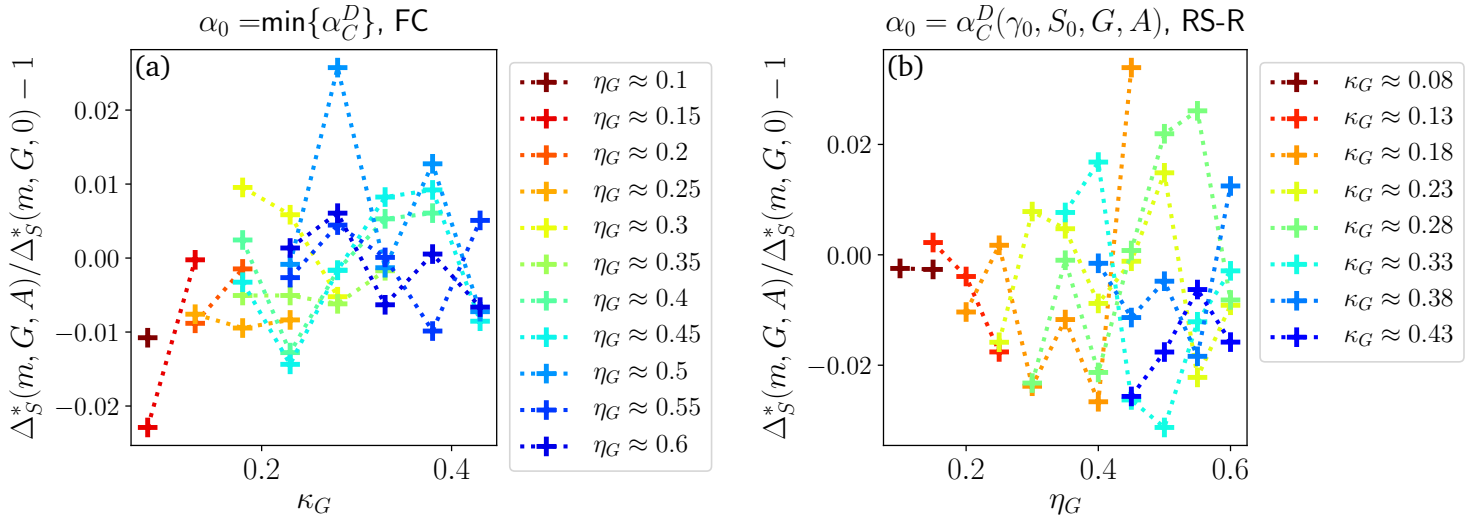


Figure 3.3.4: Typical deviation away from the “no syntropy” scenario. For all structures of the syntropy matrix considered, apart from NIS (see Fig. 3.3.5), adding a large syntropy, be it the “common” or “individual” maximum, does not significantly increase the structural stability of the microbial community.

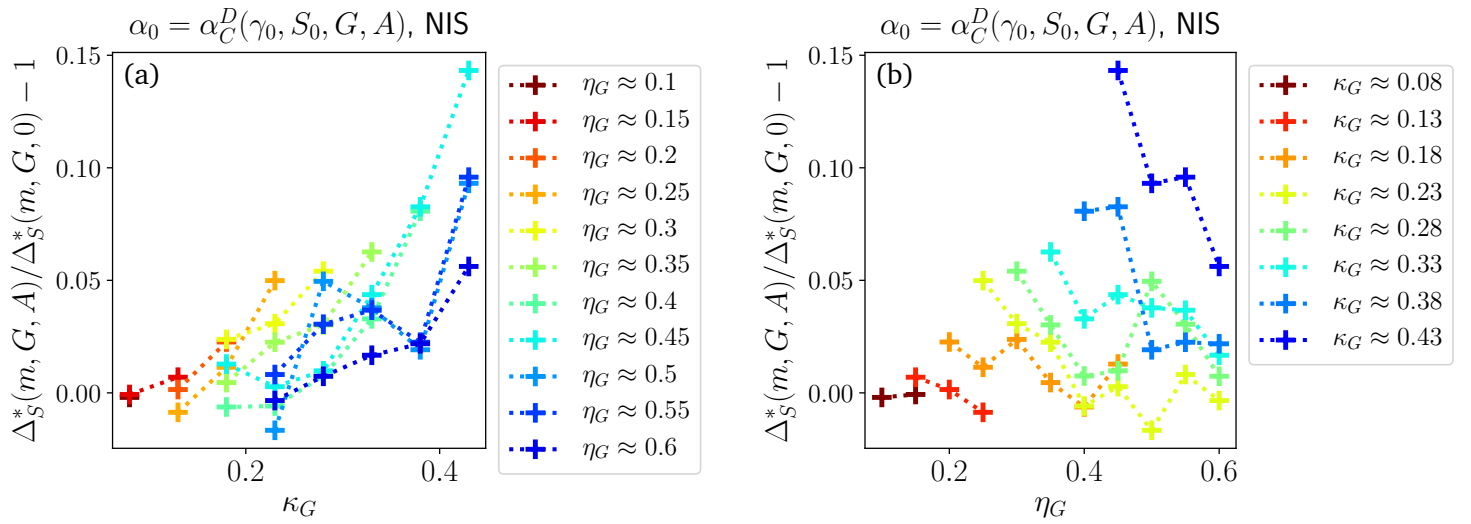


Figure 3.3.5: Deviation from the “no syntropy” case for the syntropy matrix A with a NIS structure. α_0 is taken at the critical dynamical syntropy α_C^D for each system. At the largest possible syntropy,

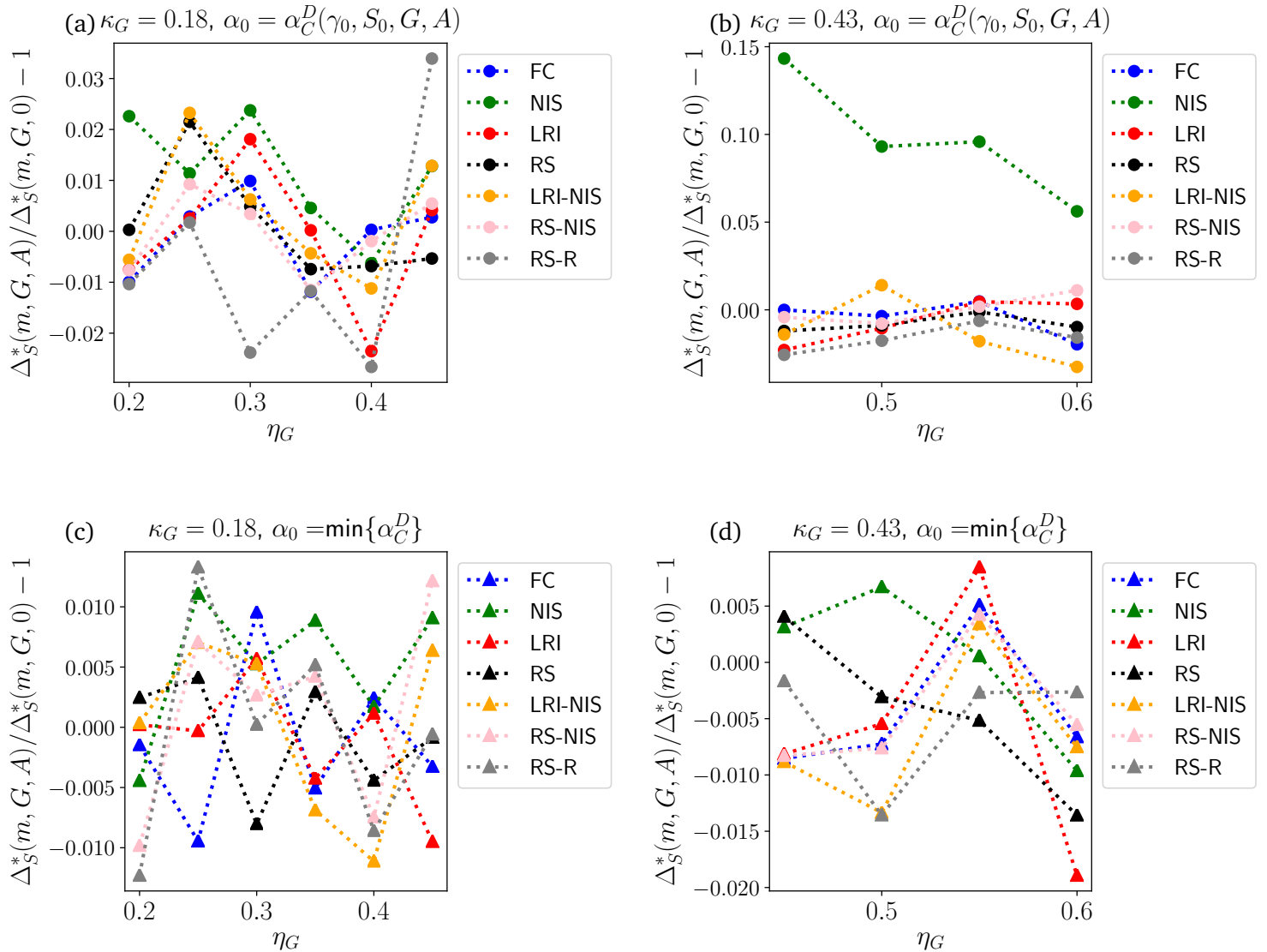


Figure 3.3.6: Difference between the critical structural perturbation with and without syntropy for different scenarios as a function of the ecological overlap for a given connectance (a)-(c) $\kappa_G = 0.18$ and (b)-(d) $\kappa_G = 0.43$. For (a)-(b) α_0 is taken at the critical dynamical syntropy (which depends on the network), for (c)-(d) at the common maximum syntropy. The different colours correspond to the different structures of A considered. A significant increase is observed only at high connectance, where the “own individual syntropy” NIS scenario is $\sim 10\%$ more structurally stable than the “no syntropy” case.

4 Discussion

The studies conducted in this Thesis allowed us to gain a more precise knowledge on the impact of syntropy on microbial communities. Although microbial communities are present in a very large number of diverse ecosystems [6, 7, 8], our grasp of their functioning is yet very crude and an improvement of the underlying mechanisms that govern their shaping may lead us to technological breakthroughs [14]. We found four important results which seem to be determinant in the dynamics of microbial communities as dictated by our model: biological trade-offs play an essential role, both in the absence and presence of syntropy; syntropy increases dynamical stability and – except under very specific conditions – neither increases nor decreases structural stability; finally, the topology of both the matrices at play is one of the main factors of the dynamics.

Microbial communities are governed by trade-offs: everything comes with a price. In the absence of syntropy, we observed that the product of the consumers' consumption uptake and abundance at equilibrium should not exceed a certain threshold. If that threshold is exceeded, the system either does not conserve biomass or has negative parameters, and it simply cannot exist. Feasible systems either have a very high consumption uptake and a low abundance of consumers at equilibrium or the other way around. The introduction of a syntrophic interaction induces an additional trade-off in the system. On one hand, syntropy reduces the number of both feasible and dynamically stable points, but on the other, the remaining points are rewarded with a better dynamical stability: they recover faster from perturbations of resources or consumers. A final trade-off was observed for the case of structural stability. It is essentially a balance between maximal attainable syntropy and increase in structural stability as a function of the structure of the syntropy network: the structure of A which allows syntropy to increase the structural stability of a microbial community is different from the one that allows the same community to withstand the largest syntropy while remaining dynamically stable. Nature is made of trade-offs. If it was not we could neither observe the diversity of systems nor the equilibria that we see. As the law of Physics show it, equilibrium comes from the confrontation of two opposite forces and if there existed a configuration of microbial community which was “optimal” towards all aspects, we most likely would observe all of them in that state. Although some studies suggest the importance of trade-offs [46, 47], to our knowledge a thorough investigation of that question in the context of microbiology remains to be done.

We also discovered that, overall, syntropy increases dynamical stability. As said above, this comes at the price that fewer systems are feasible when dynamical stability increases. That result corroborates the classical notion first claimed by May that mutualistic interactions – in our case syntropy – are detrimental to dynamical stability [48]. Additionally, because syntropy provides additional pathways for the biomass flow to the consumers, our result also confirms the conclusion of MacArthur who stated that the larger the number of such pathways, the greater the stability of the community [49].

Contrarily to dynamical stability, structural stability is in general neither improved nor worsened by syntrophic interactions. Out of the seven scenarios we tested for the structure of the syntropy matrix, the only one where syntropy improved the structural stability of the community is when every consumer releases every resource except the ones they themselves feed on. Furthermore, the improvement is more significant as the connectance of the consumption matrix grows. Why syntropy has an impact only on that scenario remains

unclear to us. It is possible that we did not observe any systematic impact of syntropy because of the assumptions of the model. Indeed we work with microbial communities that are in a chemostat environment. This means that resources available to consumers are constantly added through an external biomass flow. Because in our simulations the external biomass flow was consistently larger than the syntrophic biomass flow by at least two orders of magnitude³⁷, the impact of syntropy might have been too little to even be measured. As recent studies show [50], the role of syntropy may be more prominent in environments where resources are scarce. Investigating such environments with our model may show more decisive results in the aspect of structural stability.

Another clear result was the large influence of the consumption matrix topology on both stability and feasibility. In general microbial communities whose consumption matrix have a high connectance and a low ecological overlap are the ones that resist best to syntrophic interaction in the sense that their fully feasible and fully dynamically stable regions are the least impacted as syntropy increases. This is compatible with what was said above: a higher connectance in the consumption matrix means a larger flux of biomass available to the consumers which should increase dynamical stability. Also, a larger ecological overlap means more competition between the species which lessens the available biomass flux and reduces stability. The same trend is observed for the resistance to environmental perturbations both in the absence and presence of syntropy. For the case of structural stability, this can also be explained intuitively, in accordance to what was said about how the number of biomass flux paths is linked to the stability of the system. When a system is structurally perturbed, the external resources feeding rates get shuffled³⁸, which in turn shuffles the resources available for microbial consumption: some of them start becoming more abundant, some of them get scarcer. If a given microbial species only consumes a small number of resources, by luck it is possible that most of its resources got rarer after the environmental perturbation such that the biomass it can consume is not large enough for its survival anymore and it is driven to extinction. On the other hand, if said microbial species feeds on many resources, it is unlikely that all the resources it consumes got scarcer after the system perturbation. The lack of biomass from the scarcer resources should indeed be compensated by the additional biomass coming from the more abundant resources, which makes the species less prone to extinction. Having a larger connectance means that on average species consume more resources, which makes the system more stable and at a given connectance, having a larger ecological overlap means that they compete more for the same resources, which implies there will be some species that consume very few resources which makes the system unstable.

The way in which the topology of the syntropy matrix influences the dynamics is a question that deserves more exploration. Clear results were difficult to draw apart from the fact that a random structure of the syntropy matrix improves both feasibility and dynamical stability. It is also surprising that the LRI regime improves dynamical stability only

³⁷We can approximate the external biomass flow available for each species as $\sim N_R l_0$. On the other hand the syntrophic flow is $\sim N_R N_S \alpha_0 S_0$. With the values we used $l_0 \approx 1$ and $N_S = 25$, $\alpha_0 \approx 0.01$ and $S_0 \approx 0.05$, the syntrophic flow is way smaller than the external flow.

³⁸By “shuffling”, we mean that the l_μ change but their average value does not. Indeed, recall that the ν_μ in Eq.(1.28), have a zero average value which implies that after the perturbation l_0 remains the same, and so should the other metaparameters.

when the connectance of the consumption matrix is low. That could be due to feasibility considerations: it is indeed still unclear in which conditions the strong LRI regime is feasible, and it may happen that when the connectance of the consumption matrix is too large, such a regime simply cannot exist³⁹. It could also come from the choice of the energy function used in the MCMC LRI algorithm. That energy was indeed obtained in a heuristic way that neglected some factors, especially the role of the critical radius and its dependency on the shape of the syntropy matrix, and could be improved in a future work. It may also come from the design of the algorithm itself, which does not allow the connectance of the output matrix to be changed and therefore leaves less room to potential improvement.

Going back to a more biological picture, the results highlighted above allow us to state predictions about the behaviour of microbial communities. For instance we expect that the syntrophic microbial communities that can be found in Nature are fairly fine tuned: their consumers abundance at equilibrium should be very small compared to their resources abundance. Additionally, microbial species should feed from as much resources as they can but in a way that minimizes their interspecific competition. Evolutionary processes could also lead to the apparition of syntropy. Consider for instance a microbial community that undergoes very frequent perturbations of its abundance of consumers and resources. One could imagine an experimental setup where microbes are randomly and frequently removed from the chemostat or a less artificial environment, like the human guts [51]. In such an environment, if the other conditions (high consumption rate, etc.) are fulfilled, syntrophic interactions could appear through random genetic mutations to help the community increase its dynamical stability and recover faster from these perturbations. If structural perturbations were to occur, the community matrix would reshape itself to maximize the average number of resources that the species consume and to minimize interspecific competition. The syntropy matrix would have a structure such that species release everything except what they consume.

The next steps in the study of syntrophic microbial communities should be both experimental and theoretical. On an experimental level, one could design a setup such as the one we described above and check the accuracy of our predictions. On the theoretical side, many challenges remain to be tackled. Among the most interesting is the search for a better energy function in the LRI algorithm which would allow us to investigate the LRI regime more thoroughly. Overall a special attention should be given to a better comprehension of the role of the structure of the syntropy matrix. Understanding how its topology changes the dynamics will bring us to a better grasp of the underlying biological principles that shape microbial communities.

³⁹More specifically, the critical radius R_C strongly depends on the shape of the consumption matrix and gets larger as its connectance increases. It is possible that beyond a certain connectance, R_C gets too large and the inequality of Theorem 1 cannot be fulfilled anymore.

5 Appendices

5.1 Supplementary methods

5.1.1 Dynamical stability

Measuring the feasibility and local dynamical stability volumes

In the main text, we study how the sizes of both the fully feasible and the fully locally dynamically stable regions, respectively $\mathcal{F}_1^{G,A}(\alpha_0)$ and $\mathcal{D}_{L,1}^{G,A}(\alpha_0)$, change as a function of G , A and α_0 . It is important to explain in what way (and why in *that* way) these are computed. We define the *volume* of $\mathcal{F}_1^{G,A}(\alpha_0)$, or *feasibility volume*, as:

$$\text{Vol} \left(\mathcal{F}_1^{G,A}(\alpha_0) \right) \equiv \frac{\iint_{(\gamma_0, S_0) \in [0,1]^2} d\gamma_0 dS_0 \mathcal{F}(m, G, A)}{\iint_{(\gamma_0, S_0) \in [0,1]^2} d\gamma_0 dS_0} = \iint_{(\gamma_0, S_0) \in [0,1]^2} d\gamma_0 dS_0 \mathcal{F}((\gamma_0, S_0, \alpha_0), G, A). \quad (5.1)$$

The *volume* of $\mathcal{D}_{L,1}^{G,A}(\alpha_0)$, or *(local) dynamical stability volume* is similarly defined:

$$\text{Vol} \left(\mathcal{D}_{L,1}^{G,A}(\alpha_0) \right) \equiv \iint_{(\gamma_0, S_0) \in [0,1]^2} d\gamma_0 dS_0 \mathcal{D}_L((\gamma_0, S_0, \alpha_0), G, A). \quad (5.2)$$

The feasibility and dynamical stability volumes do not *stricto sensu* measure the area occupied by the fully feasible and fully dynamically stable regions, respectively. In the case of the feasibility volume, it is documented in the main text that the zone where $\mathcal{F}(m, G, A)$ is different from 1 or 0 is very small so measuring the volume this way does not provide a significant difference to naively counting the number of points for which the feasibility function is *exactly* 1.

However, in the case of the dynamical stability volume, this approach would provide unsatisfactory results. Indeed, $\mathcal{D}_L(m, G, A)$ is a function that may be very patchy (see Figure 3.2.5): many points are not fully dynamically stable but rather *almost* fully dynamically stable, in the sense that there are many m such that $\mathcal{D}_L(m, G, A)$ is extremely close to but not exactly equal to 1. Because of this, counting exactly the points where $\mathcal{D}_L(m, G, A) = 1$ is very prone to noise, in the sense that it depends a lot on the precision at which $\mathcal{D}_L(m, G, A)$ is evaluated. We know that a lot of points are only *almost* fully dynamically stable; if we increase the number of simulations to evaluate $\mathcal{D}_L(m, G, A)$, who can tell if the points that were previously identified as fully dynamically stable would be now only almost fully dynamically stable and hence not counted in the volume anymore?

Because of such considerations taking into account every point but pondering it by its value of the feasibility/dynamical stability function not only provides a measure close to the idea of measuring the “full volume” but also provides smoother and more robust results.

Following that line of thought, we also define the *common feasibility volume*, which is a measure of the common fully feasible region $\mathcal{F}_1^{S_M}(\alpha_0)$ of a matrix set S_M at a given syntrophic interaction strength α_0 :

$$\text{Vol} \left(\mathcal{F}_1^{S_M} \right) \equiv \iint_{(\gamma_0, S_0) \in [0,1]^2} d\gamma_0 dS_0 \min_{(G,A) \in S_M} \{ \mathcal{F}((\gamma_0, S_0, \alpha_0), G, A) \}. \quad (5.3)$$

In a completely analogous manner, the *common (local) dynamical stability volume* of a matrix set S_M is given by:

$$\text{Vol}(\mathcal{D}_{L,1}^{S_M}) \equiv \iint_{(\gamma_0, S_0) \in [0,1]^2} d\gamma_0 dS_0 \min_{(G,A) \in S_M} \{\mathcal{D}_L((\gamma_0, S_0, \alpha_0), G, A)\}. \quad (5.4)$$

In practice, the integrals appearing in the above formulas are approximated numerically. The unit square $(\gamma_0, S_0) \in [0, 1]^2$ is discretized in a set $\{(\gamma_0^i, S_0^i)\}$ with $i = 1, \dots, N_{\text{totpoints}}$ which are then summed up with their according weights, e.g. for Equation (5.1):

$$\text{Vol}(\mathcal{F}_1^{G,A}(\alpha_0)) \approx \frac{\sum_{i=1}^{N_{\text{points}}} \mathcal{F}((\gamma_0^i, S_0^i), \alpha_0, G, A)}{N_{\text{totpoints}}}. \quad (5.5)$$

Typically, as said above in Section 2.1.1, $N_{\text{totpoints}} = 100^2$ when studying matrices with $N_R = 25$ and $N_{\text{totpoints}} = 30^2$ when studying matrices with $N_R = 50$.

Center of dynamical stability

The general idea behind the center of dynamical stability ($\langle \gamma_0 \rangle_D(\alpha_0), \langle S_0 \rangle_D(\alpha_0)$) is to show that as syntropy increases, only systems with a large γ_0 and a small S_0 remain dynamically stable (and hence feasible). For the case of feasibility, that was an easy task, one only needs to look at a heat map of $\mathcal{F}_1^{S_{25}}(\alpha_0)$ (Fig.3.1.8) and see that only such zones remain fully feasible as syntropy grows. However, as explained in the main text, that figure can not be replicated for the case of dynamical stability. Because of the almost fully dynamically stable points, the fully dynamically stable region $\mathcal{D}_{L,1}^{G,A}(\alpha_0)$ of each $(G, A) \in S_{25}$ is very fragmented such that the common fully dynamically stable region $\mathcal{D}_{L,1}^{S_{25}}(\alpha_0)$ vanishes for $\alpha_0 > 0$ (Fig.3.2.6). But even though $\mathcal{D}_{L,1}^{S_{25}}(\alpha_0)$ quickly vanishes, it does not mean that there are no dynamically stable (γ_0, S_0) , on the opposite (Fig.3.2.7)! This is the reason we need another measure to show how syntropy changes the location of the dynamically stable points.

Intuitively, we would like something that tells us basically where *on average* the most dynamically stable (γ_0, S_0) are. This is very close to the physical idea of the center of gravity, which tells you where most of the mass of an object lies. In consequence we define the *center of dynamical stability* ($\langle \gamma_0 \rangle_D(\alpha_0), \langle S_0 \rangle_D(\alpha_0)$) with the same formulae, namely:

$$\langle \gamma_0 \rangle_D(\alpha_0) \equiv \frac{1}{N_{\hat{0}}^{S_{25}}} \sum_{(G,A) \in S_{25}} \frac{\iint_{(\gamma_0, S_0) \in \mathcal{D}_{L,\hat{0}}^{G,A}(\alpha_0)} \gamma_0 \mathcal{D}_L((\gamma_0, S_0, \alpha_0), G, A)}{\iint_{(\gamma_0, S_0) \in \mathcal{D}_{L,\hat{0}}^{G,A}(\alpha_0)} \mathcal{D}_L((\gamma_0, S_0, \alpha_0), G, A)} \quad (5.6)$$

and

$$\langle S_0 \rangle_D(\alpha_0) \equiv \frac{1}{N_{\hat{0}}^{S_{25}}} \sum_{(G,A) \in S_{25}} \frac{\iint_{(\gamma_0, S_0) \in \mathcal{D}_{L,\hat{0}}^{G,A}(\alpha_0)} S_0 \mathcal{D}_L((\gamma_0, S_0, \alpha_0), G, A)}{\iint_{(\gamma_0, S_0) \in \mathcal{D}_{L,\hat{0}}^{G,A}(\alpha_0)} \mathcal{D}_L((\gamma_0, S_0, \alpha_0), G, A)} \quad (5.7)$$

where $\mathcal{D}_{L,\hat{0}}^{G,A}(\alpha_0)$ is the set of points where the dynamical stability function has mass (i.e. does not vanish):

$$\mathcal{D}_{L,\hat{0}}^{G,A}(\alpha_0) = \{(\gamma_0, S_0) : \mathcal{D}_L((\gamma_0, S_0, \alpha_0), G, A) > 0\} \quad (5.8)$$

and $N_{\hat{0}}^{S_{25}}$ simply denotes the number of consumption-syntropy networks $(G, A) \in S_{25}$, which have non-zero points, *i.e.* for which $\mathcal{D}_{L,\hat{0}}^{G,A}(\alpha_0)$ is not empty.

Probability of dynamical stability when feasibility is ensured

We here define the *probability of being dynamically stable when feasible* $\text{Prob}(\mathcal{D}_L|\mathcal{F})(G, A, \alpha_0)$ for a network (G, A) and a syntropy α_0 . First consider a single point $(\gamma_0, S_0, \alpha_0)$. We use conditional probability theory [52] to get the probability $\text{Prob}(\mathcal{D}_L|\mathcal{F})$ that $(\gamma_0, S_0, \alpha_0)$ is dynamically stable if it feasible:

$$\text{Prob}(\mathcal{D}_L|\mathcal{F})(G, A, \gamma_0, S_0, \alpha_0) \equiv \frac{\text{Prob}(\mathcal{D}_L \cap \mathcal{F})(G, A, \gamma_0, S_0, \alpha_0)}{\text{Prob}(\mathcal{F})(G, A, \gamma_0, S_0, \alpha_0)}, \quad (5.9)$$

where $\text{Prob}(\mathcal{D}_L \cap \mathcal{F})$, resp. $\text{Prob}(\mathcal{F})$ are the probabilities that $(\gamma_0, S_0, \alpha_0)$ are dynamically stable and feasible, resp. feasible. Since we required feasibility in the definition of dynamical stability, we have $\text{Prob}(\mathcal{D}_L \cap \mathcal{F}) = \text{Prob}(\mathcal{D}_L)$. Using Eqs.(1.7) and (1.21), one gets from Eq.(5.9):

$$\text{Prob}(\mathcal{D}_L|\mathcal{F})(G, A, \gamma_0, S_0, \alpha_0) = \frac{\text{Prob}(\mathcal{D}_L)(G, A, \gamma_0, S_0, \alpha_0)}{\text{Prob}(\mathcal{F})(G, A, \gamma_0, S_0, \alpha_0)} = \frac{\mathcal{D}_L((\gamma_0, S_0, \alpha_0), G, A)}{\mathcal{F}((\gamma_0, S_0, \alpha_0), G, A)}. \quad (5.10)$$

Finally the probability of being dynamically stable when feasible is taken as the average over the feasible points (γ_0, S_0) of the previous quantity:

$$\text{Prob}(\mathcal{D}_L|\mathcal{F})(G, A, \alpha_0) \equiv \frac{\iint_{(\gamma_0, S_0) \in \mathcal{F}_{\hat{0}}^{G,A}(\alpha_0)} d\gamma_0 dS_0 \frac{\mathcal{D}_L((\gamma_0, S_0, \alpha_0), G, A)}{\mathcal{F}((\gamma_0, S_0, \alpha_0), G, A)}}{\iint_{(\gamma_0, S_0) \in \mathcal{F}_{\hat{0}}^{G,A}(\alpha_0)} d\gamma_0 dS_0} \quad (5.11)$$

where $\mathcal{F}_{\hat{0}}^{G,A}(\alpha_0)$ is simply the set of not unfeasible points:

$$\mathcal{F}_{\hat{0}}^{G,A}(\alpha_0) \equiv \{(\gamma_0, S_0) : \mathcal{F}((\gamma_0, S_0, \alpha_0), G, A) > 0\}. \quad (5.12)$$

Standard deviation expansion

The idea behind the standard deviation expansion is the following. Let $q_{i\mu}$ be an arbitrary matrix of size $N_S \times N_R$. The nice trick done in [26] is to write the elements of the q matrix in terms of new variables $\tilde{q}_{i\mu}$:

$$q_{i\mu} = \langle q \rangle + \sigma_q \tilde{q}_{i\mu}. \quad (5.13)$$

In that expression, $\langle q \rangle$ is the average of q , element-wise

$$\langle q \rangle \equiv \frac{\sum_{\mu,i} q_{i\mu}}{N_S N_R}, \quad (5.14)$$

and σ_q is the standard deviation of q , again element-wise:

$$\sigma_q \equiv \sqrt{\langle q^2 \rangle - \langle q \rangle^2} \text{ with } \langle q^2 \rangle \equiv \frac{\sum_{\mu,i} q_{i\mu}^2}{N_S N_R}. \quad (5.15)$$

The main advantage of this procedure is that we get a clear idea about the scales involved. A matrix element $q_{i\mu}$ is roughly the mean $\langle q \rangle$ plus a deviation σ_q multiplied by a factor of magnitude ~ 1 . Indeed the $\tilde{q}_{i\mu}$ are not large since they follow the two equalities [26]:

$$\langle \tilde{q} \rangle = 0 \text{ and } \langle \tilde{q}^2 \rangle = 1. \quad (5.16)$$

We apply this framework to our problem by noticing that if the $q_{i\mu}$ are all random samples coming from the same distribution law \mathfrak{Q} , we can write the following approximation in the case $N_R, N_S \gg 1$:

$$\langle q \rangle \approx \langle \mathfrak{Q} \rangle \equiv q_0. \quad (5.17)$$

We can then rewrite the free parameters of our model⁴⁰:

$$\left\{ \begin{array}{l} l_\nu \approx l_0 + \sigma_l \tilde{l}_\nu \\ R_\nu^* \approx R_0 + \sigma_R \tilde{r}_\nu \\ S_i^* \approx S_0 + \sigma_S \tilde{s}_i \\ \gamma_{i\nu} \approx \gamma_0 + \sigma_\gamma \tilde{g}_{i\nu} \\ \alpha_{\nu i} \approx \alpha_0 + \sigma_\alpha \tilde{\alpha}_{\nu i} \\ \sigma_{i\nu} \approx \sigma_0 + \sigma_\sigma \tilde{\sigma}_{i\nu} \end{array} \right. \quad (5.18a)$$

$$(5.18b)$$

$$(5.18c)$$

$$(5.18d)$$

$$(5.18e)$$

$$(5.18f)$$

The strategy is to assume that the standard deviations are small which allows us to proceed to a first order Taylor expansion.

5.2 Supplementary results

5.2.1 Feasibility

Estimating the fully feasible region

Biomass conservation As stated in the main text, we require that biomass is conserved in our model. This is equivalent to fulfilling Eq.(1.5), which we rewrite here:

$$\sum_\nu (1 - \sigma_{i\nu}) \gamma_{i\nu} R_\nu^* \geq \sum_\nu \alpha_{\nu i} \quad \forall i = 1, \dots, N_S. \quad (5.19)$$

Eqs.(1.34) can be used to estimate the RHS of this equation:

$$\sum_\nu \alpha_{\nu i} \approx \deg(A, i) \alpha_0, \quad (5.20)$$

where $\deg(A, i)$ is the degree of the i -th column of the α matrix :

$$\deg(A, i) = \sum_\nu A_{\nu i}. \quad (5.21)$$

⁴⁰This works with γ and α because G and A have a trivial topology. Otherwise we would have to take their structure into account and the computations would not be as easy.

Similarly,

$$\sum_{\nu} (1 - \sigma_{i\nu}) \gamma_{i\nu} R_{\nu}^* \approx (1 - \sigma_0) R_0 \sum_{\nu} \gamma_{i\nu} \approx \deg(G, i)(1 - \sigma_0) R_0 \gamma_0, \quad (5.22)$$

Energy conservation Eq.(1.5) is then equivalent to

$$\deg(A, i)\alpha_0 \lesssim \deg(G, i)(1 - \sigma_0)R_0\gamma_0 \quad \forall i = 1, \dots, N_S. \quad (5.23)$$

Since $\deg(G, i) > 0$, we have⁴¹:

$$\frac{\deg(A, i)}{\deg(G, i)}\alpha_0 \lesssim (1 - \sigma_0)R_0\gamma_0 \quad \forall i = 1, \dots, N_S. \quad (5.24)$$

This is fulfilled if :

$$\max_i \left\{ \frac{\deg(A, i)}{\deg(G, i)} \right\} \alpha_0 \lesssim (1 - \sigma_0)R_0\gamma_0. \quad (5.25)$$

Biological interpretation of the parameters Additionally, the consumers death rates d_i have to be positive. This implied Eq.(1.4a), which may be recast as :

$$\sum_{\mu} \sigma_{i\mu} \gamma_{i\mu} R_{\mu}^* > \sum_{\mu} \alpha_{\mu i} \quad (5.26)$$

Using a reasoning similar to above, we get a corresponding metaparameters inequality:

$$\max_i \left\{ \frac{\deg(A, i)}{\deg(G, i)} \right\} \alpha_0 \lesssim \sigma_0 R_0 \gamma_0. \quad (5.27)$$

Also, the resources diffusion rates m_{ν} need to be positive:

$$l_{\nu} + \sum_j \alpha_{\nu j} S_j^* > \sum_j \gamma_{j\nu} R_{\nu}^* S_j^* \quad \forall \nu = 1, \dots, N_R, \quad (5.28)$$

which is equivalent to

$$l_0 + \deg(A, \nu)\alpha_0 S_0 \gtrsim \deg(G, \nu)\gamma_0 R_0 S_0 \quad \forall \nu. \quad (5.29)$$

Since $\deg(G, \nu) > 0$, we can divide the above equations⁴² by $\deg(G, \nu) > 0$ and then recast these N_R equations into a single condition:

$$\min_{\nu} \left\{ \frac{l_0}{\deg(G, \nu)S_0} + \frac{\deg(A, \nu)}{\deg(G, \nu)}\alpha_0 \right\} \gtrsim \gamma_0 R_0. \quad (5.30)$$

⁴¹Indeed, $\deg(G, i)$ is the number of resources species i eats. We of course ask every consumer to at least consume something, otherwise they would not be part of the microbial community.

⁴²Similarly to a previous footnote, we require that every resource ν is eaten by at least one consumer, i.e. $\deg(G, \nu) > 0$, otherwise it does not belong to the community.

Combining both conditions

The two upper bounds Eqs.(5.25)-(5.27) on α_0 can be combined in a single inequality :

$$\max_i \left\{ \frac{\deg(A, i)}{\deg(G, i)} \right\} \alpha_0 \lesssim \min(1 - \sigma_0, \sigma_0) \gamma_0 R_0 \quad (5.31)$$

Note that when $\alpha_0 > 0$, we will trivially require that the syntropy matrix is not empty, *i.e.* there exists at least an i for which $\deg(A, i) \geq 1$. Also, the largest value $\deg(G, i)$ can get (for any i) is N_R . Hence,

$$\max_i \left\{ \frac{\deg(A, i)}{\deg(G, i)} \right\} \geq \frac{1}{N_R}, \quad (5.32)$$

and we can find the largest allowed theoretical non-zero α_0 :

$$\alpha_0 \lesssim \min(1 - \sigma_0, \sigma_0) \gamma_0 R_0 N_R.. \quad (5.33)$$

Finally, Eq.(5.30) and (5.31) can be combined into a single one, which characterizes the fully feasible region $\mathcal{F}_1^{G,A}$:

$$\max_i \left\{ \frac{\deg(A, i)}{\deg(G, i)} \right\} \alpha_0 \lesssim \min(1 - \sigma_0, \sigma_0) \gamma_0 R_0 \lesssim \min(1 - \sigma_0, \sigma_0) \min_\nu \left\{ \frac{l_0}{\deg(G, \nu) S_0} + \frac{\deg(A, \nu)}{\deg(G, \nu)} \alpha_0 \right\}. \quad (5.34)$$

5.2.2 Dynamical stability

Effective system

Models which involve the dynamics of species only are in general better known than consumers-resources models. In particular, a huge body of literature exists on the study of Lotka-Volterra systems [17, 28]. We may profit from this knowledge by transforming the effect of the resources dynamics into an effective consumers-only Lotka-Volterra system.

This can be done by assuming that the resources reach an equilibrium way faster than the consumers. Mathematically, that is equivalent to

$$\frac{dR_\mu}{dt} \approx 0, \forall \mu. \quad (5.35)$$

Using Eq.(1.1a), we get an explicit value for the resources:

$$R_\mu \approx \frac{l_\mu + \sum_j \alpha_{\mu j} S_j}{m_\mu + \sum_k \gamma_{k\mu} S_k}. \quad (5.36)$$

This expression can be used in Eq.(1.1b) to get an effective system which describes the dynamics of the N_S consumers:

$$\frac{dS_i}{dt} = \left(\sum_\nu \left(\frac{\sigma_{i\nu} \gamma_{i\nu} l_\nu}{m_\nu + \sum_k \gamma_{k\nu} S_k} - \alpha_{\nu i} \right) - d_i + \sum_{\nu j} \frac{\sigma_{i\nu} \gamma_{i\nu} \alpha_{\nu j}}{m_\nu + \sum_k \gamma_{k\nu} S_k} S_j \right) S_i. \quad (5.37)$$

This can be rewritten in a more compact way:

$$\frac{dS_i}{dt} = p_i(S)S_i + \sum_j M_{ij}(S)S_iS_j \quad (5.38)$$

with

$$p_i(S) = - \left(d_i + \sum_\nu \alpha_{\nu i} \right) + \sum_\nu \frac{\sigma_{i\nu} \gamma_{i\nu} l_\nu}{m_\nu + \sum_k \gamma_{k\nu} S_k} \text{ and } M_{ij}(S) = \sum_\nu \frac{\sigma_{i\nu} \gamma_{i\nu} \alpha_{\nu j}}{m_\nu + \sum_k \gamma_{k\nu} S_k}. \quad (5.39)$$

If we assume the species S_k are not too far away from their equilibrium values⁴³, *i.e.*

$$S_k \approx S_k^* \forall k, \quad (5.40)$$

then using Eq.(1.4b) we can simplify p_i . Indeed,

$$m_\nu + \sum_k \gamma_{k\nu} S_k \approx m_\nu + \sum_k \gamma_{k\nu} S_k^* = \frac{l_\nu + \sum_k \alpha_{\nu k} S_k^*}{R_\nu^*} \quad (5.41)$$

Hence, the explicit dynamical dependence on S can be removed from p_i and M_{ij} :

$$p_i(S) \approx p_i \equiv - \left(d_i + \sum_\nu \alpha_{\nu i} \right) + \sum_\nu \frac{\sigma_{i\nu} \gamma_{i\nu} l_\nu R_\nu^*}{l_\nu + \sum_k \alpha_{\nu k} S_k^*}, \quad (5.42)$$

and

$$M_{ij}(S) \approx M_{ij} \equiv \sum_\nu \frac{\sigma_{i\nu} \gamma_{i\nu} R_\nu^* \alpha_{\nu j}}{l_\nu + \sum_k \alpha_{\nu k} S_k^*}. \quad (5.43)$$

We now perform perturbation analysis on the effective system. We study a system that we put close to an equilibrium S^* , *i.e.*

$$S = S^* + \Delta S, \text{ with } \Delta S \ll 1. \quad (5.44)$$

Written this way, the effective equations of motion Eq.(5.38) are equivalent to:

$$\frac{d\Delta S_i}{dt} = p_i(S^* + \Delta S)(S_i^* + \Delta S_i) + \sum_j M_{ij}(S^* + \Delta S)(S_i^* + \Delta S_i)(S_j^* + \Delta S_j). \quad (5.45)$$

Since the deviations from equilibrium $\Delta S_i \ll 1$, we can forget the terms in higher power than quadratic:

$$\frac{d\Delta S_i}{dt} = \tilde{p}_i \Delta S_i + \sum_j E_{ij} \Delta S_j + \mathcal{O}(\Delta S^2), \quad (5.46)$$

with

$$\tilde{p}_i \equiv p_i(S^*) + \sum_k M_{ik}(S^*) S_k^*, \quad (5.47)$$

⁴³Note that this is very rarely true, especially in the context of the study of structural stability, where entire species sometimes die out.

and

$$E_{ij} \equiv \left(\frac{\partial p_i}{\partial S_j} \Big|_{S^*} + M_{ij}(S^*) + \sum_k \frac{\partial M_{ik}}{\partial S_j} \Big|_{S^*} S_k^* \right) S_i^*. \quad (5.48)$$

After some computations, we can get \tilde{p}_i and E_{ij} in terms of the initial parameters. Indeed,

$$p_i(S^*) = - \left(d_i + \sum_\nu \alpha_{\nu i} \right) + \sum_\nu \frac{\sigma_{i\nu} \gamma_{i\nu} l_\nu}{m_\nu + \sum_k \gamma_{k\nu} S_k^*} \quad (5.49)$$

and

$$M_{ik}(S^*) = \sum_\nu \frac{\sigma_{i\nu} \gamma_{i\nu} \alpha_{\nu j}}{m_\nu + \sum_k \gamma_{k\nu} S_k^*}. \quad (5.50)$$

Hence, using Eq.(5.47):

$$\tilde{p}_i = - \left(d_i + \sum_\nu \alpha_{\nu i} \right) + \sum_\nu \frac{\sigma_{i\nu} \gamma_{i\nu}}{m_\nu + \sum_k \gamma_{k\nu} S_k^*} \left(l_\nu + \sum_j \alpha_{\nu j} S_j^* \right). \quad (5.51)$$

This can be simplified using Eq.(5.41) and Eq.(1.2b):

$$\tilde{p}_i = -d_i + \sum_\nu \sigma_{i\nu} \gamma_{i\nu} R_\nu^* = \sum_\nu \alpha_{\nu i}. \quad (5.52)$$

With a similar computation, one finds

$$E_{ij} = \sum_\nu \frac{\sigma_{i\nu} \gamma_{i\nu} S_i^*}{m_\nu + \sum_k \gamma_{k\nu} S_k^*} (\alpha_{\nu j} - \gamma_{j\nu} R_\nu^*). \quad (5.53)$$

Finally, Eq.(5.46) can be recast in

$$\frac{d\Delta S_i}{dt} = \sum_j (J_E)_{ij} \Delta S_j, \quad (5.54)$$

where the effective $N_S \times N_S$ jacobian matrix J_E is defined by:

$$(J_E)_{ij} = \sum_\nu \left[\frac{\sigma_{i\nu} \gamma_{i\nu} S_i^*}{m_\nu + \sum_k \gamma_{k\nu} S_k^*} (\alpha_{\nu j} - \gamma_{j\nu} R_\nu^*) + \alpha_{\nu i} \delta_{ij} \right]. \quad (5.55)$$

We see that we without surprise we find the B , Γ and D matrices coming from the Jacobian at equilibrium:

$$(J_E)_{ij} = \sum_\nu \left[\frac{B_{i\nu} \Gamma_{\nu j}}{D_\nu} + \alpha_{\nu i} \delta_{ij} \right] \quad (5.56)$$

This matrix determines the stability of the equilibrium. Namely if the largest eigenvalue of J_E is positive, the equilibrium is unstable. If it is negative, the equilibrium is stable. If it is zero, the equilibrium is marginal.

Finding the critical radius

The Gershgorin circle theorem allows us to get a precious bound on the modulus of each eigenvalue and hence on the one that decides the dynamics of the system λ_1 . Indeed we know that all eigenvalues of J^* will be located in one of the $N_R + N_S$ discs of J^* . These are the “resources” discs:

$$\tilde{D}_\mu^R \equiv \left\{ z \in \mathbb{C} : |z + D_\mu| \leq \sum_j |\Gamma_{\mu j}| \right\} \quad \forall \mu = 1, \dots, N_R, \quad (5.57)$$

and the “consumers” discs:

$$\tilde{D}_i^C \equiv \left\{ z \in \mathbb{C} : |z| \leq \sum_\nu |B_{i\nu}| \right\} \quad \forall i = 1, \dots, N_S. \quad (5.58)$$

According to the circle theorem Eq.(2.12), all eigenvalues will be in the union of these circles, *i.e.* there exists $\forall \lambda \in \sigma(J^*)$ at least one μ^* or one i^* such that:

$$|\lambda| \leq \sum_\nu |B_{i^*\nu}| \quad (5.59)$$

or

$$|\lambda + D_{\mu^*}| \leq \sum_j |\Gamma_{\mu^* j}|. \quad (5.60)$$

The triangle inequality implies:

$$|\lambda| \leq |\lambda + D_{\mu^*}| + |-D_{\mu^*}| \leq \sum_j |\Gamma_{\mu^* j}| + |-D_{\mu^*}| = \sum_j |\Gamma_{\mu^* j}| + D_{\mu^*}. \quad (5.61)$$

The only way both Eq.(5.59) and (5.61) are satisfied for all eigenvalues, and especially the one with the highest real part λ_1 is if they are bound by the maximum of both RHS of these equations.

Proof of Lemma 1

We prove Lemma 1 below.

Proof. Let $\lambda \in \sigma(A)$. By the circle theorem, there exists $k \in \{1, \dots, N\}$ such that :

$$|\lambda - A_{kk}| \leq \sum_{j \neq k} |A_{kj}|. \quad (5.62)$$

We now use the complex identity:

$$|\lambda - A_{kk}| \geq \operatorname{Re}(\lambda - A_{kk}) = \operatorname{Re}(\lambda) - \operatorname{Re}(A_{kk}). \quad (5.63)$$

Equation (3.23) implies:

$$\sum_{j \neq k} |A_{kj}| < -\operatorname{Re}(A_{kk}). \quad (5.64)$$

Combining the two previous inequalities yields:

$$\operatorname{Re}(\lambda) - \operatorname{Re}(A_{kk}) \leq |\lambda - A_{kk}| \leq \sum_{j \neq k} |A_{kj}| < -\operatorname{Re}(A_{kk}). \quad (5.65)$$

Comparing the RHS and LHS of this inequality yields:

$$\operatorname{Re}(\lambda) < 0. \quad (5.66)$$

□

Estimation of the critical radius in terms of metaparameters

The following expression needs to be approximated:

$$\sum_j |\Gamma_{\mu j}| + D_\mu = \sum_j |\alpha_{\mu j} - \gamma_{j\mu} R_\mu^*| + \frac{l_\mu + \sum_j \alpha_{\mu j} S_j^*}{R_\mu^*}. \quad (5.67)$$

It is difficult to simplify that expression. If we assume that A has a structure such that very little intraspecific syntropy is observed then:

$$\sum_j |\Gamma_{\mu j}| \approx \sum_j \alpha_{\mu j} + \sum_j \gamma_{j\mu} R_\mu^* \approx \deg(A, \mu) \alpha_0 + \deg(G, \mu) \gamma_0 R_0. \quad (5.68)$$

In consequence we have:

$$\max_\mu \left\{ \sum_j |\Gamma_{\mu j}| + D_\mu \right\} \approx \max_\mu \left\{ \deg(G, \mu) \gamma_0 R_0 + \deg(A, \mu) \left(1 + \frac{\alpha_0 S_0}{R_0} \right) + \frac{l_0}{R_0} \right\}. \quad (5.69)$$

Similarly we find

$$\sum_\nu |B_{i\nu}| \approx \deg(G, i) \sigma_0 \gamma_0 S_0. \quad (5.70)$$

R_C is finally given by:

$$R_C \approx \max_i \left\{ \deg(G, i) \sigma_0 \gamma_0 S_0, \max_\mu \left\{ \deg(G, \mu) \gamma_0 R_0 + \deg(A, \mu) \left(1 + \frac{\alpha_0 S_0}{R_0} \right) + \frac{l_0}{R_0} \right\} \right\}. \quad (5.71)$$

When is zero part of the spectrum of J^* ?

We are interested in knowing when $\lambda = 0$ is part of the spectrum of J^* . By definition, $\lambda = 0$ is an eigenvalue if and only if it solves the master equation (3.11):

$$\det \begin{pmatrix} -D & \Gamma \\ B & 0 \end{pmatrix} = 0 \quad (5.72)$$

Using the fact that D is invertible, we can make use of the equality⁴⁴:

$$\det \begin{pmatrix} -D & \Gamma \\ B & 0 \end{pmatrix} = \det(-D) \det(BD^{-1}\Gamma). \quad (5.73)$$

Eq.(5.72) then becomes:

$$\det(BD^{-1}\Gamma) = 0 \quad (5.74)$$

which means that $BD^{-1}\Gamma$ is not full rank. Finally,

$$0 \in \sigma(J^*) \iff BD^{-1}\Gamma \text{ is not full rank.} \quad (5.75)$$

But when is $BD^{-1}\Gamma$ not full rank? The Sylvester rank inequality [53] states that:

$$\text{rank}(BD^{-1}\Gamma) \geq \text{rank}(B) + \text{rank}(D^{-1}\Gamma) - N_R. \quad (5.76)$$

Similarly,

$$\text{rank}(D^{-1}\Gamma) \geq \text{rank}(D^{-1}) + \text{rank}(\Gamma) - N_R = \text{rank}(\Gamma), \quad (5.77)$$

where we used the fact that D^{-1} is invertible so $\text{rank}(D^{-1}) = N_R$. One of the standard rank properties is:

$$\text{rank}(D^{-1}\Gamma) \leq \min\{\text{rank}(D^{-1}), \text{rank}(\Gamma)\} \implies \text{rank}(D^{-1}\Gamma) \leq \text{rank}(\Gamma). \quad (5.78)$$

In the end this yields $\text{rank}(D^{-1}\Gamma) = \text{rank}(\Gamma)$ and :

$$\text{rank}(BD^{-1}\Gamma) + N_R \geq \text{rank}(B) + \text{rank}(\Gamma). \quad (5.79)$$

We can use this inequality to enunciate a lemma about the presence of zero in the spectrum of J^* .

Lemma 2. *If $N_R \leq N_S$ and B and Γ are full rank, then $0 \notin \sigma(J^*)$.*

Proof. We assume that 0 is in the spectrum of J^* and prove it leads to a contradiction. Because $0 \in \sigma(J^*)$, Eq.(5.75) implies $BD^{-1}\Gamma$ is not full rank. Since the largest possible value for the rank of matrix is the minimum between its number of rows and columns, we have :

$$\text{rank}(BD^{-1}\Gamma) < \min(N_R, N_S) = N_R. \quad (5.80)$$

This can be used as an upper bound for Eq.(5.79) :

$$2N_R > \text{rank}(B) + \text{rank}(\Gamma). \quad (5.81)$$

However, we also know that B and Γ are full rank, *i.e.*

$$\text{rank}(B) = \text{rank}(\Gamma) = N_R. \quad (5.82)$$

Hence the previous inequality amounts to $N_R > N_R$, which is a contradiction. We conclude that the hypothesis $0 \in \sigma(J^*)$ is wrong. \square

⁴⁴This uses a formula which is trivially analogous to one found in [43].

Weak LRI regime

We prove Theorem 2.

Proof. We assume

$$(\Gamma B)_{\mu\mu} < - \sum_{\nu \neq \mu} |(\Gamma B)_{\mu\nu}| \quad \forall \mu. \quad (5.83)$$

Let $\lambda \in \mathbb{R}$, then the following will also trivially hold:

$$(\Gamma B)_{\mu\mu} - \lambda^2 < - \sum_{\nu \neq \mu} |(\Gamma B)_{\mu\nu}| \quad \forall \mu. \quad (5.84)$$

Dividing Eq.(5.84) by D_μ , we get:

$$\frac{1}{D_\mu} \left[\left(\sum_i \Gamma_{\mu i} B_{i\mu} \right) - \lambda^2 \right] < - \sum_{\nu \neq \mu} \left| \frac{\sum_i \Gamma_{\mu i} B_{i\nu}}{D_\mu} \right| \quad \forall \mu. \quad (5.85)$$

Looking at Eq.(3.19), we see that this is equivalent to:

$$S_{\mu\mu} + \sum_{\nu \neq \mu} |S_{\mu\nu}| < 0 \quad \forall \mu. \quad (5.86)$$

Using Lemma 1, we know that all the real eigenvalues of $S(\lambda)$ will have a negative real part. We can conclude with the statement of the theorem. \square

Approximation of the full spectrum

As an application to find explicit solutions for the spectrum of the Jacobian, we consider the very special case of the fully connected consumption and syntropy networks. In this “mean-field” theory, every consumer consumes and releases each resource, *i.e.*

$$G_{i\mu} = A_{\mu i} = 1 \quad \forall \mu = 1, \dots, N_R \quad \forall i = 1, \dots, N_S. \quad (5.87)$$

Our goal is to find the spectrum of systems with such consumption and syntropy networks. Barbier and Arnoldi showed that the variance of the interaction matrix plays a leading role in the dynamics of their model [26]. We follow an approach similar to theirs and perform a *standard deviation expansion*, explained in Section 5.1.1.

Rewriting the jacobian at equilibrium The different blocks of the jacobian at equilibrium (1.17) can be written with the new variables obtained in Section 5.1.1.:

$$\begin{cases} l_\mu + \sum_j \alpha_{\mu j} S_j^* = l_0 + N_S \alpha_0 S_0 + \sigma_l \tilde{l}_\mu + \sigma_\alpha S_0 \sum_j \tilde{\alpha}_{\mu j} + \sigma_\alpha \sigma_S \sum_j \tilde{\alpha}_{\mu j} \tilde{s}_j \\ R_\mu^* = R_0 + \sigma_R \tilde{r}_\mu \end{cases} \quad (5.88)$$

$$-\gamma_{j\mu} R_\mu^* + \alpha_{\mu j} = -\gamma_0 R_0 + \alpha_0 + \sigma_\gamma R_0 \tilde{\gamma}_{j\mu} + \sigma_R \gamma_0 \tilde{r}_\mu + \sigma_\alpha \tilde{\alpha}_{\mu j} + \sigma_\gamma \sigma_R \tilde{\gamma}_{j\mu} \tilde{r}_\mu \quad (5.89)$$

$$\begin{aligned} \sigma_{i\nu} \gamma_{i\nu} S_i^* = & \sigma_0 \gamma_0 S_0 + \sigma_\sigma \gamma_0 S_0 \tilde{\sigma}_{i\nu} + \sigma_\gamma \sigma_0 S_0 \tilde{\gamma}_{i\nu} + \sigma_S \sigma_0 \gamma_0 \tilde{s}_i + \sigma_\sigma \sigma_\gamma S_0 \tilde{\sigma}_{i\nu} \tilde{\gamma}_{i\nu} \\ & + \sigma_\sigma \sigma_S \gamma_0 \tilde{\sigma}_{i\nu} \tilde{s}_i + \sigma_\gamma \sigma_S \sigma_0 \tilde{\gamma}_{i\nu} \tilde{s}_i + \sigma_\sigma \sigma_\gamma \sigma_S \tilde{\sigma}_{i\nu} \tilde{\gamma}_{i\nu} \tilde{s}_i \end{aligned} \quad (5.90)$$

It's easier to work with relative standard deviations, *i.e.* we rewrite for all parameters :

$$\sigma_P \equiv \epsilon_P \langle P \rangle, \quad \forall P \in \{l_\nu, R_\nu^*, S_i^*, \gamma_{i\nu}, \alpha_{\nu i}, \sigma_{i\nu}\}. \quad (5.91)$$

The previous relations then become :

$$\left\{ \begin{array}{l} l_\mu + \sum_j \alpha_{\mu j} S_j^* \\ R_\mu^* \end{array} \right. = \frac{l_0 (1 + \epsilon_l \tilde{l}_\mu) + \alpha_0 S_0 (N_S + \epsilon_\alpha \sum_j \tilde{\alpha}_{\mu j} + \epsilon_\alpha \epsilon_S \sum_j \tilde{\alpha}_{\mu j} \tilde{s}_j)}{R_0 (1 + \epsilon_R \tilde{r}_\mu)} \quad (5.92)$$

$$-\gamma_{j\mu} R_\mu^* + \alpha_{\mu j} = -\gamma_0 R_0 (1 + \epsilon_\gamma \tilde{\gamma}_{j\mu} + \epsilon_R \tilde{r}_\mu + \epsilon_\gamma \epsilon_R \tilde{\gamma}_{j\mu} \tilde{r}_\mu) + \alpha_0 (1 + \epsilon_\alpha \tilde{\alpha}_{\mu j}) \quad (5.93)$$

$$\left\{ \begin{array}{l} \sigma_{i\nu} \gamma_{i\nu} S_i^* \\ \sigma_{i\nu} \gamma_{i\nu} S_i^* \end{array} \right. = \sigma_0 \gamma_0 S_0 (1 + \epsilon_\sigma \tilde{\sigma}_{i\nu} + \epsilon_\gamma \tilde{\gamma}_{i\nu} + \epsilon_S \tilde{s}_i + \epsilon_\sigma \epsilon_\gamma \tilde{\sigma}_{i\nu} \tilde{\gamma}_{i\nu} + \epsilon_\sigma \epsilon_S \tilde{\sigma}_{i\nu} \tilde{s}_i \\ + \epsilon_\gamma \epsilon_S \tilde{\gamma}_{i\nu} \tilde{s}_i + \epsilon_\sigma \epsilon_\gamma \epsilon_S \tilde{\sigma}_{i\nu} \tilde{\gamma}_{i\nu} \tilde{s}_i) \quad (5.94)$$

Standard deviation expansion at first order We assume the relative standard deviations are small:

$$\epsilon_P \ll 1, \quad \forall P \in \{l_\nu, R_\nu^*, S_i^*, \gamma_{i\nu}, \alpha_{\nu i}, \sigma_{i\nu}\}. \quad (5.95)$$

The previous equations can be rewritten as:

$$\left\{ \begin{array}{l} l_\mu + \sum_j \alpha_{\mu j} S_j^* \\ R_\mu^* \end{array} \right. = \frac{l_0 + N_S \alpha_0 S_0}{R_0} - \epsilon_R \frac{l_0 + N_S \alpha_0 S_0}{R_0} \tilde{r}_\mu + \epsilon_l \frac{l_0}{R_0} \tilde{l}_\mu + \epsilon_\alpha \frac{\alpha_0 S_0}{R_0} \sum_j \tilde{\alpha}_{\mu j} \quad (5.96)$$

$$-\gamma_{j\mu} R_\mu^* + \alpha_{\mu j} = -\gamma_0 R_0 + \alpha_0 - \epsilon_\gamma \gamma_0 R_0 \tilde{\gamma}_{j\mu} - \epsilon_R \gamma_0 R_0 \tilde{r}_\mu + \epsilon_\alpha \alpha_0 \tilde{\alpha}_{\mu j} \quad (5.97)$$

$$\sigma_{i\nu} \gamma_{i\nu} S_i^* = \sigma_0 \gamma_0 S_0 (1 + \epsilon_\sigma \tilde{\sigma}_{i\nu} + \epsilon_\gamma \tilde{\gamma}_{i\nu} + \epsilon_S \tilde{s}_i) \quad (5.98)$$

where we neglect all terms of order $\mathcal{O}(\epsilon^2)$. We now assume furthermore that the relative standard deviations of every parameter in the model more or less have the same value which again is assumed small, *i.e.* we set :

$$\epsilon_P \approx \epsilon \ll 1, \quad \forall P \in \{l_\nu, R_\nu^*, S_i^*, \gamma_{i\nu}, \alpha_{\nu i}, \sigma_{i\nu}\}. \quad (5.99)$$

This allows us to rewrite the jacobian at equilibrium as:

$$J^* = J_0 + \epsilon \tilde{J}, \quad (5.100)$$

with

$$J_0 = \begin{pmatrix} -D_0 & \Gamma_0 \\ B_0 & 0 \end{pmatrix} \quad (5.101)$$

where

$$(D_0)_{\mu\nu} \equiv D_0 \delta_{\mu\nu} = \frac{l_0 + N_S \alpha_0 S_0}{R_0} \delta_{\mu\nu} \quad (5.102)$$

$$(\Gamma_0)_{\mu i} \equiv \Gamma_0 = -\gamma_0 R_0 + \alpha_0 \quad (5.103)$$

$$(B_0)_{i\nu} \equiv B_0 = \sigma_0 \gamma_0 S_0 \quad (5.104)$$

and

$$\tilde{J} = \begin{pmatrix} \tilde{D} & \tilde{\Gamma} \\ \tilde{B} & 0 \end{pmatrix} \quad (5.105)$$

with

$$\tilde{D}_{\mu\nu} \equiv \left(-D_0 \tilde{r}_\mu + \frac{l_0}{R_0} \tilde{l}_\mu + \frac{\alpha_0 S_0}{R_0} \sum_j \tilde{\alpha}_{\mu j} \right) \delta_{\mu\nu} \quad (5.106)$$

$$\tilde{\Gamma}_{\mu i} \equiv \alpha_0 \tilde{\alpha}_{\mu i} - \gamma_0 R_0 (\tilde{\gamma}_{i\mu} + \tilde{r}_\mu) \quad (5.107)$$

$$\tilde{B}_{i\mu} \equiv B_0 (\tilde{\sigma}_{i\mu} + \tilde{\gamma}_{i\mu} + \tilde{s}_i) \quad (5.108)$$

Using Jacobi's formula [54], the equation $\det(J^* - \lambda \mathbb{1}_{N_R+N_S}) = 0$ can be rewritten as:

$$\det(J_0 - \lambda \mathbb{1}_{N_R+N_S} + \epsilon J^*) = \det(J_0 - \lambda \mathbb{1}_{N_R+N_S}) + \epsilon \operatorname{Tr} \left(\operatorname{adj}(J_0 - \lambda \mathbb{1}_{N_R+N_S}) \tilde{J} \right) = 0. \quad (5.109)$$

where $\operatorname{adj}(\dots)$ is the adjugate operator (*i.e.* which yields the transpose of the cofactor matrix). This equation is a complicated polynomial of degree $N_R + N_S$. We do not know how to find an easily computable solution for $\epsilon > 0$. An explicit solution can however be computed when $\epsilon = 0$.

Zero variance case When $\epsilon = 0$, Eq.(5.109) becomes:

$$\det(J_0 - \lambda \mathbb{1}_{N_R+N_S}) = \det \begin{pmatrix} -D_0 - \lambda \mathbb{1}_{N_R} & \Gamma_0 \\ B_0 & -\lambda \mathbb{1}_{N_S} \end{pmatrix} = 0 \quad (5.110)$$

If we assume that $\lambda \neq 0$, using a reasoning similar to Section 3.2.1 we can write the previous equation as:

$$\det(\lambda^2 \mathbb{1}_{N_R} + D_0 \lambda - \Gamma_0 B_0) = 0 \quad (5.111)$$

Component-wise, we have:

$$(\lambda^2 \mathbb{1}_{N_R} + D_0 \lambda - \Gamma_0 B_0)_{\mu\nu} = (\lambda^2 + D_0 \lambda) \delta_{\mu\nu} - \Gamma_0 B_0. \quad (5.112)$$

Section 2 explains how to find the non-zero solutions of Eq.(5.111). They are given by the roots of the polynomial:

$$(\lambda + D_0)^{N_R-1} (\lambda^2 + D_0 \lambda - N_R \Gamma_0 B_0) = 0. \quad (5.113)$$

That equation gives us $N_R - 1 + 2 = N_R + 1$ non-zero eigenvalues, which means that there are $N_S - 1$ zero eigenvalues. The two eigenvalues different from $-D_0$ or 0 are the roots of the second degree polynomial:

$$\lambda^2 + D_0 \lambda - N_R \Gamma_0 B_0 = 0. \quad (5.114)$$

In the end, the spectrum is given by:

- if $\Gamma_0 < -\frac{D_0^2}{4N_R B_0}$:

$$\sigma(J_0) = \left\{ 0, \dots, 0, -D_0, \dots, -D_0, -\frac{D_0}{2} \left(1 \pm i \sqrt{-\left(1 + \frac{4N_R \Gamma_0 B_0}{D_0^2} \right)} \right) \right\} \quad (5.115)$$

- if $\Gamma_0 = -\frac{D_0^2}{4N_R B_0}$:

$$\sigma(J_0) = \left\{ 0, \dots, 0, -D_0, \dots, -D_0, -\frac{D_0}{2}, -\frac{D_0}{2} \right\} \quad (5.116)$$

- if $\Gamma_0 > -\frac{D_0^2}{4N_R B_0}$:

$$\sigma(J_0) = \left\{ 0, \dots, 0, -D_0, \dots, -D_0, -\frac{D_0}{2} \left(1 \pm \sqrt{1 + \frac{4N_R \Gamma_0 B_0}{D_0^2}} \right) \right\} \quad (5.117)$$

It then becomes clear that the system is dynamically unstable if and only if $\frac{4N_R \Gamma_0 B_0}{D_0^2} > 0$. Because $N_R, B_0 > 0$, we get the condition:

$$\text{The non-variance system is dynamically unstable} \iff \Gamma_0 > 0. \quad (5.118)$$

If $\Gamma_0 \leq 0$, the fully connected system will be marginally stable. Note that the RHS of the feasibility condition Eq.(3.3) is equivalent in the fully connected case to :

$$\alpha_0 \lesssim \min(1 - \sigma_0, \sigma_0) \gamma_0 R_0 \iff \Gamma_0 \lesssim [\min(1 - \sigma_0, \sigma_0) - 1] \gamma_0 R_0 < 0, \quad (5.119)$$

which means that the case $\Gamma_0 > 0$ is simply not feasible. So in the end the feasible fully connected case is marginally stable and its non-zero eigenvalues have a negative real part.

We see that all but one non-zero eigenvalues are given by $-D_0$. However the last eigenvalue is determined by $4N_R \Gamma_0 B_0 + D_0^2$. It gives us the “deviation” away from $-D_0/2$ and hence also plays an essential role in the stability. Looking at its sign allows us to find possibly more locally dynamically stable zones of the metaparameters space \mathcal{M} . Indeed we expect to find more stable systems in the case of Eq.(5.117) if $4N_R \Gamma_0 B_0 + D_0^2$ is small, i.e.

$$4N_R \Gamma_0 B_0 + D_0^2 \ll 1 \iff 4N_R \sigma_0 \gamma_0 S_0 (\alpha_0 - \gamma_0 R_0) + \frac{l_0^2}{R_0^2} + \frac{2N_S \alpha_0 S_0 l_0}{R_0^2} + \frac{N_S^2 \alpha_0^2 S_0^2}{R_0^2} \ll 1. \quad (5.120)$$

Special determinant computation

We want to know when the determinant of the following N -dimensional square matrix is zero:

$$A_N = \begin{pmatrix} a & b & b \\ b & \ddots & b \\ b & b & a \end{pmatrix}, \text{i.e. } A_{ij} = b + (a - b)\delta_{ij}. \quad (5.121)$$

The equation we want to solve is:

$$\det(A_N) = 0. \quad (5.122)$$

Note that, using Gaussian elimination, Eq.(5.122) can be transformed in:

$$\det \begin{pmatrix} a & b & \dots & b \\ b - a & a - b & 0 & 0 \\ 0 & \ddots & \ddots & 0 \\ 0 & 0 & b - a & a - b \end{pmatrix} = 0 \quad (5.123)$$

Using Laplace's expansion, this can be written as:

$$a \det \begin{pmatrix} a-b & 0 & \dots & 0 \\ b-a & a-b & 0 & 0 \\ 0 & \ddots & \ddots & 0 \\ 0 & 0 & b-a & a-b \end{pmatrix} + (a-b) \det \begin{pmatrix} b & b & \dots & b \\ b-a & a-b & 0 & 0 \\ 0 & \ddots & \ddots & 0 \\ 0 & 0 & b-a & a-b \end{pmatrix} = 0 \quad (5.124)$$

Since the first term of the previous equation is a lower triangular matrix, its determinant is easily found:

$$a \det \begin{pmatrix} a-b & 0 & \dots & 0 \\ b-a & a-b & 0 & 0 \\ 0 & \ddots & \ddots & 0 \\ 0 & 0 & b-a & a-b \end{pmatrix} = a(a-b)^{n-1}. \quad (5.125)$$

Finding an explicit equation for the left term is a bit more involving. Let us define the general n square matrix $F_n(a, b)$:

$$F_n(a, b) = \begin{pmatrix} b & b & \dots & b \\ b-a & a-b & 0 & 0 \\ 0 & \ddots & \ddots & 0 \\ 0 & 0 & b-a & a-b \end{pmatrix}. \quad (5.126)$$

With a Laplace expansion one gets:

$$\det(F_n(a, b)) = b \det \begin{pmatrix} a-b & 0 & 0 \\ b-a & \ddots & 0 \\ 0 & b-a & a-b \end{pmatrix} + (a-b) \det \begin{pmatrix} b & b & \dots & b \\ b-a & a-b & 0 & 0 \\ 0 & \ddots & \ddots & 0 \\ 0 & 0 & b-a & a-b \end{pmatrix}. \quad (5.127)$$

This means:

$$\det(F_n(a, b)) = b(a-b)^{n-1} + (a-b) \det(F_{n-1}(a, b)). \quad (5.128)$$

It is easy to check that the solution to the previous equation is:

$$\det(F_n(a, b)) = [(n-1)b + \det(F_1(a, b))] (a-b)^{n-1}. \quad (5.129)$$

Since $\det(F_1(a, b)) = 1$, we get:

$$\det(F_n(a, b)) = n(a-b)^{n-1} \quad (5.130)$$

Inserting this in Eq.(5.124) yields:

$$\det(A_N) = 0 \iff (a-b)^{N-1} [a + (N-1)b] = 0. \quad (5.131)$$

The optimal S_0 for locally dynamically stable systems

How S_0 should be adjusted to increase the largest eigenvalue (Eq.5.120) is a bit tricky because it is present in three terms that do not have the same behaviour: one term is linear in S_0 with a negative coefficient, another is linear with a positive coefficient and another is quadratic (also with a positive coefficient). So we need to compute the minimum value the sum of these three terms is and take S_0 as the minimum we found. The consumers equilibrium abundance S_0^* that yields the minimum value is implicitly given by the condition:

$$\frac{d}{dS_0} \left[4N_R\sigma_0\gamma_0 S_0(\alpha_0 - \gamma_0 R_0) + \frac{l_0^2}{R_0^2} + \frac{2N_S\alpha_0 S_0 l_0}{R_0^2} + \frac{N_S^2\alpha_0^2 S_0^2}{R_0^2} \right]_{S_0=S_0^*} = 0. \quad (5.132)$$

The enthusiastic reader sees that this is equivalent to:

$$S_0^* = \frac{R_0^2}{N_S^2\alpha_0^2} \left(2N_R\sigma_0\gamma_0 (\gamma_0 R_0 - \alpha_0) - \frac{N_S\alpha_0 l_0}{R_0^2} \right). \quad (5.133)$$

One checks really easily that this point is indeed a minimum in S_0 . So if $S_0 > S_0^*$ it should be decreased, and otherwise increased. For $\alpha_0 \rightarrow 0$, $S_0^* \rightarrow \infty$, and for $\alpha_0 \rightarrow \infty$, $S_0^* \rightarrow 0^-$, which means we expect to find the most dynamically stable points at large S_0 for low syntropy and at low S_0 for large syntropy.



Eidgenössische Technische Hochschule Zürich
Swiss Federal Institute of Technology Zurich

Declaration of originality

The signed declaration of originality is a component of every semester paper, Bachelor's thesis, Master's thesis and any other degree paper undertaken during the course of studies, including the respective electronic versions.

Lecturers may also require a declaration of originality for other written papers compiled for their courses.

I hereby confirm that I am the sole author of the written work here enclosed and that I have compiled it in my own words. Parts excepted are corrections of form and content by the supervisor.

Title of work (in block letters):

Impact of syntrophic interactions on the stability of microbial communities under chemostat conditions

Authored by (in block letters):

For papers written by groups the names of all authors are required.

Name(s):

Buchenel

First name(s):

Léo

With my signature I confirm that

- I have committed none of the forms of plagiarism described in the 'Citation etiquette' information sheet.
- I have documented all methods, data and processes truthfully.
- I have not manipulated any data.
- I have mentioned all persons who were significant facilitators of the work.

I am aware that the work may be screened electronically for plagiarism.

Place, date

Zürich, May 12, 2020

Signature(s)



For papers written by groups the names of all authors are required. Their signatures collectively guarantee the entire content of the written paper.

Bibliography

- [1] Ashutosh Jogalekar. *Physicists in Biology; And Other Quirks of the Genomic Age*. en. Library Catalog: blogs.scientificamerican.com. URL: <https://blogs.scientificamerican.com/the-curious-wavefunction/physicists-in-biology-and-other-quirks-of-the-genomic-age/> (visited on 04/02/2020).
- [2] Erwin Schrödinger. *What is Life? The Physical Aspect of the Living Cell*. Cambridge University Press, 1944.
- [3] Hue Sun Chan and Ken A Dill. “The Protein Folding Problem”. en. In: *Physics Today* 46.2 (1993), pp. 24–32. DOI: 10.1063/1.881371.
- [4] C. K. Fisher and P. Mehta. “The transition between the niche and neutral regimes in ecology”. en. In: *Proceedings of the National Academy of Sciences* 111.36 (Sept. 2014), pp. 13111–13116. ISSN: 0027-8424, 1091-6490. DOI: 10.1073/pnas.1405637111. URL: <http://www.pnas.org/cgi/doi/10.1073/pnas.1405637111> (visited on 01/08/2020).
- [5] Alessandro Attanasi et al. “Information transfer and behavioural inertia in starling flocks”. en. In: *Nature Physics* 10.9 (Sept. 2014), pp. 691–696. ISSN: 1745-2473, 1745-2481. DOI: 10.1038/nphys3035. URL: <http://www.nature.com/articles/nphys3035> (visited on 04/02/2020).
- [6] Ruth E. Ley et al. “Worlds within worlds: evolution of the vertebrate gut microbiota”. en. In: *Nature Reviews Microbiology* 6.10 (Oct. 2008), pp. 776–788. ISSN: 1740-1526, 1740-1534. DOI: 10.1038/nrmicro1978. URL: <http://www.nature.com/articles/nrmicro1978> (visited on 04/02/2020).
- [7] Cristina Becerra-Castro et al. “Wastewater reuse in irrigation: A microbiological perspective on implications in soil fertility and human and environmental health”. en. In: *Environment International* 75 (Feb. 2015), pp. 117–135. ISSN: 01604120. DOI: 10.1016/j.envint.2014.11.001. URL: <https://linkinghub.elsevier.com/retrieve/pii/S0160412014003237> (visited on 04/02/2020).
- [8] P. G. Falkowski. “Biogeochemical Controls and Feedbacks on Ocean Primary Production”. en. In: *Science* 281.5374 (July 1998), pp. 200–206. DOI: 10.1126/science.281.5374.200. URL: <https://www.sciencemag.org/lookup/doi/10.1126/science.281.5374.200> (visited on 04/02/2020).
- [9] Brandon E.L. Morris et al. “Microbial syntrophy: interaction for the common good”. en. In: *FEMS Microbiology Reviews* 37.3 (May 2013), pp. 384–406. ISSN: 1574-6976. DOI: 10.1111/1574-6976.12019. URL: <https://academic.oup.com/femsre/article-lookup/doi/10.1111/1574-6976.12019> (visited on 04/02/2020).
- [10] Ugo Bastolla et al. “The architecture of mutualistic networks minimizes competition and increases biodiversity”. en. In: *Nature* 458.7241 (Apr. 2009), pp. 1018–1020. ISSN: 0028-0836, 1476-4687. DOI: 10.1038/nature07950. URL: <http://www.nature.com/articles/nature07950> (visited on 01/09/2020).
- [11] R. P. Rohr, S. Saavedra, and J. Bascompte. “On the structural stability of mutualistic systems”. en. In: *Science* 345.6195 (July 2014), pp. 1253497–1253497. ISSN: 0036-8075, 1095-9203. DOI: 10.1126/science.1253497. URL: <http://www.sciencemag.org/cgi/doi/10.1126/science.1253497> (visited on 01/08/2020).

- [12] E. Thebault and C. Fontaine. “Stability of Ecological Communities and the Architecture of Mutualistic and Trophic Networks”. en. In: *Science* 329.5993 (Aug. 2010), pp. 853–856. ISSN: 0036-8075, 1095-9203. DOI: 10.1126/science.1188321. URL: <https://www.sciencemag.org/lookup/doi/10.1126/science.1188321> (visited on 04/30/2020).
- [13] Alex James, Jonathan W. Pitchford, and Michael J. Plank. “Disentangling nestedness from models of ecological complexity”. en. In: *Nature* 487.7406 (July 2012), pp. 227–230. ISSN: 0028-0836, 1476-4687. DOI: 10.1038/nature11214. URL: <http://www.nature.com/articles/nature11214> (visited on 05/08/2020).
- [14] Purna C. Kashyap et al. “Microbiome at the Frontier of Personalized Medicine”. en. In: *Mayo Clinic Proceedings* 92.12 (Dec. 2017), pp. 1855–1864. ISSN: 00256196. DOI: 10.1016/j.mayocp.2017.10.004. URL: <https://linkinghub.elsevier.com/retrieve/pii/S0025619617307322> (visited on 05/10/2020).
- [15] Jeffrey D Orth, Ines Thiele, and Bernhard Ø Palsson. “What is flux balance analysis?” en. In: *Nature Biotechnology* 28.3 (Mar. 2010), pp. 245–248. ISSN: 1087-0156, 1546-1696. DOI: 10.1038/nbt.1614. URL: <http://www.nature.com/articles/nbt.1614> (visited on 03/29/2020).
- [16] Ines Thiele et al. “Multiscale Modeling of Metabolism and Macromolecular Synthesis in *E. coli* and Its Application to the Evolution of Codon Usage”. en. In: *PLoS ONE* 7.9 (Sept. 2012). Ed. by Tamir Tuller, e45635. ISSN: 1932-6203. DOI: 10.1371/journal.pone.0045635. URL: <https://dx.plos.org/10.1371/journal.pone.0045635> (visited on 04/03/2020).
- [17] A J Lotka. “Analytical Note on Certain Rhythmic Relations in Organic Systems”. eng. In: *Proceedings of the National Academy of Sciences of the United States of America* 6.7 (July 1920), pp. 410–415. ISSN: 0027-8424. DOI: 10.1073/pnas.6.7.410. URL: <https://pubmed.ncbi.nlm.nih.gov/16576509/>.
- [18] Babak Momeni, Li Xie, and Wenying Shou. “Lotka-Volterra pairwise modeling fails to capture diverse pairwise microbial interactions”. en. In: *eLife* 6 (Mar. 2017), e25051. ISSN: 2050-084X. DOI: 10.7554/eLife.25051. URL: <https://elifesciences.org/articles/25051> (visited on 04/02/2020).
- [19] James P. O’Dwyer. “Whence Lotka-Volterra?: Conservation laws and integrable systems in ecology”. en. In: *Theoretical Ecology* 11.4 (Dec. 2018), pp. 441–452. ISSN: 1874-1738, 1874-1746. DOI: 10.1007/s12080-018-0377-0. URL: <http://link.springer.com/10.1007/s12080-018-0377-0> (visited on 01/08/2020).
- [20] Robert MacArthur. “Species packing and competitive equilibrium for many species”. en. In: *Theoretical Population Biology* 1.1 (May 1970), pp. 1–11. ISSN: 00405809. DOI: 10.1016/0040-5809(70)90039-0. URL: <https://linkinghub.elsevier.com/retrieve/pii/0040580970900390> (visited on 04/02/2020).

- [21] James D. Brunner and Nicholas Chia. "Metabolite mediated modeling of microbial community dynamics captures emergent behavior more effectively than species-species modeling". en. In: *Journal of The Royal Society Interface* 16.159 (Oct. 2019). arXiv: 1907.04436, p. 20190423. ISSN: 1742-5689, 1742-5662. DOI: 10.1098/rsif.2019.0423. URL: <http://arxiv.org/abs/1907.04436> (visited on 04/02/2020).
- [22] T W James. "Continuous Culture of Microorganisms". en. In: *Annual Review of Microbiology* 15.1 (Oct. 1961), pp. 27–46. ISSN: 0066-4227, 1545-3251. DOI: 10.1146/annurev.mi.15.100161.000331. URL: <http://www.annualreviews.org/doi/10.1146/annurev.mi.15.100161.000331> (visited on 03/29/2020).
- [23] Robert M. May. "Will a Large Complex System be Stable?" In: *Nature* 238.5364 (Aug. 1972), pp. 413–414. ISSN: 1476-4687. DOI: 10.1038/238413a0. URL: <https://doi.org/10.1038/238413a0>.
- [24] Stefano Allesina and Si Tang. "Stability Criteria for Complex Ecosystems". en. In: *Nature* 483.7388 (Mar. 2012). arXiv: 1105.2071, pp. 205–208. ISSN: 0028-0836, 1476-4687. DOI: 10.1038/nature10832. URL: <http://arxiv.org/abs/1105.2071> (visited on 01/08/2020).
- [25] Stefano Allesina et al. "Predicting the stability of large structured food webs". en. In: *Nature Communications* 6.1 (Nov. 2015), p. 7842. ISSN: 2041-1723. DOI: 10.1038/ncomms8842. URL: <http://www.nature.com/articles/ncomms8842> (visited on 01/08/2020).
- [26] Matthieu Barbier and Jean-François Arnoldi. *The cavity method for community ecology*. en. preprint. Ecology, June 2017. DOI: 10.1101/147728. URL: <http://biorxiv.org/lookup/doi/10.1101/147728> (visited on 01/08/2020).
- [27] Guy Bunin. "Ecological communities with Lotka-Volterra dynamics". en. In: *Physical Review E* 95.4 (Apr. 2017), p. 042414. ISSN: 2470-0045, 2470-0053. DOI: 10.1103/PhysRevE.95.042414. URL: <http://link.aps.org/doi/10.1103/PhysRevE.95.042414> (visited on 01/15/2020).
- [28] Y. Takeuchi. *Global dynamical properties of Lotka-Volterra systems*. en. Singapore ; River Edge, NJ: World Scientific, 1996. ISBN: 978-981-02-2471-4.
- [29] Alberto Pascual-García and Ugo Bastolla. "Mutualism supports biodiversity when the direct competition is weak". en. In: *Nature Communications* 8.1 (Apr. 2017), p. 14326. ISSN: 2041-1723. DOI: 10.1038/ncomms14326. URL: <http://www.nature.com/articles/ncomms14326> (visited on 01/08/2020).
- [30] Peter Chesson. "MacArthur's consumer-resource model". en. In: *Theoretical Population Biology* 37.1 (Feb. 1990), pp. 26–38. ISSN: 00405809. DOI: 10.1016/0040-5809(90)90025-Q. URL: <https://linkinghub.elsevier.com/retrieve/pii/004058099090025Q> (visited on 03/30/2020).
- [31] Steven H. Strogatz. *Nonlinear dynamics and Chaos: with applications to physics, biology, chemistry, and engineering*. en. Studies in nonlinearity. Reading, Mass: Addison-Wesley Pub, 1994. ISBN: 978-0-201-54344-5.

- [32] Giulio Biroli, Guy Bunin, and Chiara Cammarota. “Marginally stable equilibria in critical ecosystems”. en. In: *New Journal of Physics* 20.8 (Aug. 2018), p. 083051. ISSN: 1367-2630. DOI: 10.1088/1367-2630/aada58. URL: <http://stacks.iop.org/1367-2630/20/i=8/a=083051?key=crossref.eb2ea792ef1892155c3ce3f806e602f3> (visited on 01/14/2020).
- [33] B S GoH. “Global Stability in Many-Species Systems”. en. In: *The American Naturalist* 111.977 (1977), pp. 135–143.
- [34] Stacey Butler and James P. O’Dwyer. “Stability criteria for complex microbial communities”. en. In: *Nature Communications* 9.1 (Dec. 2018), p. 2970. ISSN: 2041-1723. DOI: 10.1038/s41467-018-05308-z. URL: <http://www.nature.com/articles/s41467-018-05308-z> (visited on 02/17/2020).
- [35] Mimmo Iannelli and Andrea Pugliese. *An Introduction to Mathematical Population Dynamics*. en. Vol. 79. UNITEXT. Cham: Springer International Publishing, 2014. ISBN: 978-3-319-03025-8 978-3-319-03026-5. DOI: 10.1007/978-3-319-03026-5. URL: <http://link.springer.com/10.1007/978-3-319-03026-5> (visited on 03/10/2020).
- [36] Samuel Jonhson, Virginia Domínguez-García, and Miguel A. Muñoz. “Factors Determining Nestedness in Complex Networks”. en. In: *PLoS ONE* 8.9 (Sept. 2013). Ed. by Yamir Moreno, e74025. ISSN: 1932-6203. DOI: 10.1371/journal.pone.0074025. URL: <https://dx.plos.org/10.1371/journal.pone.0074025> (visited on 02/26/2020).
- [37] J. P. DeLong et al. “Shifts in metabolic scaling, production, and efficiency across major evolutionary transitions of life”. en. In: *Proceedings of the National Academy of Sciences* 107.29 (July 2010), pp. 12941–12945. ISSN: 0027-8424, 1091-6490. DOI: 10.1073/pnas.1007783107. URL: <http://www.pnas.org/cgi/doi/10.1073/pnas.1007783107> (visited on 05/09/2020).
- [38] Oscar Perron. “Zur Theorie der Matrices”. de. In: *Math. Ann.* 64 (June 1907), pp. 248–263. URL: <https://doi.org/10.1007/BF01449896>.
- [39] Sergej Gershgorin. “Über die Abgrenzung der Eigenwerte einer Matrix”. de. In: *Bulletin de l’Académie des Sciences de l’URSS. Classe des sciences mathématiques et naturelles* 6 (1931), pp. 749–754.
- [40] Daniel Delahaye, Supatcha Chaimatanan, and Marcel Mongeau. “Simulated Annealing: From Basics to Applications”. en. In: *Handbook of Metaheuristics*. Ed. by Michel Gendreau and Jean-Yves Potvin. Vol. 272. Series Title: International Series in Operations Research & Management Science. Cham: Springer International Publishing, 2019, pp. 1–35. ISBN: 978-3-319-91085-7 978-3-319-91086-4. DOI: 10.1007/978-3-319-91086-4_1. URL: http://link.springer.com/10.1007/978-3-319-91086-4_1 (visited on 03/09/2020).
- [41] G. Hardin. “The Competitive Exclusion Principle”. en. In: *Science* 131.3409 (Apr. 1960), pp. 1292–1297. ISSN: 0036-8075, 1095-9203. DOI: 10.1126/science.131.3409.1292. URL: <https://www.sciencemag.org/lookup/doi/10.1126/science.131.3409.1292> (visited on 04/01/2020).

- [42] Xin Wang and Yang-Yu Liu. “Overcome Competitive Exclusion in Ecosystems”. en. In: *arXiv:1805.06002 [physics, q-bio]* (May 2019). arXiv: 1805.06002. URL: <http://arxiv.org/abs/1805.06002> (visited on 04/01/2020).
- [43] Philip D. Powell. “Calculating Determinants of Block Matrices”. en. In: *arXiv:1112.4379 [math]* (Dec. 2011). arXiv: 1112.4379. URL: <http://arxiv.org/abs/1112.4379> (visited on 03/21/2020).
- [44] Mikhail Tikhonov and Remi Monasson. “Collective Phase in Resource Competition in a Highly Diverse Ecosystem”. en. In: *Physical Review Letters* 118.4 (Jan. 2017), p. 048103. ISSN: 0031-9007, 1079-7114. DOI: 10.1103/PhysRevLett.118.048103. URL: <https://link.aps.org/doi/10.1103/PhysRevLett.118.048103> (visited on 04/24/2020).
- [45] Robert Marsland et al. “Available energy fluxes drive a transition in the diversity, stability, and functional structure of microbial communities”. en. In: *PLOS Computational Biology* 15.2 (Feb. 2019). Ed. by Alexandre V. Morozov, e1006793. ISSN: 1553-7358. DOI: 10.1371/journal.pcbi.1006793. URL: <http://dx.plos.org/10.1371/journal.pcbi.1006793> (visited on 04/24/2020).
- [46] Thomas Pfeiffer and Sebastian Bonhoeffer. “Evolutionary Consequences of Trade-offs between Yield and Rate of ATP Production”. en. In: *Zeitschrift für Physikalische Chemie* 216.1 (Jan. 2002). ISSN: 2196-7156, 0942-9352. DOI: 10.1524/zpch.2002.216.1.051. URL: <http://www.degruyter.com/view/j/zpch.2002.216.issue-1/zpch.2002.216.1.051/zpch.2002.216.1.051.xml> (visited on 05/10/2020).
- [47] Diane Lawrence et al. “Species Interactions Alter Evolutionary Responses to a Novel Environment”. en. In: *PLoS Biology* 10.5 (May 2012). Ed. by Stephen P. Ellner, e1001330. ISSN: 1545-7885. DOI: 10.1371/journal.pbio.1001330. URL: <https://dx.plos.org/10.1371/journal.pbio.1001330> (visited on 05/11/2020).
- [48] Robert M May. “Qualitative Stability in Model Ecosystems”. en. In: *Late Spring* (1973), p. 6.
- [49] Robert MacArthur. “Fluctuations of Animal Populations and a Measure of Community Stability”. en. In: *Ecology* 36.3 (July 1955), p. 533. ISSN: 00129658. DOI: 10.2307/1929601. URL: <http://www.jstor.org/stable/1929601?origin=crossref> (visited on 04/23/2020).
- [50] Alan R. Pacheco, Mauricio Moel, and Daniel Segrè. “Costless metabolic secretions as drivers of interspecies interactions in microbial ecosystems”. en. In: *Nature Communications* 10.1 (Dec. 2019), p. 103. ISSN: 2041-1723. DOI: 10.1038/s41467-018-07946-9. URL: <http://www.nature.com/articles/s41467-018-07946-9> (visited on 05/10/2020).
- [51] Richard R. Stein et al. “Ecological Modeling from Time-Series Inference: Insight into Dynamics and Stability of Intestinal Microbiota”. en. In: *PLoS Computational Biology* 9.12 (Dec. 2013). Ed. by Christian von Mering, e1003388. ISSN: 1553-7358. DOI: 10.1371/journal.pcbi.1003388. URL: <https://dx.plos.org/10.1371/journal.pcbi.1003388> (visited on 05/11/2020).

- [52] Andrey N. Kolmogorov. *Foundations of the Theory of Probability*. Chelsea Pub Co, 1960. URL: [https://cml.rhul.ac.uk/resources/fop/Theory%20of%20Probability%20\(small\).pdf](https://cml.rhul.ac.uk/resources/fop/Theory%20of%20Probability%20(small).pdf) (visited on 05/03/2020).
- [53] Néstor Thome. “Inequalities and equalities for $l = 2$ (Sylvester), $l = 3$ (Frobenius), and $l > 3$ matrices”. en. In: *Aequationes mathematicae* 90.5 (Oct. 2016), pp. 951–960. ISSN: 0001-9054, 1420-8903. DOI: 10.1007/s00010-016-0412-4. URL: <http://link.springer.com/10.1007/s00010-016-0412-4> (visited on 04/15/2020).
- [54] Jan R. Magnus and Heinz Neudecker. *Matrix differential calculus with applications in statistics and econometrics*. en. Third edition. Wiley series in probability and statistics. Hoboken, NJ: Wiley, 2019. ISBN: 978-1-119-54119-6 978-1-119-54116-5.